DISS. ETH NO.

THE ROLE OF SUB-SURFACE WATER IN PLASMA-DEPOSITED VERTICAL CHEMICAL GRADIENTS

A thesis submitted to attain the degree of

DOCTOR OF SCIENCES of ETH ZURICH

(Dr. sc. ETH Zurich)

presented by

NOÉMI ELISABETH BLANCHARD

MSc in Physics, University of Fribourg

born on 27.04.1987

citizen of Tafers FR

accepted on the recommendation of

Prof. Dr. Manfred heuberger, examiner

Dr. Christophe Hollenstein, co-examiner

Prof. Dr. Nicholas Spencer, co-examiner

Dr. Dirk Hegemann, co-examiner

2015

ABSTRACT

Despite its widely accepted importance, the exact role of water in protein adsorption is still an unresolved issue. It is generally acknowledged that hydrophobic interactions are an important factor controlling the adsorption of proteins (and other amphiphilic molecules) to various types of surfaces. However, no general consensus exists about the exact role of the hydrophobic effect in adsorption processes. Adsorption is traditionally discussed with respect to the very surface properties of a material, involving only the top layer of atoms or molecules. In this thesis we want to test the central hypothesis that a vertical chemical gradient below the surface affects the adsorption of amphiphilic molecules such as surfactants or proteins.

The vertical chemical gradients used in this thesis need to meet several requirements. First of all the thickness of the gradient has to be controllable and the specific energy of the gradient should be tunable over a reasonable range of surface free energies. In addition, the vertical structure needs to be stable over time in aqueous environments and should allow for the penetration of water into the gradient. Plasma polymerization offers the possibility to deposit films meeting these requirements. However, a precise control over film deposition must be established.

To this end the plasma polymerization process of hexamethyldisiloxane (HMDSO) was investigated in more detail. Previously, it was found for other precursors used in plasma polymerization that film densification/cross-linking is mainly influenced by interactions with energetic particles at the surface. The influence of energetic conditions in the gas phase and at the surface on film

densification/cross-linking was therefore studied also for HMDSO. It was found that the degree of fragmentation of the precursor in the plasma gas phase has a similar influence on densification than energetic particle interactions. A specific map of chemical fragmentation pathways for the HMDSO precursor was then proposed. The properties of HMDSO plasma polymer films deposited applying a broad range of plasma parameters were further characterized using X-ray photoelecton spectroscopy (XPS) and contact angle measurements. Film thickness, chemical composition and wetting behavior of the HMDSO films used in this thesis can thus precisely be controlled. The aging and hydration of these films was studied by contact angle measurements after quasi equilibration in air or water. Hydration history effects related to the energetic conditions applied in the plasma process were observed. Under suitable plasma conditions effective water penetration and hydrated ion diffusion in the films was possible as evidenced by silver release studies.

In order to further investigate the response of these plasma polymer films to aqueous environments two films were deposited in hexamethyldisiloxane (HMDSO) and HMDSO/O_2 low-pressure discharges. Analysis of their chemical structures in dry state using infrared spectroscopy (IR) and neutron reflectometry (NR) revealed the hydrophobic, PDMS-like properties of the HMDSO-derived film, while the retention of carbon groups is reduced by O_2 addition yielding a more inorganic, hydrophilic SiO_x film. Both films showed a slight (vertical) density gradient perpendicular to the substrate, where the exposed film surface seems to be more oxidized indicating oxidative aging reactions upon contact with air. In a further step, the hydration and water uptake abilities of the films in aqueous environments were investigated. In situ measurements in D_2O using NR and ellipsometry measurements in humid environments were confirmed by multiple transmission-reflection IR measurements after equilibration of the films in water. While water penetrates more deeply into the

nano-porous SiO_x film, the HMDSO film is hydrated merely in an about 10 nm thick region close to the film surface (sub-surface). The HMDSO film is thus partially permeable to water.

With the acquired knowledge about the relationship between applied plasma parameters, resulting film chemistry and wetting behavior, hydrophilic-to-hydrophobic vertical chemical gradient layers could be produced by gradually tuning plasma parameters like power input and gas composition. Characterization of the obtained gradient films by XPS and contact angle measurements revealed that indeed the thickness and wettability of the gradients can be controlled.

As mentioned in the beginning, vertical chemical gradients are thought to affect the adsorption of amphiphiles. In order to test this hypothesis, the adsorption of bovine serum albumin (BSA) on the plasma polymerized vertical chemical gradients was investigated using the Transmission Interferometric Adsorption Sensor (TInAS). In comparison to the amount of protein adsorbed on plain SiO_x and HMDSO films, a reduced adsorbed amount of BSA was observed on gradient films. The exact driving forces behind this reduction remain to be revealed. Based on the obtained results and findings from existing literature, it is hypothesized that the sub-surface water contained within the gradient structures in an way that the interaction with an approaching protein is unfavorable and protein adsorption is reduced.

Further investigations will be needed to shed light on the mechanisms behind this reduction. Therefore, several strategies to clarify the role of sub-surface water in adsorption processes on vertical chemical gradients are presented.

ZUSAMMENFASSUNG

Obwohl es allgemein anerkannt ist, dass Wasser und die damit verbundenen hydrophoben Wechselwirkungen für die Adsorption von Proteinen und anderen amphiphilen Molekülen auf verschiedensten Oberflächen eine wichtige Rolle spielen, ist die genaue Funktion von Wasser in Bezug auf die Proteinadsorption noch nicht vollständig geklärt. Ein allgemeiner Konsens über die Rolle des hydrophoben Effekts in Adsorptionsprozessen konnte ebenfalls noch nicht erreicht werden. Adsorption wird üblicherweise anhand der Oberflächeneigenschaften eines Materials diskutiert, wobei nur die oberste Atom-oder Moleküllage berücksichtigt wird. In dieser Arbeit soll nun die Hypothese getestet werden, dass ein unter der Oberfläche liegender vertikaler chemischer Gradient die Adsorption von amphiphilen Molekülen wie Tensiden oder Proteinen beeinflusst.

Dazu müssen die untersuchten vertikalen chemischen Gradientenschichten präzise einstellbare Eigenschaften aufweisen, was vor allem die chemische Zusammensetzung und die Dicke des Gradienten betrifft sowie die spezifische Energie im Gradienten, die über einen angemessenen Oberflächenenergiebereich einstellbar sein sollte. Zusätzlich muss die vertikale Struktur in wässriger Umgebung über längere Zeit stabil bleiben und eine gewisse Durchlässigkeit für Wasser aufweisen. Zur Erzeugung ultradünner Schichten mit den gewünschten Eigenschaften wurde die Plasmapolymerisation als Verfahren gewählt, wobei eine hohe Prozesskontrolle erforderlich ist

Ausgehend von der Erfahrung, dass die Verdichtung und Vernetzung der Plasmapolymerschicht vor allem durch die Wechselwirkung mit energetischen Teilchen an der Oberfläche beeinflusst

wird, wurde der Plasmapolymerisationsprozess des in dieser Arbeit verwendeten Präkursor-Mono-mers, Hexamethyldisiloxan (HMDSO), genauer untersucht, um den Einfluss der energetischen Be-dingungen in der Plasmagasphase und an der Substratoberfläche auf das Schichtwachstum aufzu-klären. Es konnte gezeigt werden, dass der Fragmentationsgrad des Präkursors in der Gasphase einen ähnlich starken Einfluss auf die Schichtverdichtung hat wie die Wechselwirkung mit ener-getischen Teilchen. Die verschiedenen Reaktionswege für die Fragmentation von HMDSO wurden aufgezeigt und schichtbildende Radikale ermittelt. Die über einen breiten Parameterbereich herge-stellten HMDSO-Plasmapolymerschichten wurden daraufhin mittels Photoelektronenspektroskopie (XPS) und Kontaktwinkelmessungen auf ihre Eigenschaften untersucht. Die derart gewonnenen Erkenntnisse wurden genutzt, um die Schichtdicke, die chemische Zusammensetzung und das Be-netzungsverhalten der in dieser Arbeit verwendeten HMDSO-Schichten exakt zu kontrollieren. Des Weiteren wurde das Alterungs- und Hydrationsverhalten dieser Schichten nach Lagerung an Luft oder in Wasser untersucht. Die beobachteten Alterungs- und Hydrierungseffekte konnten dabei mit den energetischen Bedingungen im Plasmaprozess in Verbindung gebracht werden. Mit Hilfe einer Studie zur Freisetzung von Silber konnte ausserdem gezeigt werden, dass Wasser prinzipiell in hydrophobe HMDSO-Schichten eindringen kann und die Diffusion hydrierter Ionen durch die Schichten möglich ist.

Das Verhalten in wässriger Umgebung wurde für zwei Beschichtungstypen genauer untersucht; nämlich für eine im reinen HMDSO-Plasma abgeschiedenen Schicht und für eine Beschichtung aus einem HMDSO/O_2-Gasgemisch. Die chemische Struktur dieser Schichten im trockenen Zustand wurde mittels Infrarotspektroskopie (IR) und Neutronenreflektometrie (NR) ermittelt. Die reine HMDSO Schicht wies dabei hydrophobe, PDMS-ähnliche Eigenschaften auf, während die Beimi-

schung von Sauerstoff zu einem tieferen Kohlenstoffgehalt und damit zu einer eher anorganischen, hydrophilen Schicht führte. Senkrecht zum Substrat wiesen beide Schichten einen leichten (vertikalen) Dichtegradienten auf. Die freiliegende Schichtoberfläche scheint dabei stärker oxidiert zu sein, was darauf hindeutet, dass die Schichten beim Kontakt mit Luft durch Oxidation altern. In einem weiteren Schritt wurden die Hydration und Wasseraufnahmefähigkeit der Schichten in wässriger Umgebung untersucht. Die Messungen mittels NR in D_2O, Ellipsometrie in feuchter Umgebung und MTR-IR nach Lagerung der Schichten in Wasser bestätigten, dass beide untersuchten Schichttypen Wasser aufnehmen. Dabei dringt das Wasser tiefer in die nanoporöse SiO_x Schicht ein als in die HMDSO-Schicht, die nur in einem etwa 10 nm dicken Bereich an der Schichtoberfläche hydriert wird. Die nominell hydrophobe HMDSO Schicht ist also teilweise wasserdurchlässig.

Mit dem erlangten Wissen über den Zusammenhang der verwendeten Plasmaparameter und der daraus resultierenden Schichtzusammensetzung und des Benetzungsverhaltens, konnten hydrophil-zu-hydrophob Gradienten kontrolliert hergestellt werden. Die so erhaltenen vertikalen chemischen Gradienten wurden mit Hilfe von XPS und Kontaktwinkelmessungen charakterisiert, um die angestrebte Dicke und das Benetzungsverhalten der Gradienten zu verifizieren.

Wie anfangs schon erwähnt, wird angenommen, dass vertikale chemische Gradienten die Adsorption von amphiphilen Molekülen beeinflussen. Um diese Hypothese zu testen, wurde die Adsorption von Rinderserumalbumin (BSA) an den vertikalen chemischen Plasmapolymer-Gradienten untersucht. Für diese Adsorptionsstudie wurde das optische Messverfahren TInAS (Transmission Interferometric Adsorption Sensor) gewählt. Die besonderen Eigenschaften der Gradientenschichten ergaben im Vergleich zu den reinen SiO_x- und HMDSO-Schichten eine geringere Menge an adsorbiertem Protein. Es ist jedoch noch unklar, wodurch diese Reduktion im Detail verursacht wird. Gestützt

auf die gewonnenen Ergebnisse sowie Erkenntnissen aus Literatur wurde die Hypothese aufgestellt, dass sich das Wasser in den Gradienten so strukturiert, dass die Wechselwirkung mit einem Protein ungünstig wird und dadurch die Proteinadsorption reduziert.

Um den Mechanismus hinter dieser Reduktion vollends aufzuklären, werden verschiedene Strategien vorgeschlagen, um die Rolle des Wassers in Adsorptionsprozessen an vertikalen chemischen Gradienten tiefergehend zu untersuchen.

CONTENTS

INTRODUCTION

This first chapter of the thesis is thought to provide the reader with a more general introduction giving the broader context of this work. More detailed introductions regarding the main topics of this thesis are found at the beginning of each chapter. Furthermore, the scope of this thesis and its structure are presented at the end of this chapter.

1.1 General introduction

Water is the most abundant and most important solvent on earth, but also one of the least understood. Water is a liquid at ambient conditions only thanks to the strong cohesion of water molecules and their ability to form hydrogen bonds amongst each other. These strong interactions result in the high surface tension that water exhibits compared to other liquids and are also responsible for other phenomena such as hydrophobic hydration. The latter describes the ability of water to dissolve also apolar molecules by forming a so-called hydration shell around them. This hydration shell is entropically unfavorable, but enthalpically favorable, as the molecules constituting the hydration shell can

interact via stronger, more stable hydrogen bonds than in bulk water [1–4]. Hydrogen bonding is also (partially) responsible for the folding of DNA strands and proteins or the formation of micelles of amphiphilic molecules. The importance of these interactions is generally acknowledged in many fields of science. However, even if considerable effort has been devoted to the understanding of the origin of hydrophobic interactions, it is not fully understood yet [5, 6].

Over the past few decades considerable theoretical and experimental efforts have been dedicated to clarify the structure of water on surfaces and its role in mediating biological response to polymer materials (see e.g. references [3, 7–10]). However, so far no general consensus exists in this matter and the interaction of water with surfaces remains one of the most important research areas in materials science [11].

With the growing interest in bio-compatible, anti-fouling materials in the last few decades, the central question about the exact mechanisms governing protein adsorption attracted more interest and a large body of literature concerning this issue has been published (see e.g. the reviews [11–17] and references therein). As pointed out by Vogler [11] two main paradigms prevail, namely 1) to conceive protein adsorption as a process controlled by complex pair-wise interactions between the protein and the surface (see e.g. references [15, 18–20]), and 2) to understand protein adsorption as a process entirely controlled by the hydrophobic effect (for example references [11, 21–23] and references therein). In this latter approach water and its strong hydrogen bonding interactions are thought to be responsible for the adsorption process: a protein adsorbs when the displacement of water at the surface is energetically favorable. Indeed, water mediates virtually all material-biomolecule interactions via a rapidly formed water layer at the material surface when immersed into an aqueous solution. For example, before the proteins in blood reach an implant surface, a water layer is ad-

2

sorbed at the interface and it is the interaction with this water layer that determines whether a protein will adsorb to the surface or not. Several terms have been used to describe this surface-bound water: Vogler talks about "vicinal" water [24], Tanaka classifies hydrated water into "free", "intermediate" and "non-freezing" water [22], while many others simply employ the terms "interfacial" or "bound" water.

Depending on the surface properties, water hydrates surfaces to different degrees, which will affect protein adsorption. On hydrophobic surfaces, the water structure is easily disrupted because it is overall energetically more favorable to dehydrate the surface such that the protein can expose parts of its hydrophobic interior to the surface. On hydrophilic surfaces (such as e.g. self-assembled monolayers of poly(ethylene glycol) (PEG) or other non-fouling polymers [25, 26]) the interaction between water and the surface is so strong, that the protein cannot displace the water and will therefore not adsorb (or only after extended contact times) [11, 13, 22]. Such non-fouling materials are of interest in (bio)medical applications, as for example implants, to prevent undesirable protein adsorption and blood cell adhesion that could lead to coagulation or trigger an immune system response.

As outlined above, the role of water in mediating protein adsorption remains an unsolved issue. Approaching this issue using surfaces with novel, interesting properties, such as e.g. vertical chemical gradients, could add to the understanding of the phenomenon. Vertical chemical gradients represent an interesting and relatively new type of materials [27–29] with gradually changing chemistry normal to the surface. This vertical structure may affect the distribution and structure of water in sub-surface regions in a way that hydrophobic interactions are influenced. Furthermore, for gradient length scales of the order of the size of typical amphiphilic molecules, which is in the range of 1-10 nm, it is expected that the vertical structure affects the adsorption of these amphiphiles [28, 30].

Vertical chemical gradients thus present interesting surfaces to study the adsorption of proteins. Important requirements for the vertical chemical gradient structures include a controllable thickness in the nanometer range and a and a stable, covalently bound hydrophilic/hydrophobic structure. Plasma polymerization represents a convenient technique to produce such vertical chemical gradient structures: the incorporation of functional groups into the deposited films can be controlled by regulating the gas mixture and the cross-linking degree of the films can be adjusted by a precise control of the energy input into the plasma phase and at the surface [31–35].

Based on this, it was decided to develop vertical chemical gradients using plasma polymerization of HMDSO and to study the adsorption of proteins on these novel surfaces.

1.2 Scope and Outline of the thesis

The aim of this work was to develop vertical chemical gradient films with controllable thickness and wetting properties, and to investigate their influence on protein adsorption. Plasma polymerization was the method of choice for the deposition of the vertical chemical gradients. Thereby, hexamethyl-disiloxane (HMDSO) was used as a precursor due to the variety of wetting properties that can be obtained with this monomer depending on the applied plasma conditions.

As outlined above, control over thickness and wetting properties as well as film stability are fundamental requirements for the vertical chemical gradient structures. Therefore, in a first step, the plasma polymerization process of HMDSO was investigated in more detail, in order to establish a better control over the cross-linking degree and wetting properties of the resulting films. Additionally long-term aging of the deposited films after equilibration in air or water was studied.

In a further step, the degree of water penetration into two plasma polymer films deposited from HMDSO exhibiting different surface wettabilities was investigated. The interest thereby was to quantify the amount of water contained in the surface-near region of these films.

Suitable conditions to generate vertical chemical gradients were then chosen based on the results obtained in the earlier studies. Vertical gradients of different thicknesses were deposited using plasma polymerization of HMDSO and characterized by different techniques, namely XPS, AFM and contact angle measurements. In a final step, the adsorption of bovine serum albumin (BSA) on vertical chemical gradients was studied in order to test the hypothesis that the vertical sub-surface structure affects the adsorption of proteins.

This thesis is organized as follows:

Chapter 2 provides the theoretical background of this thesis. A brief introduction to plasma polymerization is given and important concepts concerning surface forces, adsorption and diffusion are discussed. First, an introduction to plasma processes and plasma polymerization is given. Then, intermolecular and surface forces are introduced, followed by some important aspects related to adsorption and basic models describing adsorption kinetics. Lastly, the concept of diffusion is introduced.

In Chapter 3 the influence of HMDSO fragmentation in the plasma gas phase and of energetic conditions at the surface on densification/cross-linking of the resulting plasma polymers was investigated. It was found that the degree of HMDSO fragmentation in the gas phase had a similar influence on densification than energetic particle interactions at the surface. Possible gas phase reaction pathways are presented. Furthermore, the aging of these films in air and water was explored by

a long term contact angle study and found to depend on energetic conditions applied in the plasma process.

In Chapter 4 the diffusion of water into a hydrophobic and a more hydrophilic plasma polymerized HMDSO film was studied using neutron reflectometry. The amount of water in the near-surface region of both films was quantified. It was shown that water not only penetrated into the more hydrophilic but also into the hydrophobic film. Additional infrared spectroscopy and ellipsometry measurements were performed to complement the obtained results.

Chapter 5 discusses the production of vertical chemical gradients by plasma polymerization of HMDSO. The obtained gradient films were characterized using X-ray photoelectron spectroscopy, atomic force microscopy and contact angle measurements. It was shown that the established plasma process control allowed tuning the thickness and surface free energy of the plasma polymerized vertical gradients.

Furthermore, the adsorption of BSA on these vertical chemical gradients was investigated using the Transmission Interfereometric Adsorption Sensor (TInAS) [36]. In comparison to plain plasma polymer films (without gradient), protein adsorption was reduced on the vertical chemical gradients. The exact mechanism behind this reduction remains unclear, but several hypotheses regarding its origin are presented showing the importance of water in the sub-surface.

Chapter 6 provides a summary of the major findings of this thesis. Additionally an outlook on how to test the hypotheses proposed in Chapter 5 is presented along with possible applications of vertical chemical gradients.

THEORETICAL BACKGROUND

2.1 An introduction to plasma processing

A substantial part of this thesis is devoted to plasma polymerization. An introduction to the theoretical principles of plasma processing and plasma polymerization, which have been investigated extensively in the past, is thus given in this section. A complete discussion of this topic is beyond the scope of this work. Therefore, only the fundamental concepts relevant for this thesis are introduced.

2.1.1 The plasma state

A plasma is a collection of different types of particles, viz. electrons, ions, neutrals (atoms and molecules in their ground or excited states) and radiation that exhibits electrical quasineutrality and shows collective behavior. Plasma was first described by Sir William Crookes in 1879, who was talking about "radiant matter"[37]. The term *plasma* was introduced by Irvin Langmuir in 1928, who suggested to "use the name *plasma* to describe this region containing balanced charges of ions

and electrons"[38]. The plasma is often referred to as the 4th state of matter, in addition to the solid, liquid and gaseous states. Phase transitions from solid to liquid to gas are induced by heating. When in the gaseous state, a further temperature increase leads to the decomposition of atoms into electrons and ions, thus reaching the plasma state. The great majority of visible matter in the universe is in the plasma state. A well-known example of a plasma is the sun with core temperatures exceeding 10^7 K. But also stars and most interstellar matter are in this state. Beside thermal plasma activation, the energy necessary to observe the plasma state can also be supplied electrically, electromagnetically, chemically or mechanically.

2.1.2 Properties of plasmas

Thermal and non-thermal plasmas

The above mentioned examples are all so-called *thermal plasmas* because the electrons are in thermodynamic equilibrium with the heavier particles. Thus, the electron temperature T_e, the ion temperature T_i and the neutral gas temperature T_n are equal and relatively high. In contrast, *non-thermal plasmas* are not in thermodynamic equilibrium, i.e. $T_e >> T_i \cong T_n$. Low pressure glow discharges used in many technical applications belong to this category and typically exhibit values of $k_B T_e = 1 - 10$ eV, where k_B is the Boltzmann constant, and electron densities $n_e = 10^8 - 10^{13}$ cm^{-3} [39]. While the electron temperature may attain temperatures of 10^4 K or higher, T_i and T_n remain close to room temperature as illustrated in Figure 2.1.

This difference is related to an inefficient heat and momentum transfer at low pressures due to the low collision frequencies. In addition, ions and neutrals lose a major part of their gained energy
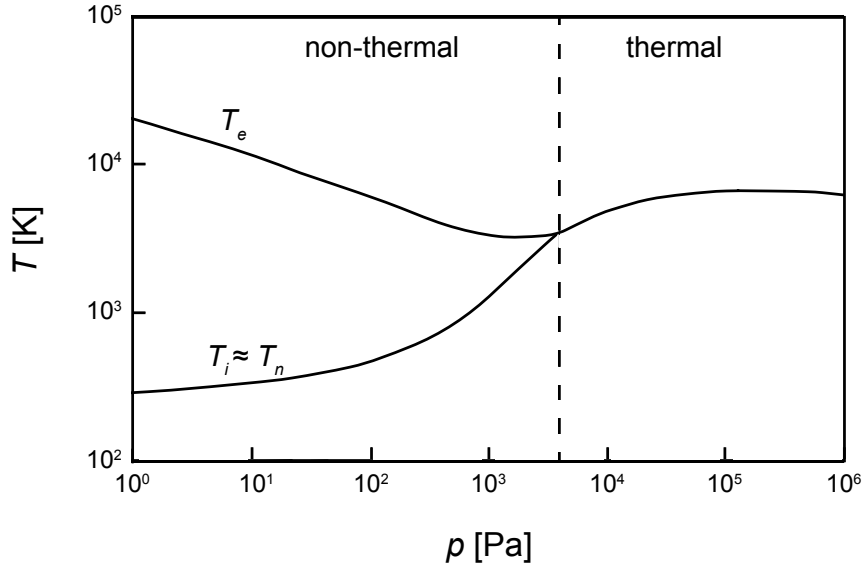
Figure 2.1: Dependence of electron, ion and neutral gas temperatures on pressure. Adapted from reference [40].

in collisions with other ions or neutrals, thus remaining "cold"[41].

The Debye length

The fundamental length scale in a plasma is the Debye length λ_{De}. It describes the distance, below which electrical quasineutrality is violated and is given by

$$\lambda_{De} = \sqrt{\frac{\epsilon_0 \, k_B T_e}{n_e \, e^2}}, \tag{2.1}$$

where ϵ_0 is the vacuum permittivity and e is the electron charge. At length scales smaller than λ_{De}, no plasma can exist because the condition of quasineutrality is not fulfilled. For typical values of the electron temperature and density in low pressure glow discharges, λ_{De} is of the order of several tenths of a millimeter.

Electron energy distribution function

Most excitation, ionization and dissociation processes in the plasma are due to collisions with electrons. The electron energy distribution function (*eedf*) is therefore an important plasma parameter. For electrons in either thermodynamic or kinetic equilibrium, and assuming that the effects of the electric field are negligible a Maxwell-Boltzmann energy distribution can be assumed [42]

$$f(E) = \sqrt{4/\pi} \, (k_B T_e)^{-3/2} \, E^{1/2} \, \exp(-E/k_B T_e) \tag{2.2}$$

with a mean electron energy of

$$E_m = \frac{3}{2} \, k_B T_e. \tag{2.3}$$

Thereby, the condition of thermodynamic equilibrium is almost never satisfied, while the condition of kinetic equilibrium is less severe. In low pressure glow discharges the electron energy distribution is often better described by a Druyvesteyn distribution

$$f(E) = \sqrt{1/\pi} \, (k_B T_e)^{-3/2} \, E^{1/2} \, \exp\left[-(0.494 \, E/k_B T_e)^2\right], \tag{2.4}$$

10

introduced by Druyvesteyn and Penning for electrons in a weak electric field undergoing (hard sphere-like) elastic collisions with neutral gas atoms with an energy-independent collision frequency [43]. A comparison of the Maxwell and the Druyvesteyn electron distribution functions for several mean electron energies is given in Figure 2.2.
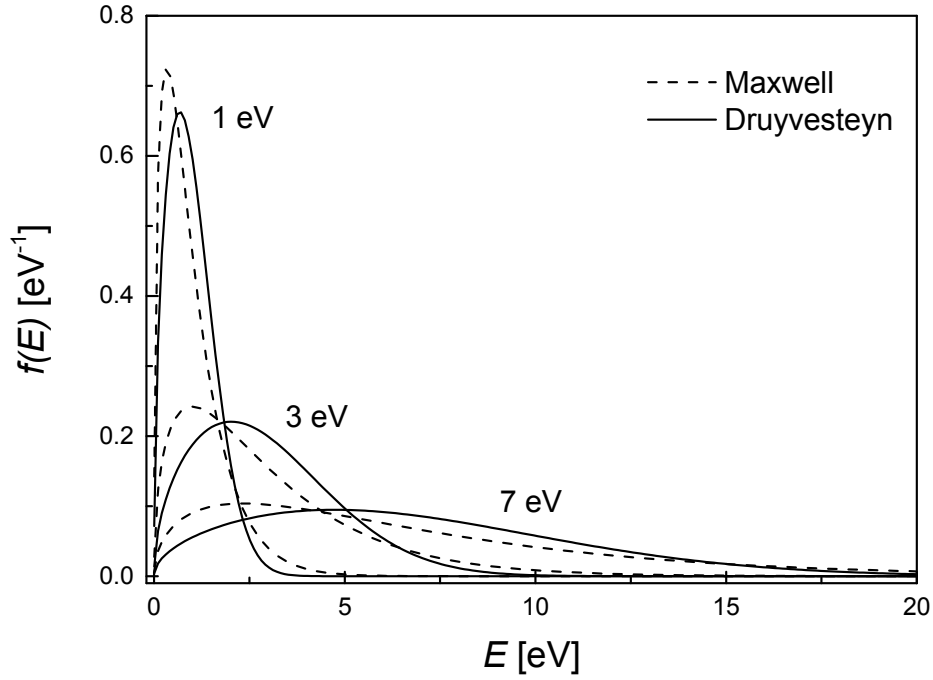
Figure 2.2: Electron energy distribution functions according to Maxwell and Druyvesteyn. The mean electron energies E_m for the three examples are indicated in the graph.

Due to the smaller amount of collisions in a low pressure glow discharge, the mean electron energies are shifted to slightly higher energies for the Druyvesteyn distribution. The threshold energies needed for excitation, ionization and dissociation of atoms or molecules are generally higher than typical E_m values. However, as is evident from Figure 2.2 for both electron energy distributions, a significant number of electrons possess energies higher than the mean electron energy and can thus initiate the above mentioned reactions.

Collisions

Ionization and excitation reactions necessary to sustain a plasma occur via charge, energy and momentum transfer in elastic or inelastic collisions. Elastic collisions are characterized by the conservation of the total kinetic energy, while in inelastic collisions kinetic energy is not conserved and part of it is transferred to internal energy causing excitation, ionization or dissociation. In plasmas exhibiting rather low ionization degrees (as is the case for low pressure capacitively coupled plasmas) collisions between electrons and neutrals are the dominant collision process [39, 40]. However, ion-neutral reactions can be important in processing plasmas as well. Table 2.1 summarizes some important collision reactions involving electrons, ions and neutrals.

Table 2.1: Collision reactions involving electrons, ions and neutrals

	Reaction
Ionization	$e^- + A \rightarrow A^+ + 2e^-$
	$A^+ + B \rightarrow A^+ + B^+ + e^-$
Excitation	$e^- + A \rightarrow A^* + e^-$
	$A^+ + B \rightarrow A^+ + B^*$
Penning ionization	$e^- + A^* \rightarrow A^+ + 2e^-$
Dissociation	$e^- + AB \rightarrow e^- + A + B$
	$A^+ + BC \rightarrow A^+ + B + C$
Dissociative ionization	$e^- + AB \rightarrow 2e^- + A^+ + B$
Dissociative attachment	$e^- + AB \rightarrow A^- + B$
Recombination	$e^- + A^+ + B \rightarrow A + B$
	$A^+ + e^- + B \rightarrow A + B$
Charge exchange	$A^+ + B \rightarrow A + B^+$
Chemical reaction	$A + BC \rightarrow C + AB$

The collision cross-section σ is the probability for collisions to take place and generally depends

on the velocity of the collision partners. In a first approximation, collisions between electrons and neutrals or ions and neutrals can be treated as collisions between hard spheres of radii r_1 and r_2. In this case, $\sigma = \pi(r_1 + r_2)^2$ independent of the respective velocities. The mean free path between collisions is given by $\lambda_{mfp} = \frac{1}{n_g\sigma}$, where n_g is the number density of (immobile) collision partners. The collision cross section between neutrals in air is of the order of 10^{-19} m^2, while the mean free path in air is of the order of a few tenths of nanometers. In low pressure technical plasmas λ_{mfp} ranges from about a millimeter to several centimeters [40]. In addition, for plasmas used in technical applications also interactions between heavy particles and the electrodes such as etching or deposition need to be considered.

2.1.3 Plasma generation

Plasmas are most commonly generated and sustained by applying an electric field to a neutral gas, thereby provoking its electrical breakdown. For low pressure plasmas, alternating electric fields are frequently applied. In order to avoid interference with telecommunication applications, the standard frequencies used in research and industry are 13.56 MHz in the radio frequency (RF) and 2.45 GHz in the microwave (MW) range, respectively [44]. In this work only RF discharges are applied and shall be discussed in more detail here.

Radio frequency driven discharges

In RF discharges the energy of the supplied electric or electromagnetic field will only be absorbed if the frequency of the field ω is lower than the electron plasma frequency ω_e given by

$$\omega_e = \sqrt{\frac{e^2\, n_e}{\epsilon_0\, m_e}}, \tag{2.5}$$

where e and m_e are the electron charge and mass, respectively [40]. The power coupling into the plasma can either be capacitive or inductive. In inductively coupled plasmas (ICPs) the RF power is applied to an inductive coil. The so developed magnetic field induces an electric field accelerating the electrons. Typically, ICP achieves high electron densities while the ion energy remains low [45]. In capacitively coupled plasmas (CCPs) the electrons are directly accelerated by responding to the applied RF field. Also in CCP, the ions nearly absorb no energy from the field due to their much larger mass and consequently lower plasma frequency ω_i, which is lower than the applied frequency ω. For typical conditions used in this work ($n_e \approx 10^9$ cm^{-3}), the electron frequency ω_e is in the order of a few GHz while the ion frequency for an argon ion ω_{Ar+} is lower than one MHz. The electrons thus activate and sustain the plasma. The associated electron heating mechanism can either be stochastic or ohmic. Ohmic heating is due to momentum transfer upon electron-neutral collisions and dominates at elevated pressures due to more frequent collisions. Stochastic heating is a mechanism, in which the electrons gain energy by reflection at the oscillating sheath edge. It is the predominant heating mechanism in capacitively coupled RF discharges at low pressures, where the sheaths oscillate strongly. In an intermediate pressure range, both mechanisms are significant and a mixed heating form is established [39]. CCPs are commonly used for materials processing and the

mutual dependence of plasma parameters is understood to some extent, such that the plasma process can be characterized by a few known parameters only [39].

Sheath formation and bias voltage

In capacitively coupled plasmas, the electrodes are typically arranged in a plane parallel configuration, as schematically shown in Figure 2.3. The larger mobility of the electrons compared to the mobility of the ions (due to $m_e << m_i$) leads to the formation of narrow zones at the electrodes, in which charge quasineutrality is violated, i.e. $n_i >> n_e$, the so called plasma *sheaths*. Because the electrons respond much faster to the applied RF field than ions, more electrons are lost to the walls leading to a net positive charging of the bulk plasma. The resulting electric field is directed towards the electrode and accelerates ions entering the plasma sheaths, while electrons are repelled and contribute to the strong excitation at the plasma bulk/sheath boundary. The plasma potential V_p is thus always positive with respect to the walls and its magnitude is at least in the order of a few times the mean electron temperature. The lack of electrons in the sheaths leads to the characteristic dark space close to the electrodes due to the low number of excitations [46]. The sheath width is typically of the order of a few Debye lengths, λ_{De}, but can extend to several millimeters in front of the RF electrode due to large potential differences. In order to leave the bulk plasma, ions need to acquire a minimum velocity

$$v_B = \sqrt{\frac{k_B \, T_e}{m_i}}.$$
(2.6)

This condition is known as the Bohm criterion and v_B is the so-called Bohm velocity. To reach this velocity, ions must be accelerated by a small electric field (Bohm potential $\approx k_B T_e / 2$) over a region

15

known as the *presheath*, which extends between the quasineutral bulk plasma and the non-neutral sheath and is typically of the order of several ion mean free path lengths (which is generally larger than the Debye length) [39, 40].
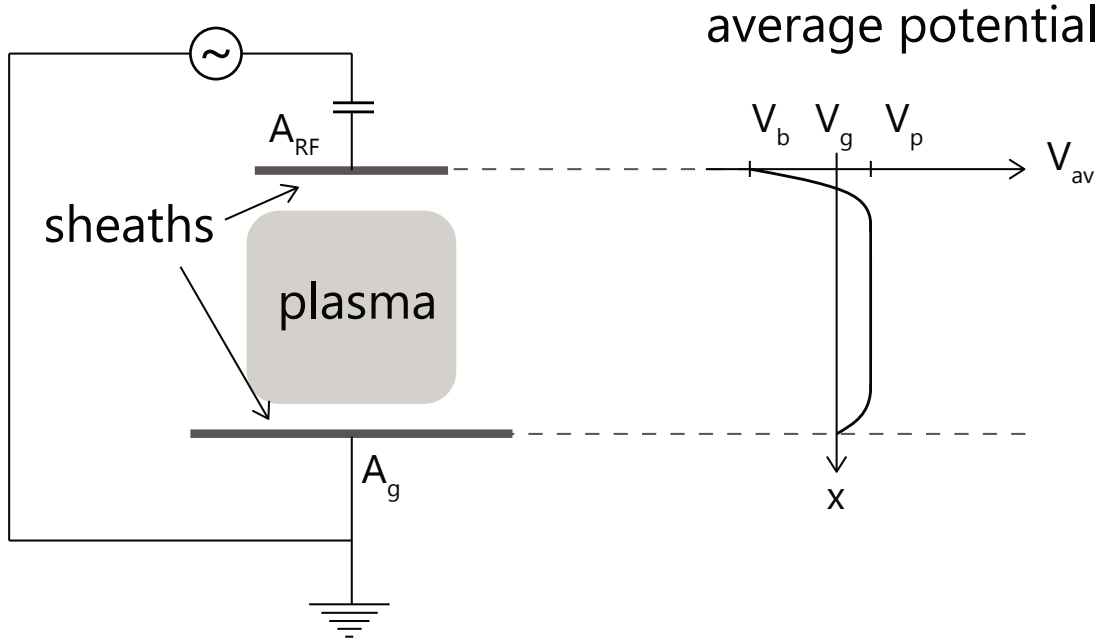

Figure 2.3: Simplified scheme of a typical asymmetric electrode configuration in a capacitively coupled plasma. The time-averaged potential across the grounded and powered electrodes having areas of A_g and A_{RF}, respectively, where $A_{RF} < A_g$, is additionally shown. Inspired by the scheme as given in reference [47].

In an asymmetric electrode configuration, as the one shown in Figure 2.3, where the area of the powered electrode A_{RF} is smaller than the area of the grounded electrode A_g an additional negative bias voltage V_b builds up at the driven electrode that strongly depends on the ratio A_{RF}/A_g [39]. During a complete RF cycle a negative charge accumulates at the driven electrode, as in the positive half cycle of the applied RF voltage more electrons are lost to the walls than ions in the negative half cycle (as long as steady-state is reached). The current density at the powered electrode is thus larger, leading to a larger potential difference between the plasma and the electrode [45]. In the case of a

symmetric electrode configuration, i.e. $A_{RF} = A_g$, the same potential drop is established at each electrode such that on average $V_b = 0$. The potential at the powered electrode $V_{RF}(t)$ is thus given by

$$V_{RF}(t) = V_0 \, sin(\omega t) + V_b, \tag{2.7}$$

where V_0 is the amplitude of the applied voltage and $\omega = 2\pi f$ with $f = 13.56$ MHz. The potential at the grounded electrode is zero. The average plasma potential V_p and sheath potential V_{sh} over which positive ions are accelerated towards the electrode are given by

$$V_{sh} = V_p = 0.39 \, V_0 \tag{2.8}$$

in the symmetric case [39] and by

$$V_{sh} = 0.39 \, V_0 - 0.73 \, V_b \tag{2.9}$$

$$V_p = 0.39 \, V_0 + 0.23 \, V_b \tag{2.10}$$

in the asymmetric case [48]. The bias voltage induces enhanced ion bombardment at the RF electrode with maximum kinetic energies of about hundred electronvolts, which is important for e.g. reactive ion etching. Furthermore, ion energies in the range of a few tens of electronvolts can be used to support the densification and cross-linking of plasma polymer films.

2.1.4 Plasma polymerization

The term plasma polymerization relates to the formation of polymeric materials under the action of plasma [41] and was discovered in the second half of the 19th century. From the 1960s on, plasma polymerization started to be investigated in more detail [49–51] and, over the years, was established as a generally accepted method of producing new materials. The new domain rapidly gained attention and it was thus suggested by Yasuda to extend the definition of plasma polymerization to a wider field, including not only organic polymeric materials, but also metallic or inorganic elements [41]. Plasma polymers are used in rather diverse technical applications and are most often deposited as thin films (50 nm - 1 μm). The possibilities to tune film properties by controlling plasma parameters and to use precursors, which are not considered monomers for conventional polymerization, along with the fact that the deposited thin films adhere well to a variety of substrates makes plasma polymerization a versatile method for thin film deposition. Moreover, multilayer films or gradient films can easily be formed using this method [52, 53].

Other than conventional polymers, films deposited via plasma polymerization do not possess regular repeating units. Plasma polymers are highly branched, randomly terminated and show a high degree of cross-linking. This random amorphous structure is obtained because all active species created in the plasma (atoms, ions, molecules, radicals and radiation) contribute to film growth. Film growth is dominated by radicals that are formed in the gas phase by collisions with energetic electrons. At the surface of the deposited film, positive ions that are accelerated by the bias voltage across the plasma sheath can cause further dissociation of the adsorbed precursor, thus forming radicals at the film surface [54], or induce cross-linking or etching. Therefore, even if the ionization degree in low pressure discharges is low (typically ranging from 10^{-6} up to 10^{-4}), ion bombardment

plays an important role in determining deposition rates and chemical composition of the deposited films. Hence, both, gas phase and surface processes, determine plasma polymerization processes.

Gas phase processes

The primary activation of a precursor in the gas phase by electron impact produces reactive intermediates (radicals, excited species, ions, ...), which then yield macromolecule formation. Due to the high complexity of the system and the lack of knowledge of important parameters (rate coefficients, collision cross sections, ...), the microscopic description of kinetics in plasma chemistry remains an unsolved problem, even if advances in modeling provided some helpful insight in the complex reaction mechanisms involved, see e.g. references [55, 56]. However, these results are often not practically applicable. Therefore, a macroscopic description, which connects the chemical conversions in the active plasma zone to the applied process parameters, is often used. The origin of macroscopic kinetics goes back to the empirical findings of Warburg and co-workers and also of Becker [57, 58], who found that the chemical decomposition of gases in the plasma is determined by the power invested per plasma volume times the residence time of the species in the plasma. The concept was then further developed and generalized [59–61]. To describe plasma polymerization processes a dimensionless reaction parameter S can be defined as

$$S = \frac{W \, \tau_{plasma} \, T}{p \, V_{plasma} \, T_0},$$

(2.11)

where τ_{plasma} is the residence time in the plasma, V_{plasma} is the volume of the plasma zone, p is the pressure, T is the temperature and T_0 the reference temperature (273 K). With the aid of the ideal gas law it can be seen that this parameter indeed describes the energy invested per particle in the plasma

zone. In addition, we have that

$$\frac{\tau_{plasma}}{V_{plasma}} = \frac{1}{F} \frac{p \, T_0}{p_0 \, T} \tag{2.12}$$

with the standard pressure $p_0 = 101325$ Pa and the gas flow rate F. Combining equations (2.11) and (2.12) an energy density ϵ_{plasma} can be defined as the energy delivered per plasma volume by the external parameters power input and gas flow:

$$\epsilon_{plasma} = \left. \frac{W}{F} \right|_{plasma}. \tag{2.13}$$

This specific energy is pressure independent and delivers the energy per molecule in the gas phase that is necessary for dissociation processes [62]. A similar relation was empirically found by Yasuda, who introduced the parameter W/FM where W is the power input, F is the gas flow rate and M is the molecular mass of the monomer [63]. Depending on reactor geometry (e.g. in an asymmetric reactor), varying the power input or the pressure leads to a change of the plasma volume, which also affects ϵ_{plasma}. Moreover, part of the gas flow might bypass the active plasma zone and thus not participate in the deposition process. Thus a factor r_{dep} can be introduced to consider the reactor geometry,

$$r_{dep} = \frac{W_{abs} \, d_{act} \, V_{gas}}{W \, d_{gas} \, V_{dis}} \tag{2.14}$$

such that

$$\epsilon_{plasma} = \left. \frac{W}{F} \right|_{plasma} = \frac{W}{F} r_{dep}, \tag{2.15}$$

where d_{act} is the width of the active plasma zone, d_{gas} is the distance the gas travels through the reactor, V_{gas} is the volume occupied by the gas, V_{dis} is the discharge volume and the factor W_{abs}/W considers the actual power absorption in the plasma (with respect to nominal power) [39, 64]. The geometrical factor r_{dep} helps in finding the real energy delivered to the plasma volume and is useful for the comparison of different reactor set-ups.

The mass deposition rate R_m resulting from the plasma chemical reactions was extensively studied by Yasuda and co-workers [63, 65]. They identified two main deposition regimes: 1) an energy-deficient regime at low energy densities, where the conversion ratio R_m/F increases nearly linearly with W/F, and 2) a monomer-deficient regime, where R_m/F is independent of the energy density. Park and co-workers found that the well-known Arrhenius equation (2.16) describing the reaction rate of a chemical reaction requiring activation (such as e.g. between colliding particles) can be adapted to reactions in plasma polymerization processes by replacing the thermal energy RT by the specific energy density W/F:

$$k = \nu \, \exp\left(-\frac{E_a}{RT}\right) \tag{2.16}$$

$$\frac{R_m}{F} = C \, \exp\left(-\frac{E_a}{W/F}\right) \tag{2.17}$$

with the reaction rate k, the collision frequency ν, the activation energy E_a and the prefactor C, which is a process and reactor dependent parameter related to the decomposition rate of the monomer. The activation energy E_a is usually obtained by a linear fit of $\ln(R_m/F)$ against $(W/F)^{-1}$. The so obtained quasi-Arrhenius relation (equation (2.17)) can be applied as long as the film-forming species are produced via a predominant chemical reaction pathway [35, 59, 64].
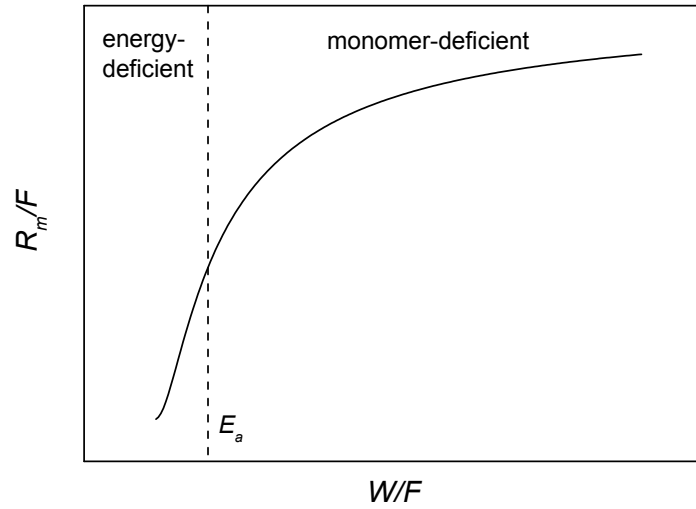
Figure 2.4: Mass deposition rate as a function of energy input for plasma polymerization processes with an activation barrier.

Relation (2.17) is illustrated in Figure 2.4. A transition regime around the activation energy now separates the energy-deficient form the monomer-deficient regime. In practice, several chemical reaction pathways with different activation energies might exist (see also Chapter 3).

When a non-polymerizable carrier or reactive gas is added to the process it also consumes part of the energy. The fraction of energy consumed can be taken into account by another correction factor r_{gas}, such that

$$F = F_m + r_{gas} \, F_c \tag{2.18}$$

with the monomer flow rate F_m and the flow rate of the carrier (or reactive) gas F_c [66]. This gas correction factor is related to the reactivity of the added gas with respect to the formation of film forming species.

Film growth processes are also influenced by reactions at the surface. The ion flux incident on

the substrate film can support film growth (by the creation of nucleation sites) or even reverse the incorporation of film-forming species (by ion assisted etching) reducing the mass deposition rate at high energy inputs. Nevertheless, for a proper selection of experimental conditions, the macroscopic approach can give valuable insights into plasma polymerization processes, while a microscopic approach involving the actual *eedf* and rate constants might still be too complex [62].

Surface processes

For surface processes, the energy density during film growth given by the ratio of the energy flux to the surface and the deposition rate has to be considered:

$$\epsilon_{surf} = \frac{\Gamma_i \, E_{mean}}{R}, \tag{2.19}$$

where Γ_i is the ion flux incident on the surface, E_{mean} is the mean ion energy and R is the deposition rate. This energy density represents the energy dissipated in the growing film volume and can be transformed into energy per deposited atom. The mean ion energy depends on the sheath voltage V_{sh} (equation (2.9)) according to

$$E_{mean} = e \, V_{sh} \, \cos \varphi, \tag{2.20}$$

where the factor $\cos \varphi$ is related to collisions in the plasma sheath and depends on the sheath length s, the type of collisions and the ion mean free path λ_i according to $\cos \varphi = (1 + c \, s/\lambda_i)^{-1}$ where $c = 0.5$ for elastic collisions and $0.5 < c < 1$ for charge exchange [67]. The ion flux incident on the

substrate can be estimated by

$$\Gamma_i = n_0 \, v_B \, \cos\theta \qquad (2.21)$$

with the bulk plasma density n_0 (equal to n_e for electropositive plasmas) and the Bohm velocity v_B given by equation (2.6) [39]. The factor $\cos\theta$ considers the reduction of the number of ions fulfilling the Bohm criterion due to collisions in the plasma bulk and depends on the plasma length l and λ_i via $\cos\theta = 0.86\,(3 + (l/2\lambda_i))^{-0.5}$. The ion flux is also related to gas phase processes: a lower power density in the gas phase reduces fragmentation and thereby the electron (and bulk plasma) density. A reduction of the energy input into the gas phase can thus lead to a lower energy flux towards the surface, even if the mean ion energies are comparable. However, a change in electron density affects the deposition rate in a similar way as the energy flux such that these effects almost cancel out. The often observed good agreement between film properties and bias voltage is thus not surprising. At the surface the reactivity of film-forming species (sticking probability) determines whether and how they are adsorbed. Physisorption requires only low energies (< 1 eV per adsorbed atom) while the energy necessary to create a covalent bond is significantly higher. This energy is provided by the flux of energetic ions incident on the surface. The energy density at the surface thus enables the creation of nucleation sites and cross-linking of the film, but also ion-assisted etching [62].

Regarding the densification of plasma polymer films, it has been shown that this mechanism is rather momentum than energy driven, i.e. collision cascades within the growing film are important [68–70]. The momentum transfer

$$\pi_{surface} = \sqrt{2 \, m_i \, E_{mean}} \, \frac{\Gamma_i}{R} \qquad (2.22)$$

with the ion mass m_i thus governs densification during plasma polymer film growth above a certain threshold energy (typically of the order of bond energies).

Plasma polymerization can thus be characterized based on the energy density in the gas phase and at the surface [35].

2.2 Surface forces

The interactions at surfaces most relevant for this work will briefly be outlined below. These include electrostatic interactions, van der Waals interactions, surface and interfacial energy as well as hydrophobic and hydration forces. The content of this section is mainly based on the textbook by Israelachvili [71].

2.2.1 Electrostatic interactions

The free energy for the Coulomb interaction between two charges Q_1 and Q_2 separated by a distance r is given by

$$w_{Clb}(r) = \frac{Q_1 Q_2}{4\pi\epsilon_0\epsilon r} = \frac{z_1 z_2 e^2}{4\pi\epsilon_0\epsilon r}, \tag{2.23}$$

where ϵ_0 is the vacuum permittivity, ϵ is the relative permittivity of the medium between Q_1 and Q_2, z_1 and z_2 are the valencies and e is the elementary charge. Due to its dependence on $1/r$, the Coulomb interaction is a long-range interaction. To obtain the interaction between larger bodies consisting of a large number of molecules the pair potentials between the molecules of each body

should be summed, assuming that the pair potentials are additive [71]. It can be shown that the interaction energy between a probing charge $Q = e$ and a uniformly charged surface of surface charge density σ and radius R is given by

$$w_{c-s}(r) = \frac{\sigma e}{2\pi\epsilon_0\epsilon} \left[\sqrt{D^2 + R^2} - D \right].$$ (2.24)

The corresponding force is obtained by derivation of the interaction energy:

$$F_{c-s}(D) = \frac{dw_{c-s}(r)}{dD} = \frac{\sigma e}{2\pi\epsilon_0\epsilon} \left[\frac{D}{\sqrt{D^2 + R^2}} - 1 \right] \xrightarrow{R \longrightarrow \infty} -\frac{\sigma e}{2\pi\epsilon_0\epsilon}.$$ (2.25)

The force depends only slightly on distance and in the limiting case of an infinitely extended surface is shown to be independent of distance. Thus, a uniformly charged surface might easily dominate the interactions between charges.

2.2.2 Van der Waals interactions

The most prominent contributions to van der Waals interactions are rotating dipole-dipole (Keesom), dipole-induced dipole (Debye) and dispersion (London-van der Waals) interactions. The Keesom energy describes an interaction between two permanent dipoles that depends on their relative orientation. A permanent charge or dipole induces dipoles in non-polar (but polarizable) molecules, which then interact through the Debye energy. The London-van der Waals dispersion interactions are quantum mechanical in nature. These interactions act between all molecules making them universal in nature and thus the most important contribution to van der Waals interactions. The pair potentials of all of these interactions show (approximately) a distance dependence of $1/r^6$ and can in a simplified

way be described by

$$w_{vdW}(r) = -\frac{C}{r^6},$$

(2.26)

where C is the interaction constant. For the interaction between a molecule at a distance D from a surface (again assuming additivity) it can be shown that

$$w_{m-s}(D) = -\frac{\pi C\rho}{6D^3},$$

(2.27)

where ρ is the number density of molecules in the solid constituting the surface. Often, the part of the interaction, which is related to the properties of the interacting materials, is combined in the Hamaker constant $A = \pi^2 C\rho_1\rho_2$ [72]. For a sphere of radius R interacting with a solid surface the potential is found to be

$$w_{sph-s}(D) = -\frac{AR}{6D} \quad \text{for} \quad D << R \quad \text{and} \quad w_{sph-s}(D) = -\frac{2\pi C\rho(4\pi R^3\rho/3)}{12D^3} \quad \text{for} \quad D >> R,$$

(2.28)

where for $D << R$ the interaction energy is proportional to the radius of the sphere and decays much slower than the pair potential, while for $D >> R$, $(4\pi R^3\rho/3)$ is number of molecules in the sphere and a relation similar to the one for a molecule interacting with a surface is obtained. The van der Waals interaction per unit area between two planar surfaces consisting of the same material is given by

$$w_{s-s}(D) = -\frac{\pi C\rho^2}{12D^2} = -\frac{A}{12\pi D^2}.$$

(2.29)

The relations derived above are valid in vacuum. The presence of a medium between the interacting objects may affect the strength as well as the sign of the van der Waals interaction. This rather complex multi-body problem, where the pair-potentials are not additive, can be treated in the framework of continuum theory, in which the forces between large bodies are derived from bulk properties such as dielectric constants and refractive indices. This approach only changes the way, in which the Hamaker constant is calculated, such that the relations derived above remain valid also for objects interacting through a medium.

2.2.3 Surface and interfacial energy

The van der Waals interaction between two planar surfaces (equation (2.29)) is derived by summation of the pair potentials between all atoms of one surface with all the atoms of the other surface. Thereby the interactions of the atoms within the same surface have been neglected. Considering these interactions, an additional term $W' = -W_c + A/12\pi D_0^2$, where W_c is the cohesive energy of atoms with its nearest neighbors situated at $D = D_0$, appears. The second, always positive, term in W' stems from the unsaturated bonds at the surface. In order to minimize this energetically unfavorable contribution, a free liquid always tries to minimize its surface area. The total energy between two planar surfaces at a distance D is thus given by (neglecting the cohesive energy W_c)

$$W(D) = \frac{A}{12\pi D_0^2} \left(1 - \frac{D_0^2}{D^2} \right) \quad \text{per unit area.} \tag{2.30}$$

When the two surfaces are in contact ($D = D_0$) the interaction energy is zero, while when the surfaces are infinitely far apart ($D \longrightarrow \infty$), $W = \frac{A}{12\pi D_0^2} = 2\gamma$ with the surface energy γ, which is the change in energy when the surface area is increased by unit area. The energy W at ($D \longrightarrow \infty$) is

also called the adhesion energy or work of adhesion. The surface energy γ is thus half the adhesion

energy, i.e. half the energy needed to separate two surfaces from contact to infinity.

The interfacial energy or interfacial tension γ_{12} between two immiscible solvents (or a solvent

and a solid) is free energy cost to increase their "interfacial" area by unit area. This expansion process

consists of the creation of unit areas of media 1 and 2 that are subsequently brought into contact. The

total change in free energy is therefore

$$\gamma_{12} = \frac{1}{2}W_{11} + \frac{1}{2}W_{22} - W_{12} = \gamma_1 + \gamma_2 - W_{12}, \tag{2.31}$$

where W_{11} and W_{22} are the adhesion energies for the respective media, whereas W_{12} is the adhesion

energy between the two media. For a solid-liquid interface this is generally expressed as $\gamma_{SL} =$

$\gamma_s + \gamma_L - W_{SL}$.

The surface and interfacial energies determine how a droplet deforms, when it adheres to a

surface. The equilibrium contact angle θ_0 of a liquid droplet on a solid surface is given by Young's

equation

$$\cos\theta_0 = \frac{\gamma_{SV} - \gamma_{SL}}{\gamma_{LV}}, \tag{2.32}$$

where γ_{SV}, γ_{SL} and γ_{LV} are the solid-vapor, solid-liquid and liquid-vapor interfacial tensions, re-

spectively.

The surface free energy of a solid γ_{SV} can be determined by measuring the contact angle of

various liquids of known surface tension. In an often applied approach by Owens, Wendt, Rabel and

Kaelble (OWRK method) [73–75] the solid-vapor and liquid-vapor interfacial tensions are divided

into a polar and a non-polar, dispersive part: $\gamma_{SV} = \gamma_{SV}^D + \gamma_{SV}^P$ and $\gamma_{LV} = \gamma_{LV}^D + \gamma_{LV}^P$. In addition, it is assumed that the adhesion energy between the solid and the liquid is given by the geometric mean of the disperse an polar parts such that

$$\gamma_{SL} = \gamma_{SV} + \gamma_{LV} - 2\left(\sqrt{\gamma_{SV}^D\gamma_{LV}^D} + \sqrt{\gamma_{SV}^P\gamma_{LV}^P}\right). \tag{2.33}$$

Combined with Young's equation (2.32), and using several liquids of known polar and disperse parts for measuring the contact angle, the surface free energy of the solid can be obtained.

2.2.4 Hydrophobic interactions

The strong tendency of water molecules to form hydrogen bonds amongst them influences the interaction of water with other molecules. Molecules or surfaces that strongly interact with water are called hydrophilic, while molecules or surfaces that show a weak interaction with water are called hydrophobic. When in contact with a non-polar (hydrophobic) molecule, water molecules maximize the number of hydrogen-bonds they can form by structuring around the hydrophobic molecule to minimize the contact area. The reorientation of the water molecules around the hydrophobic molecule is entropically unfavorable, which explains the poor solubility of e.g. hydrocarbons. This low water solubility of non-polar molecules is often called the hydrophobic effect. Hydrophobic interactions describe the strong attraction (often stronger than in free space) between hydrophobic molecules or surfaces in water. This hydrophobic attraction is associated with the entropy penalty due to the rearrangement of water molecules in the overlapping solvation zones of molecules or surfaces approaching each other. Hydration forces are not additive and a rigorous theoretical framework does not exist. Nevertheless, because they play a central role in many surface and biological phenomena

such as micelle formation or the conformation of proteins (in solution and adsorbed on a surface), increasing effort has been put into their understanding.

2.3 Adsorption at the solid-liquid interface

One major part during this project focused on protein adsorption at solid-liquid interfaces of different chemical structure and the resulting adsorption kinetics. Therefore, some relevant concepts of adsorption theory are presented in this section and several kinetic models are discussed in subsection 2.3.3. The contents of this section are inspired by the textbook of Atkins [76].

Adsorption is defined as „an increase in the concentration of a dissolved substance at the interface of a condensed and a liquid phase due to the operation of surface forces" according to the IUPAC Compendium of Analytical Nomenclature [77]. The adsorbed substance is called the adsorbate, while the interface it adsorbs to is termed adsorbent or substrate. An important quantity is the surface coverage, θ_s, which is given by the ratio of the number of occupied to the number of total adsorption sites present on the adsorbent. The inverse process, i.e. molecules leaving the surface, is called desorption.

2.3.1 Physisorption and Chemisorption

Physisorption relies on van der Waals interactions or weak dipole-dipole or electrostatic interactions between adsorbates and the substrate and is completely non-specific. The binding energies involved are of the order of a few tens of kJ/mol or about 10-100 meV/molecule. Due to the low change in enthalpy upon adsorption, molecular structure and electronic characteristics of the adsorbing molecules

are generally preserved (or altered only slightly). Physisorption of molecules can be a preliminary step of chemisorption.

Chemisorption occurs when the adsorbate forms a chemical bond (strong ionic or covalent bond) with the adsorbent. It is thus a process with a high chemical specificity. The binding energies for chemisorption are about one order of magnitude higher than for physisorption, i.e. a few hundreds of kJ/mol or about 1-10 eV/molecule. In comparison, chemical bonds usually exhibit binding energies of 5-10 eV. For spontaneous processes such as adsorption the change in free energy is negative, $\Delta G = \Delta H - T\Delta S < 0$. Upon adsorption the adsorbed molecule looses freedom of movement, the entropy change, ΔS, is thus usually negative. Therefore, the change in enthalpy, ΔH, must be negative in order to have $\Delta G < 0$, i.e. chemisorption is an exothermic process. Note that there are also a few special cases (e.g. the dissociative adsorption of H_2 on glass), where $\Delta S > 0$ and thus $\Delta G < 0$ despite the endothermic ($\Delta H > 0$) nature of the process.

2.3.2 Adsorption isotherms

Adsorption and desorption are competitive processes. At equilibrium, the adsorbed phase chemical potential μ_{ads} equals the bulk phase chemical potential μ_{bulk}:

$$\mu_{ads}(c, T, \theta_s) = \mu_{bulk}(c, T) \tag{2.34}$$

with the concentration c, the temperature T and the surface coverage θ_s, which needs to be considered, as ΔH_{ads} usually depends on the amount of molecules already present at the surface. Thus, a relationship between θ_s, c and T exists. Usually, adsorption isotherms (i.e. the variation of surface

coverage with concentration at constant temperature) are experimentally determined and described using on of the following models:

The Langmuir isotherm

A relatively simple and often applied isotherm is the Langmuir isotherm [78]. It is based on the following assumptions:

- Adsorption does not proceed beyond a monolayer.

- All adsorption sites on the surface are equal and the surface is uniform.

- The adsorption ability of a molecule at a given site is independent of the occupation of neighboring sites, i.e. there are no interactions between adsorbed molecules.

A dynamic equilibrium between dissolved molecules A and available surface sites B of the form

$$A(dissolved) + B(surface) \rightleftharpoons AB(surface) \tag{2.35}$$
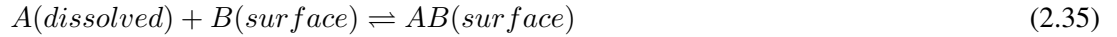
is established with rate constants for adsorption, k_{ads}, and desorption, k_{des}. The rate of change of surface coverage due to adsorption is proportional to concentration c and the number of available surface sites

$$\frac{\mathrm{d}\theta_s}{\mathrm{d}t} = k_{ads}c(1 - \theta_s), \tag{2.36}$$

while the change in surface coverage due to desorption depends on the number of adsorbed molecules:

$$\frac{\mathrm{d}\theta_s}{\mathrm{d}t} = k_{des}\theta_s. \tag{2.37}$$

At equilibrium, both rates must be equal and thus the Langmuir isotherm is obtained:

$$\theta_{s,eq} = \frac{Kc_{eq}}{1 + Kc_{eq}}, \tag{2.38}$$

where $K = k_{ads}/k_{des}$ and c_{eq} is the equilibrium concentration.

The BET isotherm

Often, the assumptions made for the Langmuir isotherm are not fulfilled. For example, an adsorbed layer may serve as a substrate for the adsorption of further layers of molecules [79]. Such multilayer adsorption processes are better described by the BET isotherm derived by Brunauer, Emmet and Teller [80], which is often represented as total adsorbed volume V relative to the volume adsorbed in a monolayer V_{mono}:

$$\frac{V}{V_{mono}} = \frac{Cz}{(1-z)[1-(1-C)z]} \tag{2.39}$$

with $z = c/c_{sat}$, where c_{sat} is the solubility of the adsorbate and C is a constant.

The two isotherms presented above are amongst the most widely applied isotherms. However, as the BET isotherm itself also relies on assumptions that are not generally fulfilled, several other empirical isotherms are often used to describe experimental results [81, 82].

2.3.3 Adsorption kinetics

In this subsection several kinetic models describing the adsorption of molecules from solution to a solid surface are discussed. This can be a rather complex process and its kinetics depend on many different factors. Nevertheless, several models, which successfully describe these kinetics, have been derived and some of the most often discussed models are outlined below.

The Lagergren equation

In 1898 Lagergren suggested a rate equation to describe the adsorption of dissolved particles to a solid substrate [83]:

$$\frac{\mathrm{d}q}{\mathrm{d}t} = k_1(q_e - q), \tag{2.40}$$

where q is the adsorption density (mass adsorbate per mass adsorbent) and q_e its value at equilibrium and k_1 is the rate constant of the process. Integrating equation (2.40) yields

$$q = q_e(1 - \exp(-k_1 t)). \tag{2.41}$$

This pseudo first order model is purely empirical and therefore also applied with ample success in the description of experimental data [84–86]. However, due to its empirical character, it is valid only for a specific set of experimental conditions [87].

Pseudo-second-order model

Another empirical model that has been used frequently in recent years is the pseudo-second-order model [88]

$$\frac{\mathrm{d}q}{\mathrm{d}t} = k_2(q_e - q)^2, \tag{2.42}$$

where k_2 is the pseudo-second-order rate constant, which is a function of initial concentration of solute molecules [89]. Integrating and rearranging yields the linear form

$$\frac{t}{q} = \frac{1}{k_2 q_e^2} + \frac{1}{q_e}t \tag{2.43}$$

that is often successfully applied to describe the sorption of metal ions from solution (c.f. the review article by Ho and McKay [88] and references therein).

Mixed-order model

The mixed-order equation was derived to cover a broader range of adsorption behavior, as the pseudo first and second order equations only represent the limiting cases of typical kinetic experiments. To this end, Marczewski introduced the dimensionless adsorption progress F as the ratio of the adsorbed amount a to its equilibrium value a_{eq}: $F = a/a_{eq}$ [90]. The mixed order equation is then written as

$$\frac{\mathrm{d}F}{\mathrm{d}t} = k_{1a}(1 - F) - k_{2a}a_{eq}(1 - F)^2, \tag{2.44}$$

36

where the k_{ia} are the kinetic rate coefficients. A similar equation has also been derived by Liu and Shen [86] for the adsorption coverage rather than the adsorption progress. Introducing contribution coefficients, f_i for the i-th order kinetic terms

$$f_i = \frac{k_{ia} a_{eq}^{i-1}}{k_{1a} + k_{2a} a_{eq}} \quad \text{and} \quad f_1 + f_2 = 1, \tag{2.45}$$

the mixed order equation can then be written

$$\frac{\mathrm{d}F}{\mathrm{d}t} = (k_{1a} + k_{2a} a_{eq})[f_1(1 - F) - f_2(1 - F)^2]. \tag{2.46}$$

If $f_2 < 1$ then a simpler form can be obtained

$$\frac{\mathrm{d}F}{\mathrm{d}t} = \frac{k_{1a}}{1 - f_2}(1 - F)(1 - f_2 F), \tag{2.47}$$

which can be integrated to obtain

$$a = a_{eq} \frac{1 - \exp(-k_{1a}t)}{1 - f_2 \exp(-k_{1a}t)}. \tag{2.48}$$

If the contribution to the second-order term is zero ($f_2 = 0$) the Lagergren first order equation is obtained. If, on the other hand, $f_1 = 0$, equation (2.44) becomes a pure second-order equation.

Langmuir kinetics

The Langmuir model described above can also be used to characterize adsorption kinetics provided that the assumptions made in the derivation of the Langmuir isotherm (equation (2.48)) are fulfilled.

Then,

$$\frac{\mathrm{d}\theta_s}{\mathrm{d}t} = k_{ads}c(1-\theta_s) - k_{des}\theta_s, \tag{2.49}$$

which at equilibrium converts to the Langmuir isotherm (equation (2.48)). A relatively simple, complete analytical solution has recently been presented [91] and will briefly be outlined below. Thereby, the dimensionless adsorption progress F and a relative change in concentration, $u = 1 - c/c_0$, where c_0 is the initial concentration, are used to account for the changes in concentration and adsorption. The Langmuir rate equation can then be expressed as

$$\frac{\mathrm{d}\theta_s}{\mathrm{d}t} = k_{ads}c_0(1-u_{eq}F)(1-F\theta_{eq}) - k_{des}F\theta_{eq} = k_{ads}c_0\left[(1-u_{eq}F)(1-F\theta_{eq}) - \frac{\theta_{eq}}{Kc_0}\right]. \tag{2.50}$$

The equilibrium coverage is defined in terms of the equilibrium uptake u_{eq} and the initial concentration c_0 according to the Langmuir isotherm

$$\theta_{eq} = \frac{Kc_{eq}}{1+Kc_{eq}} = \frac{Kc_0(1-u_{eq})}{1+Kc_0(1-u_{eq})}, \tag{2.51}$$

such that the Langmuir rate equation can be rearranged to obtain the more simple equation with the Langmuir batch factor $f_{eq} = u_{eq}\theta_{eq}$

$$\frac{\mathrm{d}\theta_s}{\mathrm{d}t} = k_{ads}c_0(1-F)(1-f_{eq}F) \qquad \text{or} \qquad \frac{\mathrm{d}F}{\mathrm{d}t} = \frac{k_{ads}c_0}{\theta_{eq}}(1-F)(1-f_{eq}F). \tag{2.52}$$

By defining the first order rate coefficient, k_1, through the parameters of the Langmuir rate equation (2.40) it follows that

$$\frac{\mathrm{d}F}{\mathrm{d}t} = \frac{k_1}{1 - f_{eq}}(1 - F)(1 - f_{eq}F).$$ (2.53)

The properties of these last two equations change gradually from first order for $f_{eq} = 0$ to pure second order for $f_{eq} = 1$, for which case equation (2.53) cannot be used directly. This behavior is illustrated in Figure 2.5.
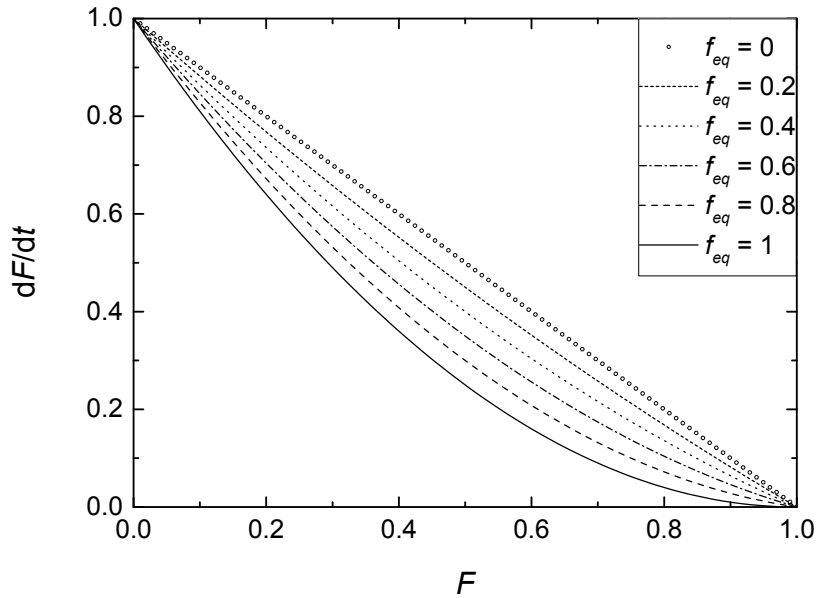

Figure 2.5: Variation of adsorption rate dF/dt for different values of f_{eq}, including the boundary cases $f_{eq} = 0$ and $f_{eq} = 1$.

For $f_{eq} < 1$, equation (2.53) can be integrated to obtain

$$F = \frac{1 - \exp(-k_1 t)}{1 - f_{eq}\exp(-k_1 t)}.$$ (2.54)

The mixed-order equation (2.48) is identical to the Langmuir equation (2.44), when the parameters

of the mixed-order equation (k_1 and f_2) are determined by the parameters governing the Langmuir rate equation (k_a, c_0, u_{eq} and θ_{eq}). Generally, the Langmuir rate equation should only be used to describe systems for which the adsorption equilibrium can be described by the Langmuir isotherm (i.e. the assumptions made in the derivation of the Langmuir isotherm must also be fulfilled). If this is not the case, the mixed-order equation without the interpretation of $f_2 = f_{eq} = u_{eq}\theta_{eq}$ can be used successfully as an empirical model to describe also non-Langmuirian systems.

The two-step model for protein adsorption

The adsorption of proteins is more complicated than the adsorption of e.g. ions, rigid particles or surfactants, due to their tendency to change conformation once they reach a surface. In addition, protein adsorption is often irreversible (or possesses desorption times that are experimentally not easily accessible). Krisdhasima and co-workers developed a simple model describing the adsorption of proteins as a two-step process, which is schematically illustrated in Figure 2.6 [92].
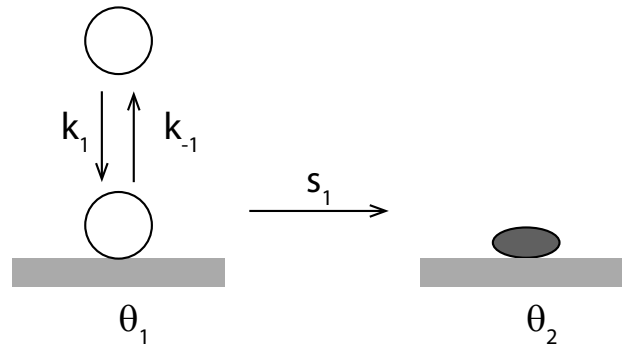

Figure 2.6: Illustration of the two-step adsorption process. The protein adsorbs reversibly with a rate k_1, then either desorbs (rate k_1) or changes its conformation leading to an irreversibly adsorbed form (rate s_1). Adapted from reference [92].

In a first step, at the initial stage of adsorption, the protein reversibly adsorbs to the surface keep-

ing its native conformation. In a second step, the presence of the surface induces a conformational change to an irreversibly adsorbed form. The rate of surface coverage in each of the states can be written as

$$\frac{\mathrm{d}\theta_1}{\mathrm{d}t} = k_1 c(1 - \theta_1 - \theta_2) - (k_{-1} + s_1)\theta_1 \tag{2.55}$$

and

$$\frac{\mathrm{d}\theta_2}{\mathrm{d}t} = s_1 \theta_1. \tag{2.56}$$

with the rate constants k_1, k_{-1}, s_1 and the concentration c. These equations can be solved analytically to obtain the total surface coverage

$$\theta = \theta_1 + \theta_2 = A_1 \exp(x_1 t) + A_2 \exp(x_2 t) + A_3, \tag{2.57}$$

where A_1, A_2 and A_3 are constants and x_1 and x_2 are always < 0 and given by complicated functions of the rate constants k_1, k_{-1}, s_1 and the concentration c. Equation (2.57) can also be expressed in terms of adsorbed mass

$$a = a_{max}(A_1 \exp(x_1 t) + A_2 \exp(x_2 t) + A_3). \tag{2.58}$$

Equation (2.58) is illustrated in Figure 2.7 for different values of x_1.
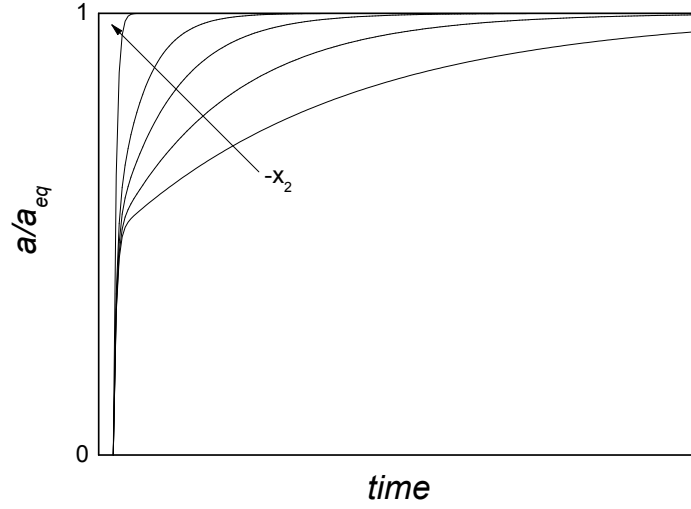
Figure 2.7: Illustration of the functional form of (2.58) for different values of x_1.

It can additionally be shown that

$$x_1 + x_2 = -(k_1 c + k_{-1} + s_1) \qquad \text{and} \qquad x_1 x_2 = s_1 k_1 c. \tag{2.59}$$

However, a third relationship would be needed in order to determine the absolute values of the rate constants. Simulations indicate that as s_1 and k_1 increase, θ and θ_2 reach their plateau value faster [92]. This model thus describes the adsorption of proteins in a more realistic way by taking into account the conformational change upon adsorption. However, the drawback of this model is that the obtained parameters x_1 and x_2 cannot directly be interpreted as kinetic rate constants of the process.

Random sequential adsorption model

The random sequential adsorption model, in its simplest form, considers the random placement of spherical disks on a surface [20, 93]. Thereby the disks are not allowed to overlap and are adsorbed

irreversibly. The rate of change of the number n of disks with area A on the surface is described by $dn/dt = C_m\phi$, where ϕ is the average fraction of the surface available to the center of a new disk and C_m is a parameter related to the mass transport to the surface (or initial deposition rate to an empty surface). dn/dt may be expressed as a power series in the number of deposited particles [94]. Using $\theta = An$ up to the third order the rate is then given by [94]

$$\frac{\mathrm{d}n}{\mathrm{d}t} = C_m[1 - 4\theta + (6\sqrt{3}/\pi)\theta^2 + (40/\sqrt{3}\pi - 176/3\pi^2)\theta^3]. \tag{2.60}$$

The jamming limit was determined to be 55%, indicating that the distribution of proteins on the surface at saturation level is highly inefficient [94]. The random sequential adsorption model is thus thought to describe protein adsorption in a more realistic way taking into account the dimensions of the proteins adsorbed on the surface [15]. However, its complicated form is not very convenient for fitting experimental data.

Due to the complexity and heterogeneity of proteins and the poor understanding of the exact mechanisms governing time-dependent changes in adsorption, desorption and protein conformation, each of the models described above has its drawbacks. Nevertheless, these models can give valuable insights into adsorption kinetics of proteins, if applied with care.

2.4 Diffusion

2.4.1 Fick's laws of diffusion

Diffusion refers to the transport of molecules down a concentration gradient due to random thermal motion. The equations describing diffusion processes were derived by Fick [95]. The driving force for diffusion is a gradient in chemical potential μ, which for low concentrations can be approximated by $\mu = \mu^{st} + RTln(c/c^{st})$, where the superscript st refers to the standard state and R is the universal gas constant. Thus, in one dimension, the flux of particles J due to diffusion is given by

$$J = -C \left(\frac{\partial \mu}{\partial x} \right)_{p,T},$$

(2.61)

where C is a constant related to the mobility of the diffusing particles. Then, by calculating the derivative and inserting into equation (2.61), Fick's first law is obtained:

$$J = -\frac{CRT}{c} \frac{\partial c}{\partial x} = -D \frac{\partial c}{\partial x}$$

(2.62)

with the diffusion coefficient $D = CRT/c$. Fick's first law applies to steady state situations. Fick's second law, on the other hand, describes how the concentration changes with time due to diffusion. It can be derived from the continuity equation (conservation of mass):

$$\frac{\partial c}{\partial t} = -\frac{\partial J}{\partial x} = -\frac{\partial}{\partial x} \left(-D \frac{\partial c}{\partial x} \right) = D \frac{\partial^2 c}{\partial x^2}.$$

(2.63)

A general solution to this equation in the case of an inexhaustible source and semi-infinite geometry (i.e. the sample extents from $x = 0$ to $x = \infty$) is given by

$$c(x,t) = A + B \mathrm{erf}\left(\frac{x}{2\sqrt{Dt}}\right),$$

(2.64)

where A and B are constants that can be determined from the boundary conditions and $\mathrm{erf}(z)$ is the error function ($\mathrm{erf}(z) = (2/\sqrt{\pi})\int_0^\infty \exp(-\xi^2)d\xi$), erf(0)=0 and erf($\infty$)=1). For the initial condition $c(x,0) = c_0$ and boundary conditions $c(0,t) = c_s$ and $c(\infty,t) = c_0$,

$$c(x,t) = c_s + (c_0 - c_s)\mathrm{erf}\left(\frac{x}{2\sqrt{Dt}}\right).$$

(2.65)

The time and distance dependence of the concentration according to equation (2.65) is illustrated in Figure 2.8. At short times the concentration profile falls off quickly with distance to the surface, while at very long times, steady state is reached resulting in a linear concentration profile. At x=0, $c = c_s$, while at large distances from the origin the concentration is almost constant with time approaching the boundary value c_0.
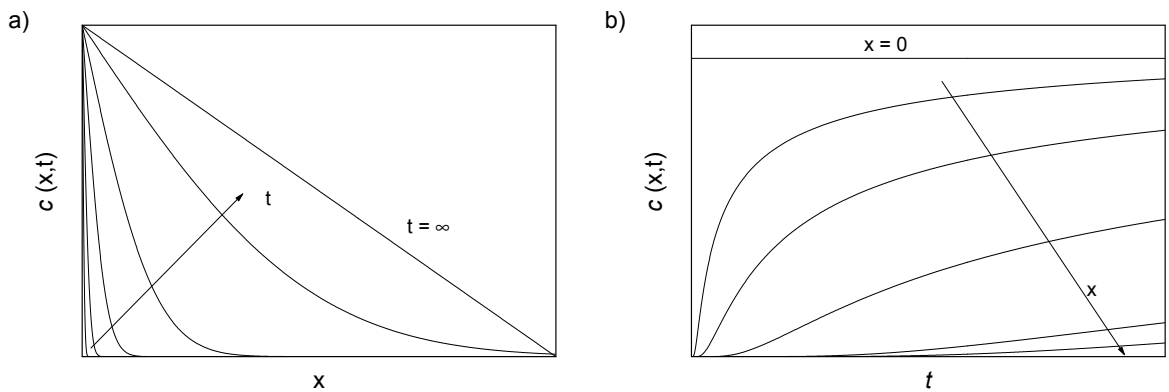

Figure 2.8: Variation of the concentration c a) with distance x at different times t and b) with time t for different values of x.

2.4.2 Diffusion of water in silica glass

The mechanism of diffusion of water into silica has been described by Doremus [96] as resulting form the diffusion of molecular water into the silica glass and its subsequent reaction with the Si-O-Si network to form silanol groups according to

$$Si - O - Si + H_2O \rightleftharpoons 2SiOH. \tag{2.66}$$

For diffusion plus chemical reaction the equation of continuity can be written as

$$\frac{\partial c}{\partial t} = -D\frac{\partial^2 c}{\partial x^2} - \frac{\partial X}{\partial t}, \tag{2.67}$$

where c is the concentration of molecular water, X is the concentration of reacted immobile OH groups and D is the diffusion coefficient of molecular water. For the case, in which the forward reaction of (2.66) controls the formation of SiOH groups (i.e. the reverse reaction rate is negligibly small), $\partial X/\partial t = \lambda c$, where λ is the reaction rate coefficient of the forward reaction. With initial concentration $c(x,0) = c_0$, boundary conditions of constant surface concentration $c(0,t) = c_s$ and semi-infinity geometry (i.e. $c(\infty,t) = c_0$) it can be shown that for $\lambda t >> 1$, i.e. approaching steady state,

$$c(x) = c_0 + (c_s - c_0)\exp\left(-x\sqrt{\frac{\lambda}{D}}\right). \tag{2.68}$$

For situations, where the reverse reaction is also relevant, a more complicated relation involving a time dependent diffusion coefficient is obtained [96].

In summary, the fundamental theoretical concepts necessary to understand the content of this thesis were discussed. Furthermore, experimental models, which will be used in this thesis were introduced.

DENSIFICATION AND HYDRATION OF HMDSO PLASMA

POLYMERS

In this chapter the influence of energetic conditions in the plasma gas phase and at the surface on fragmentation of hexamethyldisiloxane (HMDSO) and densification of the resulting plasma polymers is investigated. Additionally, the aging of these films in air and water is studied. The issues addressed in this chapter are important for the development of stable vertical chemical gradients with tunable thickness and film chemistry.

The work reproduced in this Chapter was published in Plasma Processes and Polymers in 2015 [97]. For this publication, I have planned and performed all experiments (except the silver release study) and prepared the first version of the manuscript. Barbara Hanselmann assisted in plasma deposition and Johannes Drosten performed the silver release study. Manfred Heuberger corrected the manuscript and gave valuable inputs to data interpretation. Dirk Hegemann supervised this work, corrected the manuscript and helped develop the ideas therein.

3.1 Introduction

The deposition of functional coatings by plasma polymerization is a versatile coating technique. Beneficial attributes include adhesion to a variety of substrates as well as the possibility to control the modulus, the hardness and the wettability via the degree of cross-linking [31–33, 98–100]. Adjusting these properties requires, however, a precise control and understanding of the plasma gas phase energetics and plasma surface growth processes. For the particular starting molecule (commonly named "monomer" in plasma polymerization) used in this study, namely hexamethyldisiloxane (HMDSO), their respective role in the dissociation and the densification/ cross-linking for plasma polymer deposition is still under discussion [101, 102]. For the predominant plasma chemical reaction pathway, however, good arguments have been given that it mainly proceeds via the opening of one Si-O bond in the HMDSO monomer [103–105]. The activation and fragmentation of the monomer in the plasma is controlled by the energy supplied per molecule, which is proportional to the steady state energy density in the gas phase. A steady state description of the plasma polymerization processes via externally accessible parameters, namely the power input per monomer gas flow rate, W/F_m (macroscopic description) was considered [35, 64]. As long as the production of film-forming species in the plasma proceeds via a predominant chemical reaction pathway that can be described by an apparent activation energy E_a , the mass deposition rate R_m can be related to the steady state energy density in the gas phase using a quasi-Arrhenius approach, where the thermal energy kT is replaced by the specific energy W/F_m [63, 106]:

$$\frac{R_m}{F_m} = C exp\left(-\frac{E_a}{(W/F_m)}\right).$$

(3.1)

The pre-factor C is a reactor and process dependent factor related to the conversion of monomer into film growth [107]. The measured mass deposition rate depends on the sticking probability of the film forming species, which should be constant over the examined W/F_m range in order to justify the quasi-Arrhenius method of approach [103].

For the quality of the growing film the impinging ion energy (also named deposited energy or energy density) during film growth, ϵ_{surf}, is an important parameter; it can be described as follows

$$\epsilon_{surf} = \frac{E_{mean}\Gamma_i}{R} \tag{3.2}$$

with E_{mean} the mean kinetic energy of the ions impinging on the substrate, Γ_i the ion flux towards the substrate and R the deposition rate. ϵ_{surf} thus gives the general energy deposited per condensing particles during film growth from ion bombardment [35, 99, 108]. Energetic particle bombardment at the surface promotes densification (cross-linking) of larger fragments or facilitates the chemisorption of physisorbed molecules [109]. Along these lines, the energetic balance during film growth can affect the sticking probability or yield ion-induced etching [103]. Recently, it has been shown for plasma polymers generated from hydrocarbon precursors that above a certain threshold energy the densification and cross-linking of the films scales with the deposited momentum given by

$$\pi_{surf} = 2\sqrt{2m_i E_{mean}}\frac{\Gamma_i}{R} \tag{3.3}$$

where m_i is the average ion mass [70]. For these types of films, the momentum transfer per condensing particles through energetic particle interactions at the growing film surface thus plays

an important role in defining the film properties. In the here relevant case of the organosilicon monomer HMDSO on the other hand, the influence of momentum transfer on film density is not fully established yet, while some work on the importance of ion bombardment has been performed [31, 110, 111]. Note that in the absence of etching the film growth rate corresponds to the flux of film forming species towards the substrate, Γ_{dep}. In this case, either one of the two quantities can be used to calculate the deposited energy and momentum respectively. Otherwise, part of the energy at the surface is consumed for etching processes, which reduces the deposition rate and thus the effective flux of film forming species, Γ_{dep}, should be considered [103, 112].

Organosilicon plasma polymers are used in many applications such as optics, barrier coatings, sensors or biomedical applications [100]. HMDSO is widely used as a starting molecule for plasma polymers because it has a suitable vapour pressure at ambient conditions, is relatively non-toxic and is commercially easily available. Numerous reports on its use in applications including pervaporation membranes, barrier coatings for controlled release of molecules, humidity sensors, biocompatible coatings and anti-bacterial nanosilver-composite materials have been published [113–120]. These examples suggest that plasma polymerized HMDSO films are stable in water and that (at least to some extent) water penetrates into these hydrophobic films (i.e. film hydration is possible). In this work, the importance of surface processes (deposited energy and momentum) as well as gas phase processes (fragmentation of the monomer) on the densification and wetting properties of HMDSO plasma polymers is investigated. In addition, the stability of these coatings in air and in aqueous environments is assessed with a focus on film hydration.

3.2 Experimental Section

For the deposition of HMDSO plasma polymers capacitively coupled RF discharges ($f = 13.56$ MHz) were used. The films were deposited in a rather large asymmetrical reactor equipped with a gas shower head mounted at a distance of 5 cm from the driven electrode providing a uniform, vertical gas flow through the plasma zone towards the electrode. The driven electrode had an area of $A_{dep} = 1470$ cm^2, while the area of the grounded counter electrode, which consisted of the chamber walls, was considerably larger. The asymmetry of the reactor led to a concentration of the luminous plasma in front of the driven electrode (near the plasma-sheath boundary) and thus a (negative) bias voltage, V_{bias}, was established. The potential drop over the plasma sheath can be approximated by the linear relationship obtained by averaging over one RF cycle $V_{sh} \approx 0.39V_0 - 0.73V_{bias}$ [48], where V_0 is the amplitude of the RF excitation $V_{RF} = V_0 sin(2\pi ft)$. A V/I probe (ENI Model 1065) was used to measure the excitation voltage V_0, the bias voltage V_{bias} and the absorbed power. The plasma expansion was considered by correcting the plasma parameter W/F_m for the internal power absorption and for the specific reactor geometry as described earlier [64, 107]. The applied power was varied from 30 to 150 W. In addition, microwave interferometry (JE PlasmaConsult MWI2650) was used as a line-of-sight, integrated measurement of the electron density by guiding the MW radiation (26.5 GHz) through the bright plasma zone near the plasma-sheath boundary [109, 121]. Electron density was determined to increase nearly linearly from 3×10^9 cm^{-3} to 1×10^{10} cm^{-3} in the considered power range. The HMDSO monomer was purchased from Fluka and the HMDSO tank (as well as the tubing) was stabilized at a temperature of 43°C outside the reactor. The HMDSO total gas flow rate was kept constant at 4 sccm using a thermo-stabilized mass flow controller (also at 43°C). To fill the rather large plasma chamber and to stabilize the plasma, 20 sccm of Ar (Carbagas)

was added as carrier gas. The gases were mixed outside the plasma chamber and introduced via the same gas shower. The process pressure was fixed at 7 Pa. To determine the deposition rate and the film density, reference glass slides and silicon wafers were coated. The deposited mass was determined by weighing the glass slides directly before and after the deposition process. The film thickness was measured over a masked film edge with a profilometer (Veeco, Dektak 150). The film density was then calculated from the volume and the mass of the coatings. The chemical composition of the films was analysed by X-ray photoelectron spectroscopy (XPS) measurements. The films were measured within 2 days after deposition. The analyses were carried out using a PHI 5600 LS spectrometer equipped with a hemispherical electron analyser and a Mg-Kα (300 W, 1253.6 eV) X-ray source. The base pressure was approximately 10^{-6} Pa. Survey and high resolution spectra were recorded using pass energies of 187.85 eV and 29.35 eV and step widths of 0.400 eV and 0.125 eV, respectively. The atomic concentrations were calculated with CasaXPS Version 2.3.12 software using instrument specific sensitivity factors. Charging effects were compensated by referencing the C 1s peak to 285.0 eV. For peak fitting of the Si peak a method according to Alexander [122] was applied using the following binding energies: Si(-O) (101.2 eV), Si(-O)$_2$ (101.9 eV), Si(-O)$_3$ (102.6 eV), and Si(-O)$_4$ (103.5 eV). A tolerance of ± 0.1 eV was allowed for these positions. The full width at half maximum of the peaks was kept equal for all four peaks but was allowed to vary between samples; typically, values in the range of 1.8-2.1 eV were obtained. Water contact angles were determined using a software controlled drop shape analyser (DSA 25, Krüss). For each sample several drops at different positions on the sample were measured. For testing the long term stability of the films, some samples were stored at 20°C and RH 65%; others were stored in deionized water. For the contact angle measurements the latter samples were taken out of the water, gently blown dry and measured within 1-2 minutes. The silver released from a silver layer (150 nm deposited

by Magnetron sputtering) across different $\approx$ 100 nm thick pp-HMDSO films was determined by multilayer coating in a Petri dish. The samples were incubated with 4 ml of deionized water for variable durations. The analysis of the amount of silver released through the HMDSO films was carried out by ICP-OES using an Optima 3000 Perkin Elmer instrument. For the analysis, the Ag now dissolved in the supernatant was dissolved in 2 ml concentrated nitric acid and diluted with 8 ml water up to 10 ml. The silver-containing solution was then injected into the ICP-OES and optically analysed (Ag lines at 328.068 nm and 338.289 nm). The calibration was performed using an external Ag standard solution of $1 \mathrm{mg\ ml}^{-1}$. The detection limit was $\leq 0.075\ \mu\mathrm{g\ ml}^{-1}$.

3.3 Results and Discussion

The HMDSO molecule, $(CH_3)_3$-Si-O-Si-$(CH_3)_3$, is more complex than other typical monomers used for plasma polymerization. Therefore, a wealth of different species is expected during its fragmentation in the gas phase [123–125]. Many of these species show a low affinity towards the surface and thus have a low probability of being incorporated into the growing film (rather yielding volatile products that can be detected in the gas phase). The radical created by breaking one Si-O bond of HMDSO (bond energy of 5.9 eV) [126], $(CH_3)_3$-Si-O$^\bullet$, on the other hand, has a sticking coefficient close to one and can thus be assumed to be the predominant film forming species [62, 105, 127]. A Si-O-Si network (similar as in polydimethylsiloxane (PDMS)) can then be established by further abstraction of a methyl group at the surface or in the gas phase. This requires overcoming the surface barrier for chemisorption in the order of several eV [128] or breaking further Si-C bonds (bond energy of 4.6 eV). Provided that enough energy is supplied to the gas phase and/or at the surface, assuming a predominant chemical reaction pathway involving Si-O breakage and CH_3 abstraction is therefore an

adequate approximation. As shown in Figure 3.1 a) and observed previously [34, 129, 130] the deposition rate of HMDSO plasma polymers can indeed be described using a quasi-Arrhenius approach (equation (3.1)).
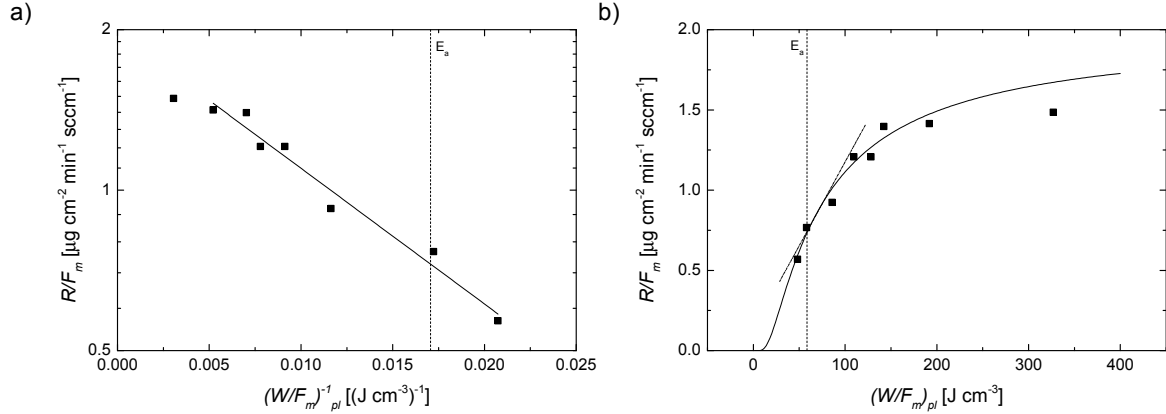

Figure 3.1: a) Arrhenius-like plot of the deposited mass of HMDSO plasma polymers. The data points were fitted using equation (3.1); the dashed line indicates the obtained activation energy $\langle E_a \rangle = 13.6$ eV/molecule. b) Deposited mass of HMDSO plasma polymers as a function of energy density in the gas phase depicted according to Yasuda [63]. The solid line illustrates equation (3.1); the dashed line indicates $\langle E_a \rangle$ and the dashed dotted line indicates the linear increase of R_m/F_m around $\langle E_a \rangle$.

Due to the rather high energies involved in the formation of film forming species, also a relatively high activation energy is expected. For the experimental conditions used in this work, an apparent activation energy of $\langle E_a \rangle = 55.8$ J cm^{-3} corresponding to 13.6 eV/molecule was obtained (indicated by the dashed line in Figure 3.1 a) and b)). Over a broad range the deposition rate follows an Arrhenius-like behaviour (solid line in Figure 3.1 a) and b)). The dash-dotted line in Figure 3.1 b) indicates the energy density range around $\langle E_a \rangle$, in which the deposition rate increases almost linearly with W/F_m.

The elemental composition of the films was assessed using X-ray photoelectron spectroscopy. The main component of the C 1s peak was attributed to saturated hydrocarbons and charge referenced to 285.0 eV. A minor component ($\leq 5\%$ of the total peak area) appeared at slightly higher binding

energies ($\approx$ +2 eV) and was attributed to ether or hydroxyl groups, but not analysed further. The O

1s peak was symmetrical and its position remained constant for all samples (533.2 $\pm$ 0.1 eV). The

elemental compositions obtained are presented for three different samples in Table 3.1.

Table 3.1: XPS results for samples A, B and C, respectively (see Figure 3.1 and Figure 3.2); Si(PDMS) and Si(SiO$_2$) as defined in the text.

Sample	C [at %]	O [at %]	Si [at %]	C/Si	O/Si	Si(PDMS)/Si	Si(SiO$_2$)/Si
A	49.2	24.2	26.6	1.85	0.91	55	45
B	49.3	24-6	26.1	1.89	0.94	52	48
C	47.4	27.3	25.3	1.88	1.08	47	53

The results are in good agreement with previous HMDSO plasma polymers produced under sim-

ilar conditions [131, 132]. While around $\langle E_a \rangle$ (samples A and B) the elemental composition remains

constant, a slight oxidation can be observed at higher energy inputs (sample C). This becomes even

more apparent in the O/Si ratio which is increasing with energy input. For the C/Si ratio, on the other

hand, no clear trend could be observed when increasing the power input from sample A to sample C.

As described in the experimental section, the silicon peak was fitted using four peaks corresponding

to the four different oxidation states of the Si atom according to Alexander et al. [122] To describe

the less cross-liked (PDMS-like) network the quantity Si(PDMS) is defined which comprises the

contributions to the peak areas associated with one or two oxygen atoms bound to the silicon. Ac-

cordingly, Si(SiO$_2$) is given by the two peaks representing three or four oxygen atoms attached to

the silicon. This quantity thus represents a denser (SiO$_2$-like) network. Increasing the power input

into the plasma clearly leads to a decrease of methyl content in the network. Nevertheless, all three

samples contain significant amounts of PDMS-like network, suggesting that the film forming species

indeed mainly consist of the predominant (PDMS-like) fragment $^\bullet$(CH$_3$)$_2$-Si-O$^\bullet$. These XPS results

are in agreement with MTR-IR measurements of the pp-HMDSO films, which will be published in the near future.

Besides the deposition rate, the variation of the film density with the applied plasma conditions was evaluated. The film density increases with ϵ_{surf} (equation (3.2)), as illustrated in Figure 3.2 a).
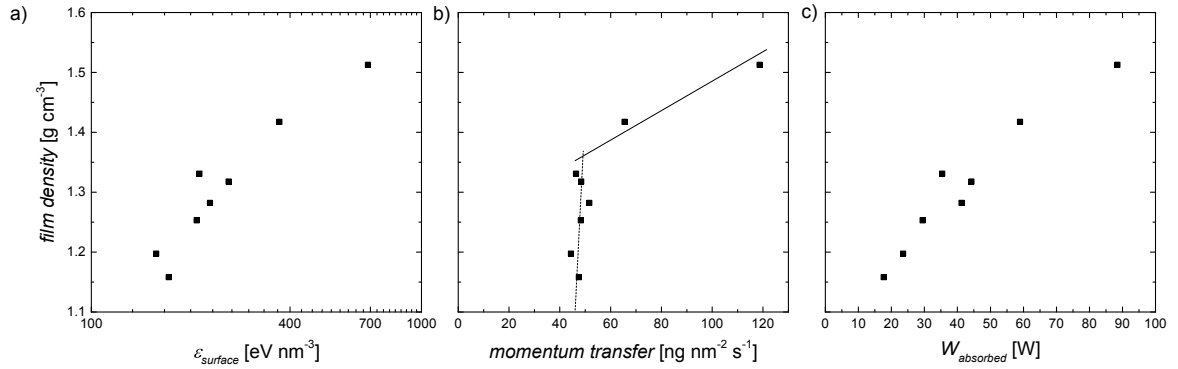

Figure 3.2: a) Increase of film density with deposited energy at the surface; b) Influence of deposited momentum on film density. The dashed line indicates the increase of film density in the range of (almost) constant deposited momentum, while the solid line indicates the recovery of the linear dependence with increasing values; c) Dependence of film density on power absorbed by the plasma. Note that, as the monomer gas flow was kept constant, this is equivalent to the energy input into the gas phase.

This indicates the importance of energy input at the surface for the densification of plasma polymerized HMDSO, since ϵ_{surf} provides the energy for surface diffusion processes and for nucleation (creation of binding sites for film forming species) as well as for bond opening and cross-linking. It has recently been shown that for pure ethylene discharges as well as for mixtures of ethylene with carbon dioxide or ammonia the film density increases linearly with deposited momentum [70], which was taken as an indication that densification through momentum transfer (above a certain energy threshold, i.e. sufficient energy is provided for film formation) might be an important process in general. However, for HMDSO plasma polymer deposition the densification might be more complex.

Figure 3.2 b) shows the film density versus deposited momentum as calculated using equation (3.3). Because the ion flux towards the substrate, Γ_i, scales roughly linearly with delivered power [99] and also the deposition rate R increases nearly linearly with power in the parameter range around $\langle E_a \rangle$ (c.f. Figure 3.1 b)), the deposited momentum is almost constant in this first range. Nevertheless, the film density significantly increases from 1.15 g cm^{-3} to about 1.35 g cm^{-3}, seen as nearly vertical distribution of data points. Hence, at different power inputs but similar energetic conditions at the surface, coatings with a broad range of densities were produced. In this particular parameter range, the densification of pp-HMDSO does thus not proceed primarily via momentum transfer. This suggests that gas phase processes, i.e. the extent of fragmentation of the monomer, which increases with increasing energy input [104], might be of similar importance for the densification of pp-HMDSO. A fragmentation mechanism of the HMDSO molecule as illustrated in Figure 3.3[1] is thus proposed, which includes formation of free radicals with multiple dangling bonds (free radical sites / binding sites) already in the gas phase that significantly contribute to the observed cross-linking in the film.

Starting from the monomer molecule, two main initial dissociation mechanisms are suggested: the abstraction of a methyl group requiring 4-6 eV (reaction 1) and the cleavage of a Si-O bond requiring 6-9 eV (reaction 2). Note that for direct electron impact dissociation the bond energy needs to be exceeded by typically 1-3 eV [133, 134]. Starting from the abstraction of a methyl group, the $(CH_3)_2$-$^\bullet$Si-O-Si-$(CH_3)_3$ - radical can be further decomposed by breaking an Si-O bond (6-9 eV, reaction 1a)). Both possible ways of breaking this bond lead to film forming species. Either the bi-radical $(CH_3)_2$-$^\bullet$Si-O$^\bullet$ with $m = 74$ amu or the mono-radical $(CH_3)_3$-Si-O$^\bullet$ with $m = 89$ amu is formed. While the former fragment is likely incorporated directly into the growing film, the latter fragment can either be incorporated as mono-radical or a further methyl group might be abstracted

---

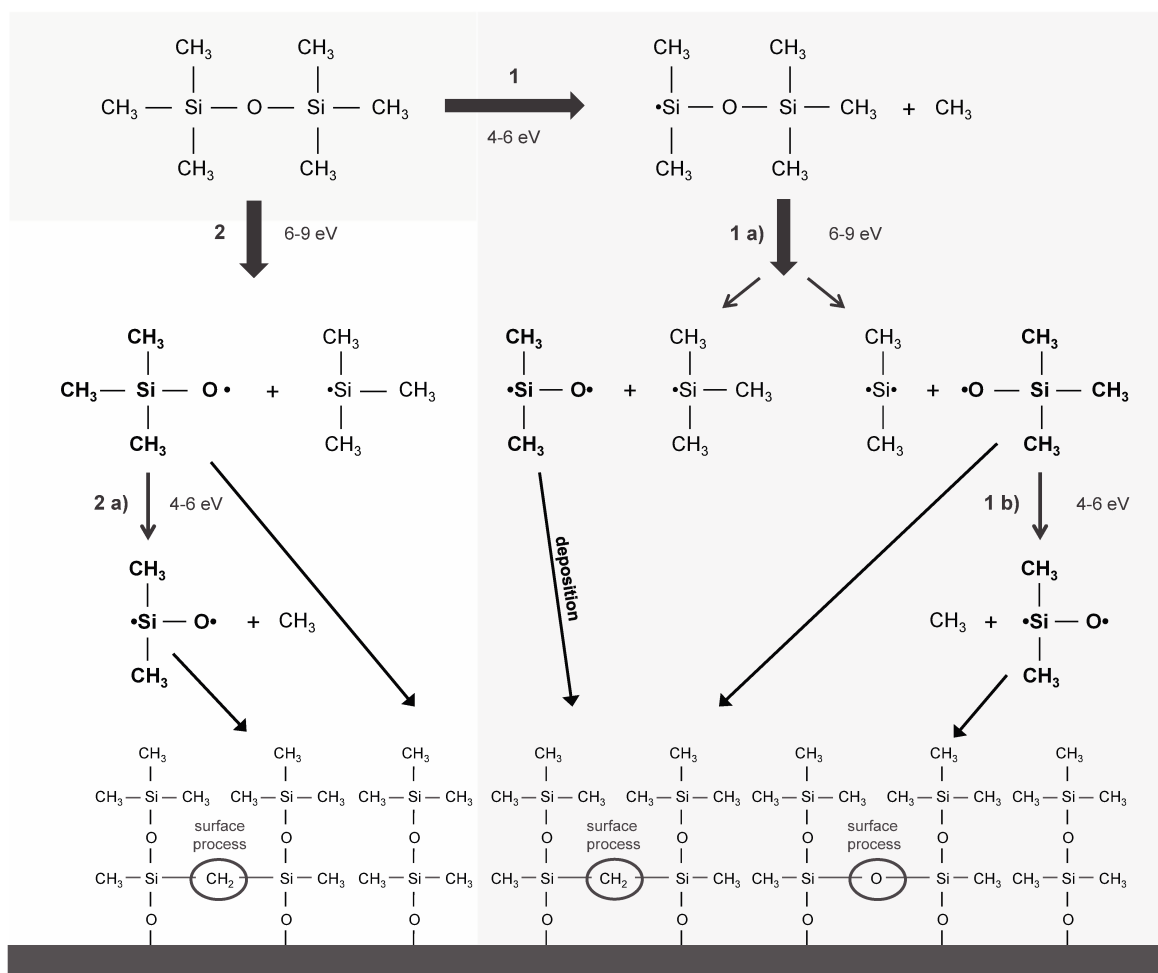[1]The design of this scheme was inspired by Rügner at al. [105]

58

Figure 3.3: Schematic representation of the dissociation processes in a HMDSO plasma yielding film forming species (in bold). The energies needed for bond dissociation are indicated in the figure. Possible surface reactions yielding cross-linking and densification are also suggested (encircled). Different gray levels in the background are used to guide the eye along different predominant chemical pathways.

in the gas phase (4-6 eV reaction 1 b)) to yield the same bi-radical. Starting with reaction 2, the monomer is directly decomposed into the film-forming mono-radical. Again, this unit might either be incorporated directly into the growing film or another CH_3-group is abstracted to yield the bi-radical $(CH_3)_2$-$^\bullet$Si-O$^\bullet$ (4-6 eV, reaction 2a)). The so formed film network can then lose further hydrocarbon groups at the surface and/or can be cross-linked/densified via the formation of -CH_2-links or Si-O bonds depending on the energy available (indicated as surface processes in Figure 3.3).

For the films produced in this study, the film density increases with increasing energy input into the gas phase and consistently the PDMS-like part of the films decreases in the range of constant deposited momentum, while the chemical composition remains constant (compare sample A and B, Table 3.1). This could be explained by the production (gas phase) and incorporation (surface) of a higher fraction of larger fragments (i.e. the mono-radical $(CH_3)_3$-Si-O$^\bullet$ with m = 89 amu) at lower energy input into the gas phase. The energy at the surface is then used to abstract a further methyl group which is required for film formation, i.e. creation of nucleation sites (binding sites for film-forming species), and thus not available for film densification. As the energy input into the gas phase increases, fragmentation becomes more important and more film forming units with m = 74 amu (i.e. the bi-radical comprising only two methyl groups) are incorporated in the film. The energy at the surface can thus partly be used for densification, partly for the abstraction of methyl groups. In both cases, PDMS-like films with a constant film composition, but different film densities are obtained (samples A and B). Above $\langle E_a \rangle$, where the energy input into the gas phase is high enough to essentially produce film forming species with abstracted methyl groups, most of the energy at the surface can be used for densification, and, the film density then resumes the linear

dependence on deposited momentum as observed for hydrocarbon discharges (as seen in Figure 3.2 b) from sample C on). Moreover, further abstraction of methyl groups can be expected which is reflected in the increasing inorganic part (Si(SiO$_2$)) within the pp-HMDSO films. Indeed, the progressive abstraction of methyl groups for HMDSO molecules with increasing energy input has previously been shown using high resolution mass spectrometry [125] and tunable infrared diode laser absorption spectroscopy [135].

The importance of gas phase processes for the densification of HMDSO plasma polymers is also illustrated in Figure 3.2 c). The film density scales with the power delivered to the plasma, which, in this work, is equivalent to the energy input into the gas phase (W/F_m), as the monomer flow is kept constant.

It is important to note that the proposed fragmentation mechanism of the HMDSO molecule presented in Figure 3.3 yields film-forming species via several plasma chemical reaction pathways. Each of these pathways should be individually described using a quasi-Arrhenius approach with the respective activation energy: ≈ 15 eV for reaction 1a), ≈ 21 eV for reaction 1b), ≈ 9 eV for reaction 2, and ≈ 15 eV for reaction 2 a). This theoretical distinction is illustrated in Figure 3.4 (left hand side).

Nevertheless, despite the fact that the HMDSO film deposition results from monomer fragments created via different chemical pathways and with different activation energies, the superposition of these three Arrhenius-like functions again yields an Arrhenius-like function with an effective activation energy $\langle E_a \rangle \approx 14$ eV/molecule, see Figure 3.4. Hence, the quasi-Arrhenius behaviour observed for samples produced in this work with an effective activation energy of $\langle E_a \rangle = 13.6$ eV/molecule (Figure 3.1 a)) plausibly results from a superposition of the here proposed reaction pathways. For
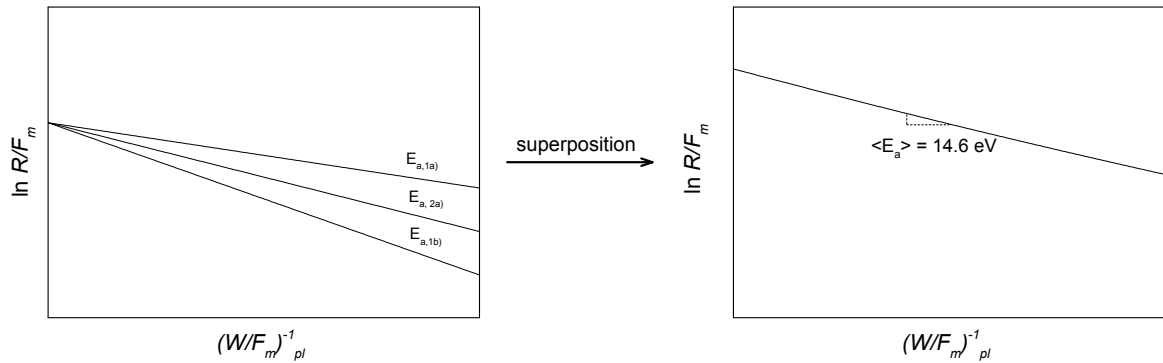
Figure 3.4: The superposition of three Arrhenius-like graphs with three different activation energies (e.g. $E_{a,1a)} = 15$ eV $= E_{a,2a)}$, $E_{a,1b)} = 21$ eV and $E_{a,2} = 9$ eV - left hand side) again yields an Arrenius-like graph with an effective activation energy $\langle E_a \rangle \approx 14$ eV/-molecule (right hand side).

a significant superposition to occur, comparable sticking probabilities are assumed to enter into the observed deposition rate, which is indeed reasonable for the considered film-forming species $(CH_3)_n$-SiO as long as sufficient nucleation sites are present [103]. Note that for all process parameters applied the deposited energy at the surface is high enough, i.e. >10 eV per deposited film-forming unit $SiO(CH_3)_2$, to allow for the abstraction of CH_3-groups resulting in the formation of binding sites or for the cross-linking via methylene groups. At energy inputs above $\langle E_a \rangle$ the films are thus densified mainly via the abstraction of hydrogen and methyl groups in the gas phase and further cross-linked via the formation of $-CH_2$- groups at the surface. Additional CH_3 abstraction at the surface results in even higher $Si(SiO_2)$ content in the film. For energy inputs near the activation energy, on the other hand, the film density is mainly determined by gas phase processes, i.e. the degree of fragmentation, since the momentum transfer per condensing molecules remains almost constant for increasing W/F_m (see Figure 3.2). These considerations are in agreement with the findings by Rügner et al. who described the HMDSO film growth mechanism at atmospheric pressure conditions [105]. A similar plasma chemical reaction pathway for the deposition of pp-HMDSO films at low and atmospheric pressure was already suggested by Sawada et al [136]. Differences in film growth are

thus mainly caused by surface processes (surface diffusion, creation of binding sites, cross-linking, and densification). Limited formation of binding sites constrains the actual film growth rate as it is observed for remote or atmospheric pressure plasmas (in the absence of oxygen) [137, 138].

A study of film hydration can yield additional insights. The water contact angles of the pp-HMDSO films produced in this study were found to decrease with increasing film density as shown in Figure 3.5.
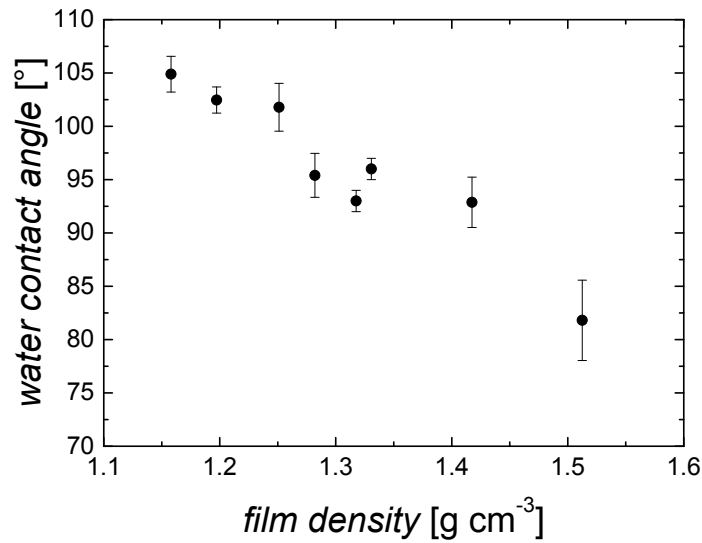

Figure 3.5: Variation of water contact angle with film density. The error bars represent the standard deviation of several measurements.

These results agree well with the obtained XPS results indicating an increasing O/Si ratio and Si(SiO_2) fraction for samples deposited at higher energy input and thus higher film density. The cross-linking degree of the films thus seems to play an important role in determining the surface chemistry.

Many applications of HMDSO plasma polymers require a long term stability of the coatings in different media depending on the exact use. In regard of these requirements the stability of the surface chemistry of the pp-HMDSO films was evaluated when stored in air or in deionized water

for several days using contact angle measurements.

The evolution of the water contact angle of samples A, B and C after storage in air under controlled conditions (20°C, RH 65%) is shown in Figure 3.6.
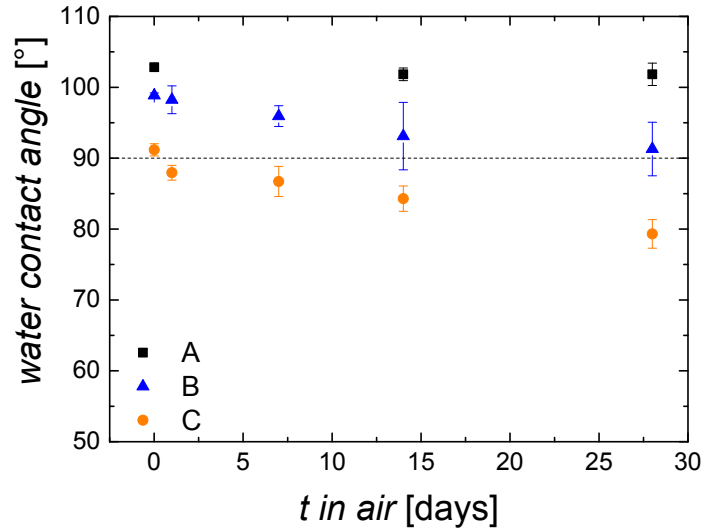

Figure 3.6: Evolution of water contact angle after sample storage in air under controlled conditions (20°C, RH 65%). The dotted line indicates the transition from hydrophobic to hydrophilic coatings at a water contact angle of 90°. The error bars represent the standard deviation of several measurements.

The water contact angle on sample A remains constant and high over the four weeks of storage time. This suggests exposition of significant quantities of methyl groups at the surface of the more loosely cross-linked pp-HMDSO [139]. Samples B and C, on the other hand, show a slight decrease of water contact angle over time, which is stronger for sample C produced at higher energy input. This trend is attributed partly to the slow oxidation of unreacted radical sites present after plasma polymerization of HMDSO [140]. As the concentration of remaining radicals increases with power [132], this is in line with the stronger decrease in contact angle of sample C as compared to sample B produced at lower energy input. After extended storage times, the contact angle converges - indicating that the responsible radicals are consumed in the process.

Storage in bulk water has a stronger effect on the contact angle immediately measured after dry blowing, as shown in Figure 3.7.
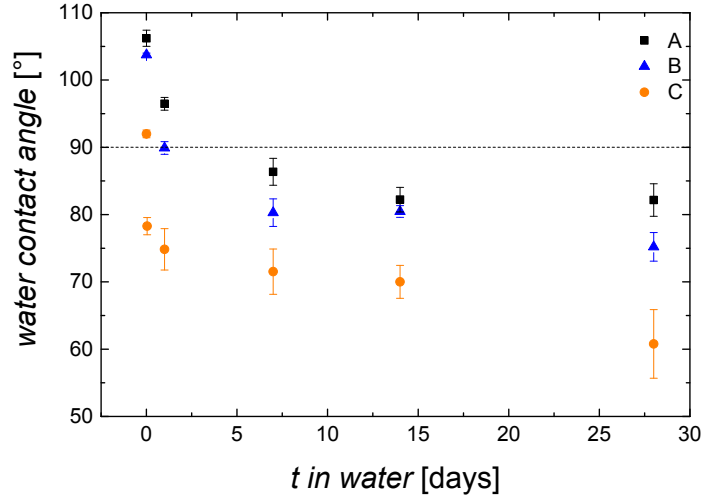

Figure 3.7: Evolution of contact angle after storage in deionized water. The dotted line indicates the transition from hydrophobic to hydrophilic coatings at a water contact angle of 90°. The error bars represent the standard deviation of several measurements.

All samples show a strong decrease in water contact angle upon the first few days of immersion in water, before eventually approaching a coating-specific asymptotic contact angle value. The water contact angle decreases at significantly higher rates than for the samples stored in air, and, in addition, the value reached after four weeks in water is significantly lower. The oxidation of trapped radicals hypothesized above cannot account for such strong decrease in water contact angle. Note that the decrease of contact angle during the first 24 h of immersion correlates with the $Si(SiO_2)$ fraction (about 10° decrease for coating A (starting contact angle $\approx 106°$, $Si(SiO_2) = 45\%$) against about 17° for coating C (starting contact angle $\approx 92°$, $Si(SiO_2) = 53\%$)). In addition, no significant differences in aging of C:H:O plasma polymers when stored in water or in air could be observed [141]. It is thus suggested that mainly the Si-O-Si network can act as hydrophilic moiety due to the presence of silanol (Si-OH) groups or its formation in contact with water [142, 143]. Water diffusion into

the pp-HMDSO films which comprise a substantial amount of voids [144, 145] is thus promoted. Successive hydration of the films leads to a more polar surface, which is in line with the observed decrease of water contact angles. As contact angle measurements are very surface sensitive, this reasoning applies for the top few nanometres of the films.

Therefore, and to assess the hydration of the complete films, water penetration throughout the film was quantified with an indirect detection method. The silver released from a metallic silver layer below the pp-HMDSO plasma polymers was measured in the supernatant. The release process is chiefly hydration/diffusion limited; water and oxygen need to penetrate through the HMDSO film and oxidize the silver surface to initiate a silver release [146–148]. The hydrated silver ions then also need to diffuse out to be detected in the supernatant. As confirmed by XPS, the samples A$'$ and C$'$ (100 nm film thickness on Ag-coated Petri dishes) are similar to samples A and C, respectively. Sample D$'$ in contrast was produced adding substantial amounts of oxygen to the discharge (O$_2$/HMDSO 10:1) in order to significantly reduce the carbon content in the films while ensuring a residual carbon content providing pores/voids. A pure silver surface was measured as reference. The results of the release studies are presented in Table 3.2. For sample A$'$ no silver could be detected after 14 days of storage

Table 3.2: O/Si and C/Si ratios for samples A$'$, C$'$ and D$'$ as determined by XPS and concentration of silver in the eluate after different storage times. A pure silver surface was measured as a reference.

	O/Si	C/Si	Ag 1 d [μm ml^{-1}]	Ag 7 d [μm ml^{-1}]	Ag 14 d [μm ml^{-1}]
Sample A$'$	0.9	1.9	0	0	0
Sample C$'$	1.1	1.7	0	0.1	0.1
Sample D$'$	1.7	0.4	1.9	6.1	7.0
Reference	-	-	5.1	15.1	19.1

in water. The slightly more hydrophilic coating C$'$ already releases a small, yet measurable amount

of silver, while sample D′, which contains only a low amount of hydrophobic groups but mainly Si-O-Si units, shows a strong silver release. Again, presence of the more polar Si-O-Si network (comprising silanol groups) also seems to play a key role in the diffusion of hydrated ions. Hence, the higher the fraction of Si-O-Si network in the films, the higher the silver release (as long as no compact SiO_2-like barrier layer is deposited).

For sample A, only the top few nanometres of the surface seem to be hydrated as evidenced by the absence of silver in the supernatant (sample A′). For comparison, sample D′, which consists mainly of Si-O-Si units, exhibits distinct silver ion release.

In fact, numerous reports in the literature have implicitly made use of the hydration of such nominally hydrophobic HMDSO coatings [113–119]. For example, Saulou and co-authors have shown that composite materials consisting of a pp-HMDSO matrix with embedded silver nanoparticles act as anti-microbial coatings [116]. The anti-microbial effect was ascribed to the release of silver ions. The pp-HMDSO must thus have been (partially) hydrated to allow for the diffusion of hydrated silver ions.

The amphiphilic character of such plasma polymerized HMDSO films, which might further be enhanced by gradually changing the hydrophobic/hydrophilic part during film growth, is potentially interesting for applications where coatings are needed that respond in a differentiated and delayed manner to changing conditions.

3.4 Conclusion

The elemental composition and the film density of plasma-polymerized HMDSO films have been studied. The energetics of mass deposition of HMDSO plasma polymers can be described using a quasi-Arrhenius approach invoking an effective activation energy $\langle E_a \rangle$. This effective activation energy $\langle E_a \rangle$ results from the superposition of the activation energies of several reaction pathways controlling the fragmentation of the HMDSO molecule in the gas phase. The proposed fragmentation mechanism yields film-forming species of different masses, namely the mono-radical $(CH_3)_3$-Si-O$^\bullet$ with $m = 89$ amu and the bi-radical $^\bullet(CH_3)_2$-Si-O$^\bullet$ with $m = 74$ amu. Depending on the applied energetic conditions both plasma gas phase fragmentation as well as ion bombardment at the surface contribute, in balance, towards film crosslinking and densification. While the generation of highly reactive bi-radical fragments in the gas phase becomes important at high energy input, methyl abstraction by ion bombardment at the film surface is also relevant at lower energy input. It is concluded that the densification of HMDSO plasma polymers films is thus governed by an interplay of gas phase and surface processes. This might also be true for other more complex starting molecules used for plasma polymerization.

FOUR

THE RESPONSE OF PLASMA POLYMERIZED HMDSO FILMS TO AQUEOUS ENVIRONMENTS

In this chapter two films deposited using plasma polymerization of HMDSO exhibiting different surface wettabilities are studied with respect to their response to aqueous environments. The amount of water in a near-surface region was quantified for both films.

The work reproduced in this chapter has been submitted for publication. For this publication, I have planned all experiments, performed the neutron reflectomery experiments, analyzed most of the data and prepared the first version of the manuscript. Vikrant Naik performed the IR measurement and helped with data interpretation, Thomas Geue introduced me to neutron reflectometry and assisted in analysis of the obtained reflectometry curves, Olaf Kahle performed the ellipsometry measurements and did a first analysis of the data, Dirk Hegemann corrected the manuscript and gave valuable inputs to data interpretation. Manfred Heuberger supervised this work, corrected the manuscript and helped develop the ideas therein.

4.1 Introduction

Thin films prepared via plasma polymerization are suitable for a wealth of applications, including protective and/or barrier coatings, as well as sensor or biomedical applications [100]. In addition, plasma polymerization offers the possibility of tuning film properties such as hardness, elastic modulus, wettability and chemical composition by accurately controlling the energetic conditions in the plasma gas phase and at the substrate surface [31, 62, 70, 97]. In comparison to conventional polymers, plasma polymers are more branched and cross-linked and contain additional chemical structural elements not found in conventional polymers [104, 149, 150]. Hexamethyldisiloxane (HMDSO) is widely used as a precursor monomer for plasma polymerization due to its suitable vapor pressure (at ambient conditions) and non-toxicity. Moreover, depending on the deposition conditions and admixture of reactive gases such as oxygen, the obtained film properties range from hydrophobic, PDMS-like, to more hydrophilic nano-porous, finally to more inorganic hard films that are based on a stable Si-O-Si backbone containing a small amount of residual hydrocarbon groups. It is thus not surprising that plasma polymerized HMDSO films (pp-HMDSO films) are used in rather diverse applications such as anti-bacterial nanosilver-composite materials, pervaporation membranes, humidity sensors, hydrophobic protective coatings or barrier films [48, 114, 116, 117, 119, 151–154]. In numerous applications the plasma polymer films prepared from HMDSO are in contact with water and, depending on the specific application, need to meet special requirements regarding film stability and film hydration (i.e. penetration of water into the films): a hydrophobic protective film should keep its water repelling properties over long time periods, while for anti-bacterial applications water needs to diffuse through the plasma polymer matrix in order to leach silver ions, which provide the anti-bacterial effect. While many studies report the long term functionality of the respective ap-

plications [114, 117, 119, 152], only few investigate the response of plasma polymerized HMDSO films in aqueous environments directly [119, 155]. Water migration in polymer films is affected by many factors such as porosity, film chemistry or mechanical properties of the film. Models describing the diffusion of water in such systems are thus often highly system-specific and complicated by the different mechanisms involved (pore filling in the cross-linked film, adsorption of water at the pore walls and diffusion of water molecules through the network of interconnected nanometer-sized voids) [156–160]. In addition, siloxane bonds present in HMDSO films can hydrolyze in the presence of water creating hydrophilic Si-OH groups facilitating further the migration of water in the films, which thus leads to a concentration dependent diffusion [96, 161, 162].

Neutron reflectivity (NR) is a technique that is sensitive to fluctuations of scattering length density (SLD) normal to the surface and is suitable to investigate thin films. Moreover, the possibility of increasing contrast between the film and the solution by deuteration makes this method well suited to study the penetration of deuterated water into thin plasma polymerized HMDSO films. Nelson et al. [155] have investigated hydrophilic allylamine (AA) and hydrophobic HMDSO plasma polymer films using neutron reflectometry and showed that the pp-AA film swells considerably in D_2O, while the pp-HMDSO film was found to be essentially impermeable to deuterated water. The same group also conducted a similar study with plasma polymers containing reactive amines, in which they showed that a small change in monomer composition (heptylamine vs. allylamine) results in quite different cross-linking degrees as well as different water uptake and functional group retention [163]. In other neutron reflectometry studies the influence of deposition conditions on film properties and efficacy against protein fouling of plasma polymerized PEG-like films was investigated [150] or the micro-structure of plasma polymerized methylmethacrylate was characterized [164]. In this work,

two plasma polymer films deposited from HMDSO monomer with and without admixture of oxygen [97] were selected and characterized in air using neutron reflectometry and IR measurements. The hydration of the films in aqueous environments was studied in situ with neutron reflectometry. Additional IR measurements after the equilibration of the films in water have been performed and compared to the NR results.

4.2 Experimental Section

4.2.1 Plasma polymerization

The plasma polymers were deposited in a capacitively coupled, RF driven ($f = 13.56$ MHz) reactor described in detail elsewhere [97]. For this study, two different films were deposited according to well established protocols [97, 165]: i) SiO:CH film deposited from a HMDSO discharge and ii) SiO$_x$ film deposited from a plasma with a fixed oxygen-to-HMDSO-ratio of 10:1. The HMDSO monomer was purchased from Fluka and the HMDSO tank including the tubing was stabilized at a temperature of 43°C outside the reactor. The HMDSO total gas flow rate was kept constant at 4 sccm using a thermo-stabilized mass flow controller (also at 43°C). For both deposition conditions, argon (20 sccm) was added as carrier gas. Oxygen and argon were purchased from Carbagas, Switzerland. The gases were mixed outside the plasma chamber and introduced via the same gas shower. The process pressure was fixed at 7 Pa. The HMDSO film and the SiO$_x$ film were deposited using power inputs of 50 W and 100 W yielding a negative self-bias voltage of 70 V and 110 V at the RF electrode, respectively. Prior to deposition of plasma polymer films the substrates were pre-cleaned in Ar/O$_2$ plasma (80 sccm/20 sccm). For neutron reflectometry measurements the films were deposited onto

72

double side-polished silicon blocks (<100>, dimensions: 1 cm $\times$ 5 cm $\times$ 10 cm, SPM, Liechtenstein), while for IR measurements double side-polished silicon wafers (<111>, Si-Mat, Germany) were used as substrates. To coat the silicon blocks, a special sample holder was designed ensuring that the coating conditions at the block surface were homogeneous and comparable to those at the RF electrode (mainly by embedding the block into the RF electrode). The films used for ellipsometry measurements were deposited onto silicon wafers. Reference glass slides and silicon wafers were coated to determine the deposition rate and the film density. The deposited mass was determined by weighing the glass slides directly before and after the deposition process. The film thickness was measured over a masked film edge with a profilometer (Veeco, Dektak 150). The film density was then calculated from the volume and the mass of the coatings.

4.2.2 Neutron reflectometry

Neutron reflectometry measurements were performed using the AMOR reflectometer at the Swiss Spallation Neutron Source (SINQ) at PSI, Villigen, Switzerland [166]. The reflectometer was operated in a time-of-flight mode covering a wavelength range of 0.35 nm to 1.2 nm and the reflectivity was recorded at three angles of incidence (0.5°, 1.5° and 3.2°). Because AMOR is an energy-dispersive instrument, the reflectivity could be obtained in a q-range of 0.01 $\text{Å}^{-1} \leq q_z \leq 0.19 \text{ Å}^{-1}$, where q_z is the magnitude of the momentum transfer vector $\vec{q}$, $q_z = (4 \, \pi/\lambda) \sin \theta$. The reflectivity R of the sample was obtained by dividing the intensity of the reflected beam by the intensity of the incoming beam and normalizing to one. For the measurements in solution, deuterated water (Sigma-Aldrich, 99.9 atom % D) was used instead of "normal" water due to the larger scattering length density (SLD) of D_2O ($\rho = 6.366 \cdot 10^{-6} \text{ Å}^{-2}$) compared to H_2O ($\rho = -5.610 \cdot 10^{-7} \text{ Å}^{-2}$) providing

better contrast between the film and the penetrating solution. The coated silicon substrates were mounted in a liquid cell connected to a cooling/heating system. Each of the investigated films was measured four times: in dry state (i.e. against air), in D_2O at 20°C, then the system was equilibrated for three hours at 60°C before measuring for the third time and the last measurement of each series was again performed at 20°C after letting the system cool down to reach stable conditions.

The data was modeled using the Parratt formalism [167] with the "Parratt32" program [168]. The data was fitted as $\log R$ vs. q_z using a multi-layer model, which includes the silicon block, the native SiO_2 layer, the plasma polymer and the surrounding medium (air or D_2O). If necessary, the plasma polymer layer was subdivided into several layers to approximate a vertical SLD gradient. The SLDs used in the models for Si, SiO_2 and D_2O were $2.073 \cdot 10^{-6}$ Å^{-2}, $3.476 \cdot 10^{-6}$ Å^{-2} and $6.366 \cdot 10^{-6}$ Å^{-2}, respectively.

4.2.3 IR measurements

Multiple transmission-reflection (MTR) FTIR measurements were performed on a home-built MTR set-up (Prof. Shoujun Xiao, University of Nanjing, China) [169]. The double side polished Si wafer was placed between two gold mirrors, 2 mm apart, such that its distance from the two mirrors was 0.3 and 1.2 mm, and the simplified number of transmission passes was six. Only one side of the wafer was coated with plasma polymer film. The spectra were acquired on a Bruker IFS66v FTIR spectrometer in vacuum at a resolution of 4 cm^{-1}, measured using a mercury cadmium telluride (MCT) detector, cooled by liquid nitrogen. A bare, plasma cleaned (conditions as described above) Si wafer was used as background. Each sample and background measurement consisted of 256 scans. The high sensitivity provided by this method allows for the study of thin films as produced in this

work. The films have been measured shortly after deposition and after equilibration in deionized water for 3 weeks (at room temperature).

4.2.4 Ellipsometry

Ellipsometric measurements were performed on a spectroscopic Ellipsometer SE850 from Sentech Instruments equipped with a humidity chamber. The humidity is controlled by mass flow controllers; the humidity range is limited to values between 2% and 80% relative humidity. The incident angle is fixed to 70°. The ellipsometer software is adapted to control and record the humidity. The thickness of the investigated films was 100 ± 5 nm. The films were equilibrated at minimum humidity for 30 minutes before the humidity dependent measurements began. The humidity-time-profile was as follows: ramping from 2% to 80% relative humidity in 40 minutes, holding at maximum humidity for 4 hours, ramping down to 2% humidity in 40 minutes, holding at minimum humidity for 4 hours. Measurements were performed every 2 minutes, i.e. 280 ellipsometric measurements were done for one complete humidity cycle.

The measured ellipsometric angles Ψ and Δ were converted to the thickness d and the (dispersion of) refractive index n by a fitting process using a simple ellipsometric layer model consisting of the silicon substrate, the native SiO_2 layer and the plasma polymer film. The optical properties of the Si-Wafer layer and the 2 nm thick native SiO_2 layer are described by literature data. The plasma polymer layer (HMDSO or SiO_x) was fitted to the Sellmeier equation [170]. A wavelength range from 360 to 800 nm was used. A single value for n is calculated at $\lambda = 589$ nm. Combining n and d allows the calculation of a relative mass of the layer, i.e. with ellipsometric investigations changes in relative mass of the film, Δm_{rel}, (e.g. by water uptake) can be determined, where $\Delta m_{rel} = (m - m_0)/m_0$

with the initial mass m_0.

4.3 Results and Discussion

In this study, two plasma polymer films deposited from the same precursor, namely hexamethyl-disiloxane (HMDSO), with or without the admixture of oxygen to the plasma process have been studied with respect to their chemical structure and response to aqueous environments. Both, the HMDSO film as well as the SiO_x film, have been characterized previously [97]. The here relevant film properties are briefly summarized in Table 4.1.

Table 4.1: Film properties of HMDSO and HMDSO/O_2 (1:10)-derived plasma polymer films

	O/Si	C/Si	film density [g cm^{-3}]	contact angle [°]
HMDSO	0.93 ± 0.01	1.87 ± 0.02	1.24 ± 0.02	102 ± 1
SiO_x	1.91 ± 0.02	0.49 ± 0.01	1.89 ± 0.02	72 ± 2

The reported atomic ratios reveal that the film deposited from the HMDSO plasma is rather PDMS-like, while the addition of oxygen to the process yields films with a more inorganic character. However, the SiO_x film still retains a significant amount of carbon ensuring a certain porosity within the films [162]. To assess the vertical density profile of these plasma polymer films in dry and hydrated state, neutron reflectometry measurements were performed. Neutrons are well suited to investigate polymer films because they interact with the atomic nuclei and thus provide a good contrast also for lighter atoms. In addition, the possibility to increase this contrast by using deuterated water further helps to study the changes in the vertical density profile of the films when in contact with D_2O.

4.3.1 Characterization of dry films

Typical neutron reflectivity curves of HMDSO and SiO_x films measured against air (i.e. in dry state) are shown in Figure 4.1 a). The observed oscillations are Kiessig fringes [171] that arise due to the interference of neutrons reflected at the polymer/air and polymer/substrate interface, respectively. The periodicity of these Kiessig fringes is characteristic for the total thickness of the polymer film, while their amplitude is related to the contrast at the interfaces [172].
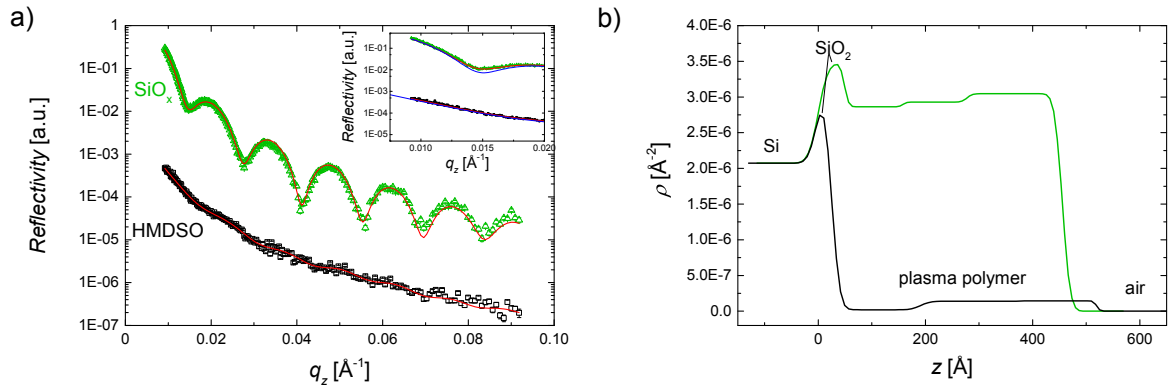
Figure 4.1: a) Neutron reflectivity of plasma polymer films in dry state. Experimental data is shown as green open triangles (SiO_x) and black open squares (HMDSO), respectively. The solid red lines represent the best fits to the experimental data. The HMDSO data are vertically shifted by a factor of 10^{-2} for the sake of clarity. The inset shows an enlargement of the low-q_z range including reflectivity curves resulting from a single-layer model (blue lines). b) Scattering length density profiles resulting from the best fits shown in a) as a function of layer depth z, where the origin of the z-axis is set at the Si/SiO_2 interface.

A layer model including the silicon substrate, the native SiO_2 layer, the plasma polymer layer and the respective medium was assumed for fitting. Modeling the plasma polymer as a single layer of uniform density did not yield satisfying fitting results as shown by the inset in Figure 4.1 a), indicating that the films do not exhibit a homogeneous density perpendicular to the surface. The dry plasma polymer films were thus approximated by three layers of variable thickness and SLD to account for this vertical density gradient. The scattering length density profiles resulting from

the best fits to the experimental data are shown in Figure 4.1 b) and the resulting fit parameters are reported in Table 4.2. The HMDSO film exhibits scattering length densities from $0.02 \cdot 10^{-6}$ Å^{-2} to $0.15 \cdot 10^{-6}$ Å^{-2}, which are similar to the SLD of PDMS [173] highlighting the PDMS-like character of this film. These SLDs present a very weak contrast to air resulting in Kiessig oscillations of low amplitude in the neutron reflectivity. On the other hand, the SLD of the dry SiO$_x$ film varies from $2.86 \cdot 10^{-6}$ Å^{-2} close to the silicon substrate to $3.05 \cdot 10^{-6}$ Å^{-2} at the film/air interface. This film thus provides a good contrast to air and therefore the Kiessig fringes are of higher amplitude. Due to the different contrast of the two films also the deviations of the unsatisfactory one-layer fit in the inset of Figure 4.1 a) seem less pronounced for the HMDSO film than for the SiO$_x$ film.

Table 4.2: Parameters resulting from the best fits to the neutron reflectivity data for the dry films.

		$\rho\,[10^{-6}\,\text{Å}^{-2}]$	thickness [Å]	roughness [Å]
HMDSO			496	
	SiO$_2$		24	14
	layer 1	0.02	167	12
	layer 2	0.14	190	14
	layer 3	0.15	139	5
SiO$_x$			406	
	SiO$_2$		49	14
	layer 1	2.86	109	6
	layer 2	2.93	119	5
	layer 3	3.05	178	8

Pre-cleaning of the substrate in an Ar/O$_2$ plasma leads to rather thick native silicon dioxide layers of 2.4 and 4.9 nm respectively, i.e. thicker in the case of O$_2$ admixture during film deposition. The roughness of the film surface is in accordance with values previously reported from AFM measurements [31, 174, 175]. On the other hand, the roughness parameter of the interlayers can be

understood as smoothness of transition between the layers rather than roughness between two layers with a sharp SLD boundary. These two cases cannot be distinguished by reflectivity measurements [176]. The here fitted scattering length density gradient extends the result of Nelson et al., who observed a homogenous density for a HMDSO film [155]. We cannot exclude that the vertical gradient was induced by post-deposition aging reactions upon contact with air, as it was not possible to measure the films in situ immediately after the deposition. The relatively harsh plasma conditions (ion bombardment and vacuum ultraviolet (VUV) radiation) introduce free radicals within the film that can further react with ambient oxygen or water, leading to the formation of silanol, carbonyl and siloxane groups and a decrease of Si-H within the film [177, 178]. These reactions lead to an overall higher oxygen and lower hydrogen content and thus to an increase of the SLD for neutrons. As these aging reactions depend on diffusion of oxygen (and water) into the films [178], the degree of aging is expected to decrease from the film surface towards the substrate, resulting in a vertical SLD gradient.
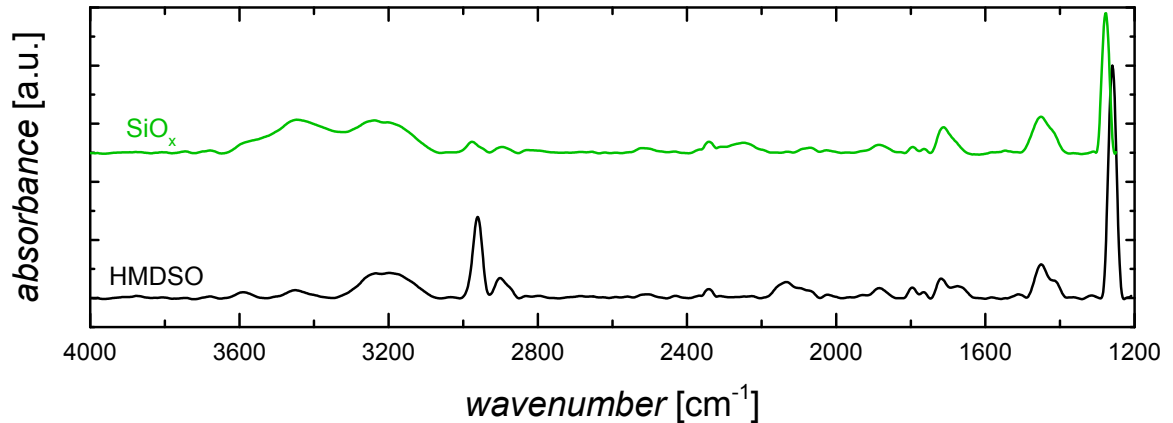
Figure 4.2: IR spectra of the freshly deposited films. Curves are shifted vertically for clarity.

The IR spectra of the plasma polymer films measured shortly after deposition are presented in Figure 4.2. Characteristic peaks were assigned according to literature data [104, 179, 180]. The

HMDSO spectrum exhibits several peaks revealing the PDMS-like structure of this film: asymmetric (2960 cm^{-1}) and symmetric (2905 cm^{-1}) CH$_3$ stretching, asymmetric (1410 cm^{-1}) and symmetric (1260 cm^{-1}) CH$_3$ bending in Si-(CH$_3$)$_x$ with x=1,2,3. The position of this rightmost peak depends on the degree of oxidation of the Si-environment and shifts to higher wavenumbers for higher oxidation states [181, 182]. In addition to these peaks, the spectrum of the plasma polymerized film also exhibits the following peaks: Si-CH$_2$-Si (1355 cm^{-1}), CH$_x$ bending (1455 cm^{-1}), C=O (1710 cm^{-1}), Si-H (2130 cm^{-1}) and -OH (3200 cm^{-1}). In the spectrum of the SiO$_x$ film also shown in Figure 4.2 the peaks related to methyl groups (CH$_3$ stretching and bending) are significantly less intense indicating the lower retention of methyl groups. Additionally, several peaks are shifted to higher wavenumbers confirming the stronger cross-linking and more oxidized Si-environment [181, 183–185]: the peak related to CH$_3$ symmetric bending in Si-(CH$_3$)$_x$ (1277 cm^{-1}), the Si-H stretching vibration (2248 cm^{-1}) and the CH$_3$ asymmetric stretching (2975 cm^{-1}). Also, the C=O peak and the peak around 1450 cm^{-1} (resulting from an overlap of several CH$_x$ bending and/or scissoring vibrations) are more intense and broader confirming the stronger cross-linking of this film. The intensity of the -OH band is higher and broadened exhibiting an additional peak around 3400 cm^{-1} attributed to water or more strongly hydrogen-bonded silanol species [186]. It should be noted here that the region below about 1800 cm^{-1} is difficult to interpret for two reasons: 1) In organosilicon plasma polymers, many chemical bonds like CH$_x$, Si-C related bonds, C=O, C=C show vibrations in this region which may overlap [180] and, in addition, the position of some of these vibrations is dependent on the electronegativity of the surroundings. This complicates an accurate peak assignment. 2) As the films are deposited on silicon wafers, the Si-O-Si stretching vibration around 1050 cm^{-1} (see Supporting Information), to which not only the film, but also the substrate contributes, results in a broad and very intense peak. This band dominates the measured spectrum and also the background

in this region [154, 187], which makes direct comparison of peak intensities difficult. Indeed, in the literature this region of the spectrum is often either not commented on, even if some features are clearly visible, or not shown at all [154, 175, 179, 185, 187–190].

Overall, the information about film density, structural film composition as determined by IR measurements and the chemical surface composition as determined by XPS, the measured scattering length density can be readily reproduced with the aid of the NIST SLD calculator [191] by adjusting the film composition until the calculation matches the experimentally observed SLD. It was thereby assumed that the chemical composition as determined by XPS measurements corresponds to the composition of the outermost layer (i.e. layer 3). For the HMDSO film, the composition reported by Nelson et al. for a similar film [155] was used as a starting point. In addition, based on the IR spectrum, it was assumed that the majority of hydrogen atoms present in the film are present as CH_3. The as-obtained film composition for the outermost layer was $Si_{68}O_{63}C_{131}H_{379}$. In order to account for an aging reactions reported above, a higher hydrogen content and a $\approx 5\%$ lower O/Si ratio was assumed for the innermost layer resulting in a film composition of $Si_{68}O_{56}C_{131}H_{392}$. For the SiO_x film the following film compositions were derived: $Si_{68}O_{130}C_{34}H_{21}$ for the film/air and $Si_{68}O_{126}C_{34}H_{38}$ for the Si-block/film interfaces, respectively. The so determined film compositions are somewhat ambiguous (mainly regarding the exact H content). However, here these compositions should serve more as an estimate of the fraction of hydrogen atoms retained within the films than as exact film compositions. In combination with the independently determined film parameters (density, chemical structure and composition) this estimate seems consistent and yields values of H/C of 2.9 to almost 3 and 0.6 to 1.1 for the HMDSO and SiO_x film, respectively.

4.3.2 Response of plasma polymer films to aqueous environments

Ellipsometry measurements of the two plasma polymer films indicate that the SiO_x film behaves differently in a humid environment than the HMDSO film, as illustrated in Figure 4.3, where we report the relative change in mass upon increase in relative humidity.
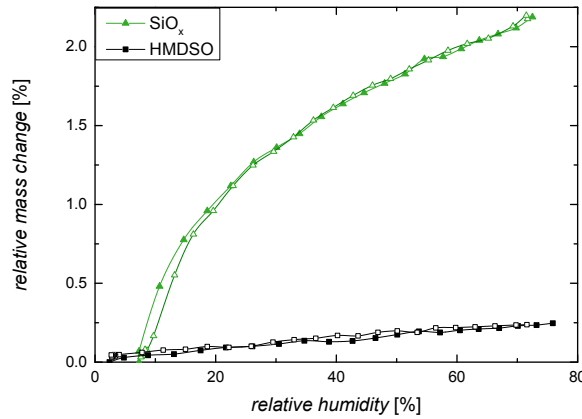

Figure 4.3: Progress of the relative change in mass for the SiO_x (green triangles) and HMDSO film (black squares) measured by ellipsometry as a function of relative humidity. Filled symbols represent increasing relative humidity; open symbols represent decreasing relative humidity.

The increase in relative mass is more pronounced for the SiO_x film ($\approx 2.2\%$) than for the HMDSO film ($\approx 0.25\%$). In addition, the SiO_x film seems to exhibit a slight hysteresis (as seen by the deviation of the open triangles from the filled triangles for a humidity lower than 25%). It is also observed that the change in relative mass is nearly instantaneous (within a few minutes) and that no change occurs over time when holding the humidity constant at 80% (data not shown). This raises the question, whether the observed increase in mass is due to the formation of a water layer on top of the films or rather due to the penetration of water into the films. To discriminate surface film condensation from water penetration, NR measurements have been realized with both films immersed in liquid (where no water layer can be formed on top of the samples).

The behavior in aqueous environment of the two different films was studied by neutron reflectivity measurements in D_2O at room temperature (20°C) and at an elevated temperature (60°C). The measurement at elevated temperature was performed in order to investigate the effect of water surface tension on the degree of solvent penetration. Increasing the temperature to 60°C decreases the surface tension of D_2O by about 10%, which might facilitate D_2O penetration into the films, as the energetic barrier presented by the hydrophobic groups can be overcome more easily by a solvent with lower surface tension. A second measurement at 20°C was performed afterward in order to investigate the reversibility of the respective plasma polymer/D_2O system.
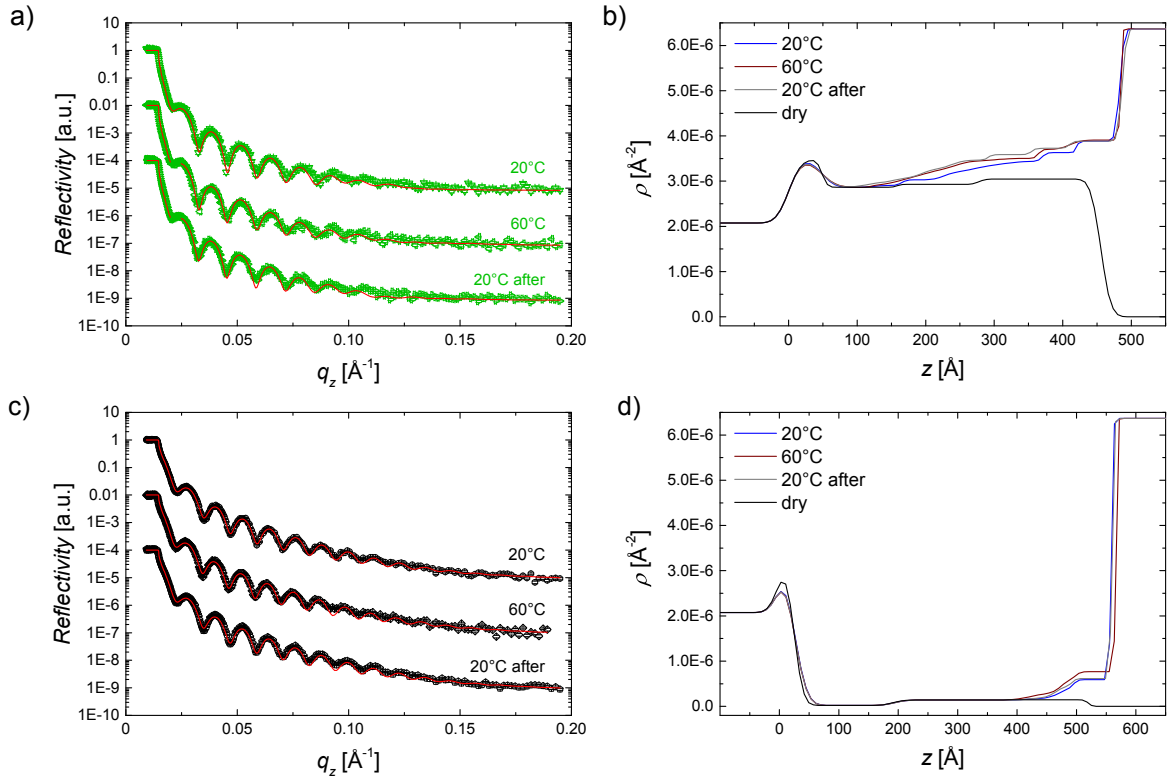
Figure 4.4: Neutron reflectivity of SiO_x a) and HMDSO c) films measured in D_2O at different temperatures. Experimental data are shown as symbols, while the solid red lines represent the best fits. The data sets for different temperatures are shifted vertically for the sake of clarity. Scattering length density profiles for the SiO_x b) and HMDSO d) films as a function of layer depth z, where the origin of the z-axis is set at the Si/SiO_2 interface.

In the NR fitting models for the films measured in D_2O, the roughness and thickness of the SiO_2 layer were fixed to the values obtained for the fitting of the dry films, but to obtain a satisfying agreement between the fit and the experimental data, more layers had to be added (see Supporting Information). In the case of the SiO_x film depicted in Figure 4.4 a), the plasma polymer layer was best approximated by eight similarly thick sublayers, where the thickness of the layers was kept variable during the fitting procedure. The SLD of each layer was allowed to vary within the limiting bounds of the SLDs of the plasma polymer film and D_2O in order to account for possible solvent penetration. The resultant scattering length density profiles are presented in Figure 4.4 b) and the obtained fitting parameters are reported in Table 4.3. A gradual increase of the scattering length density towards the film surface can be observed for all measurements. In addition, the SiO_x film swells by about 7% compared to the dry state and its thickness increases slightly from 434 Å to 438 Å with immersion time in D_2O.

The reflectivity of the HMDSO film is shown in Figure 4.4 c). The model best describing the vertical structure of the plasma polymerized film consisted of a subdivision of the polymer layer into six layers: two thicker layers close to the silicon block and four thinner layers at the film surface. Again, the thickness and SLD of each layer were allowed to adjust to accommodate possible solvent penetration. The SLD profiles resulting from the best fits to the data are shown in Figure 4.4 d). Upon immersion of the film in D_2O at 20°C an increase in SLD at the film surface can be noted, while the SLD close to the silicon substrate remains the same as for the dry polymer. The HMDSO film swells by a similar amount as the SiO_x film compared to the dry state. Increasing the temperature to 60°C results in a pronounced increase of the scattering length density in the outermost layer and to a slight increase in the inner layers. The SLD profile obtained after the second measurement at 20°C is

almost identical to the SLD profile obtained for the first measurement at this temperature indicating

reversibility.

Table 4.3: Parameters resulting from the best fits to the neutron reflectivity data recorded at different temperatures in D_2O. The thickness d and roughness σ of the layers are given in Å, the SLD ρ is given in 10^{-6} Å^{-2}. The total thickness of the films is also indicated for each measurement.

		20°C			60°C			20°Cafter		
		d	ρ	σ	d	ρ	σ	d	ρ	σ
SiO_x		434			436			438		
	layer 1	75	2.86	14	73	2.86	18	67	2.86	16
	layer 2	41	2.91	10	36	2.91	5	39	2.99	18
	layer 3	61	3.03	6	42	3.07	18	39	3.06	10
	layer 4	44	3.19	12	46	3.26	20	45	3.27	14
	layer 5	50	3.36	22	59	3.45	17	53	3.47	14
	layer 6	50	3.44	21	61	3.51	19	63	3.59	5
	layer 7	50	3.63	5	46	3.70	5	55	3.73	5
	layer 8	63	3.88	3	73	3.91	13	77	3.88	5
HMDSO		535			541			537		
	layer 1	169	0.02	17	169	0.02	17	170	0.02	17
	layer 2	190	0.14	16	190	0.14	16	190	0.14	16
	layer 3	38	0.15	16	39	0.15	16	35	0.15	16
	layer 4	52	0.17	16	52	0.29	20	47	0.18	10
	layer 5	22	0.44	17	24	0.62	12	28	0.47	14
	layer 6	63	0.59	5	67	0.77	7	67	0.62	5

The software limitation to a layer model to analyze reflectivity data makes the obtained results

somewhat ambiguous, even if the applied model is based on sound knowledge of the sample compo-

sition. Thus, additional ellipsometry measurements in a humid environment and IR measurements

after equilibration of the films in deionized water for three weeks have been performed to indepen-

dently verify hydration of the films. Figure 4.5 shows the IR spectra after equilibration in water in

comparison to the freshly prepared films.
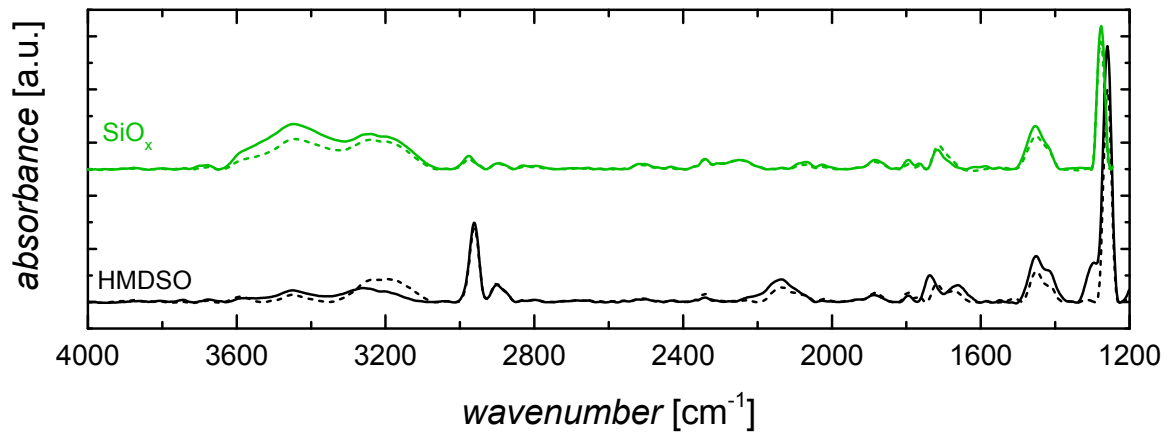
Figure 4.5: IR spectra of the SiO$_x$ and HMDSO film, respectively, after equilibration in water for three weeks (solid lines). The dry spectra are shown as references (dashed lines).

The main differences between the spectra measured in dry and hydrated state can be observed in the OH-region (3000-3800 cm^{-1}). For the SiO$_x$ film the intensity of the OH band increases; especially the peak around 3400 cm^{-1} attributed to more strongly hydrogen-bonded SiOH groups or water [186] is more intense compared to the dry film. For the HMDSO film the intensity of the band around 3200 cm^{-1} decreases slightly, which could be explained by secondary condensation reactions of silanols with water to form siloxane bonds [178]. The other regions of the spectra look very similar in dry and in hydrated state. Slight increases in the CH$_x$ vibrations around 1450 cm^{-1} are observed. It is however not entirely clear whether those changes are due to changes within the films after equilibration in water or due to the large background generated by the broad Si-O-Si vibration band, which makes quantification difficult. Overall, the IR measurements of the hydrated films confirm the picture obtained from the neutron reflectometry study: The SiO$_x$ film is effectively hydrated as shown by the increased intensity of the OH band attributed to water. The two methods used here have rather different sensitivities and resolutions towards vertical gradients: NR is sensitive to vertical changes in SDL on the order of less than 1 nm, while in the IR measurement the signal

is averaged over the complete thickness of the film. A thin layer of different composition at the film surface does not significantly contribute to the total IR signal and may thus be overlooked. The films used for IR measurements were about 100 nm thick, i.e. roughly twice as thick as the films prepared for NR measurements. The absence of water in the IR spectrum for the hydrated HMDSO film does therefore not contradict the result of the neutron reflectivity study, which suggests that some water indeed penetrates into the outermost surface layer of the hydrophobic HMDSO film. Both films are thus effectively hydrated, however not to the same extent.

The increase of scattering length density upon equilibration in heavy water observed in the reflectivity measurements may result from two simultaneous processes: the observed penetration of D_2O into the film and the exchange of hydrogen by deuterium within the film. For the HMDSO film, a deuteration level of 6% can be assumed according to the measurement by Nelson et al. [155] in a similar film. For the SiO_x film on the other hand, the level of proton exchange is not known. Thus, for this film two limiting cases can be considered: the maximal exchange of protons (i.e. all H atoms are replaced by D atoms) and a deuteration level equal to that of the HMDSO film. Assuming the exchange of all hydrogen atoms by deuterium, the NIST calculator [191] yields a scattering length density of $\rho_{film,calc} = 3.60 \cdot 10^{-6}$ Å^{-2} for the SiO_x film. This SLD is lower than the value obtained from the best fit for the outermost layer ($\rho_{film,meas} = 3.88 \cdot 10^{-6}$ Å^{-2}), suggesting that rather D_2O penetrates into the pores of this film. Pore filling by water molecules in similar films has indeed already been observed by others [162, 192]. Using a volume fraction weighted addition [155] of the film scattering length density ($\rho_{film,calc}$) and the solvent scattering length density (ρ_{D_2O}) to explain the determined scattering length density ($\rho_{film,meas}$), gives a solvent volume fraction of about 10% in the outermost layer. A similar degree of solvent penetration was found for hydrophilic heptylamine

plasma polymers [163]. For the other limiting case, i.e. when assuming a lower deuteration level of 6% for this film, a solvent volume fraction of about 25% in the outermost layer is obtained. Thus, the actual solvent content in the outermost layer of the SiO_x film probably lies between these two limits. Towards the inside of the film, the SLD gradually decreases indicating that less solvent reaches the inner sublayers. The roughly 75 Å thick plasma polymer layer closest to the SiO_2 interface still shows the same SLD as in dry state revealing that the heavy water did not reach the substrate surface in significant amounts during the approximately four hours incubation. Nevertheless, the water within the film is not only present at the film surface (top 1-2 nm of the film), but also in an extended sub-surface region. Increasing the temperature to 60°C (i.e. decreasing the surface tension of D_2O) leads to a SLD increase of the inner sublayers of the SiO_x film, while the SLD at the film surface (i.e. in the outermost layer) remains the same. However, the thickness of the outermost layer increases from 63 to 73 Å. The heavy water thus seems to penetrate further into the film, while all the accessible pores at the film surface are filled completely already at 20°C. After reducing the temperature again to 20°C, a slight further increase in SLD in the inner layers of the film is observed indicating a further hydration of the film. The penetration of heavy water into the SiO_x film does thus not seem to be at equilibrium here and the D_2O surface tension seems to play a minor role, while the time of exposure to the solvent appears to be an important factor.

On the other hand, for the HMDSO film a proton exchange of 6% was assumed according to Nelson et al. [155] (i.e. 23 of the 379 H atoms were replaced by D atoms). The NIST calculator then yields a scattering length density of $\rho_{film,calc} = 0.50 \cdot 10^{-6}$ Å^{-2} for the HMDSO film. This SLD is lower than the SLD of the outermost layer as determined by fitting ($\rho_{film,meas} = 0.59 \cdot 10^{-6}$ Å^{-2}) suggesting water penetration into the porous film. Also, this film swells slightly in aqueous environ-

ment and thus indeed does not seem to be completely impermeable to water. Applying the volume fraction weighted addition of the solvent SLD (ρ_{D_2O}) and film SLD ($\rho_{film,calc}$) to account for the observed SLD ($\rho_{film,meas}$) as described above then yields a solvent volume fraction of 2% within the outermost layer of the HMDSO film. This outermost layer extends over about 6 nm in thickness implying that also for the HMDSO film water is present in the sub-surface region. The increase in SLD upon an increase in temperature to 60°C can be explained by a higher amount of solvent (5% in volume fraction) present within the film. The similarity of the SLD profiles obtained at 20°C before and after the heating cycle suggests that the D$_2$O penetration into the HMDSO film is reversibly temperature dependent on the time scale of the experiment. This effect can be attributed partly to the largely retained chain mobility of these films, which allow the methyl groups to optimize their orientation depending on the surrounding medium [139, 193]. The surface tension of the penetrating aqueous solvent thus is also a driving force for hydration of this more hydrophobic film. Note that also the exposure time to the aqueous environment is important for these films: in a previous study, it has been shown that the water contact angle measured after exposure to water for different time periods reaches its equilibrium value only after about two weeks in water [97].

The volume fractions of water within the films obtained above can be transformed into changes in relative mass in order to quantitatively compare the results obtained by neutron reflectometry and ellipsometry. For the SiO$_x$ and HMDSO film Δm_{rel} values of 5-13% and 1.6%, respectively, were calculated using the volume fractions of water in the outermost film layer obtained by NR compared to 2.2% and 0.25%, respectively, from the ellipsometry measurements. Within the error of estimation, both methods thus show a similar amount of water in/on the films. However, for both films the kinetics seem to be different in these experiments: the change in relative mass as determined

89

by ellipsometry is nearly instantaneous and remains constant over a time period of 4 hours, while the SLD profiles as determined by neutron reflectometry evolve with exposure time to D_2O (i.e. more heavy water seems to penetrate into the films with time). In summary, these observations indicate that a quantitatively similar amount of water is taken up by the plasma polymer films as evidenced by ellipsometry and NR, but the kinetics is very different. We therefore conclude that the ellipsometer data shows differences in surface condensation whereas the NR data clearly indicates water penetration into the plasma polymer film.

The diffusion of water in plasma polymer networks containing siloxane bonds is concentration dependent due to the hydrolysis of Si-O-Si bonds and it follows a diffusion-reaction mechanism described by Doremus [96] (see also Chapter 2, section 2.4). Under the assumption that the concentration of so formed silanol groups inside the films is directly proportional to the local concentration of molecular water within the film, c, this model yields a concentration profile that is exponentially decreasing with distance from the film surface for a system approaching equilibrium. Assuming that the change in scattering length density upon penetration of D_2O is directly proportional to the concentration of heavy water in the films, i.e. $\Delta \rho = \rho_{film,meas} - \rho_{dry} \propto c$, this model can be applied to explain the observed SLD profiles. Thus, for each layer in the models $\Delta \rho$ was calculated and plotted as a function of the distance from the surface. Thereby, the "position" of each layer was characterized by the position of the middle of each layer, e.g. the position of the outermost layers was set to be 31.5 Å. Figure 4.6 shows the so obtained profiles for the HMDSO and SiO_x, respectively, measured at 20°C including the fit according to the model described above.

An agreement between the data and the fit is obtained, indicating that the proposed diffusion-reaction mechanism can describe the diffusion of water into the HMDSO and SiO_x plasma polymer
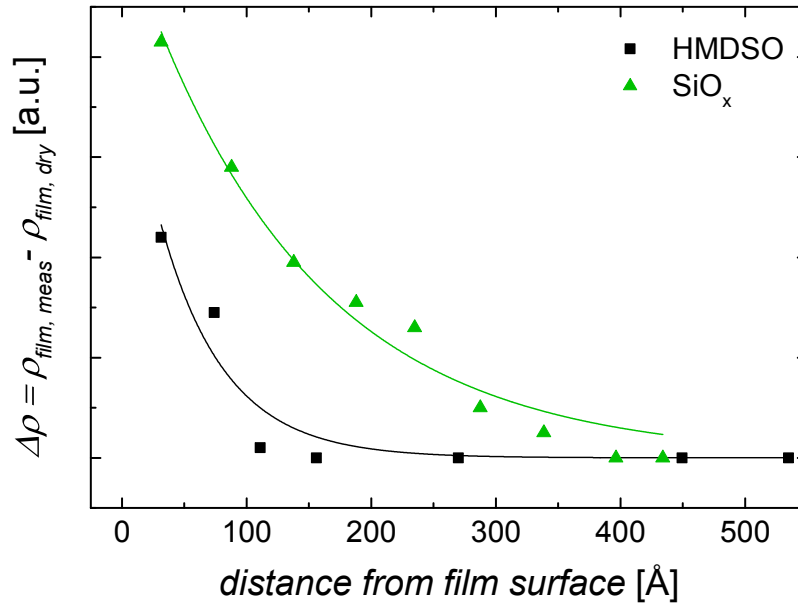
Figure 4.6: $\Delta\rho$ as a function of distance from the film surface for the SiO_x and HMDSO film, respectively. The lines are fits to the data using an exponentially decreasing function according to [96].

films. Water thus reacts with the siloxane network within the film to form more hydrophilic silanol groups that promote further penetration into the films. It is thus not surprising that the outermost surface of the nominally hydrophobic HMDSO film does not remain impermeable to water. Indeed, even PDMS is known to swell in water at equilibrium, albeit at extended equilibration times [194] indicating that the water penetration depth in HMDSO plasma polymers might increase even further on a time scale of several weeks. The outermost region of the HMDSO film that reached saturation is approximately 6 nm thick. Thus, in the more hydrophobic HMDSO film water is not only present at the very surface (top 1-2 nm), but also as sub-surface water in deeper film regions reaching about 15 nm in depth, as indicated by the film region experiencing a significant increase in SLD upon exposure to D_2O. Significantly thicker films can thus serve as kinetic barrier layers against water penetration. Thinner films, on the other hand, can be hydrated and might become interesting for different applications such as, for example, drug release, protein adsorption and bio-sensors. Note

that for both films, the slight gradient observed in dry state might additionally facilitate solvent penetration into the films.

Previously published results of a silver release study through such films ($\approx$ 100 nm thick) are in agreement with the above picture: no silver is released through the HMDSO film (i.e. the water necessary to leach silver ions from the underneath silver layer does not reach the silver layer within the time frame of the experiment) while for the SiO$_x$ film a considerable amount of silver is detected already after one day in water [97].

4.4 Conclusion

The chemical structure and hydration behavior of two siloxane-based plasma polymer films were characterized using neutron reflectometry and complementary IR measurements. In dry state, for both films an intrinsic small density gradient perpendicular to the surface was observed. Seen as a whole, the more hydrophobic HMDSO film was shown to exhibit PDMS-like characteristics, while the more hydrophilic SiO$_x$ film possesses a more inorganic nature and exhibits a higher scattering length density. The behavior of the films in aqueous environments was investigated using in situ neutron reflectometry in D$_2$O at different temperatures. Characteristic SLD profiles reflecting film hydration could be extracted for each film. Both films are hydrated: water penetrates into the nano-porous SiO$_x$ film reaching deep sub-surface regions, while in the nominally hydrophobic HMDSO film the water reaches sub-surface regions in a depth of 10-15 nm. This film is thus not completely impermeable to water. The amount of water diffusing into the films depends on the chemical structure of the plasma polymer film and was found to be 5-13% for the SiO$_x$ film and around 1-2% for the

HMDSO film. The extent of water penetration into the HMDSO film seems to depend on the surface tension of the penetrating aqueous solution and exhibits reversible temperature dependence due to the large chain flexibility of this PDMS-like film. For both films, the diffusion of water into the films can be explained by a reaction-diffusion mechanism, where silanol groups are created along the siloxane network within the film upon reaction with water.

Acknowledgments

4.5 Supporting Information

4.5.1 Fitting of Neutron reflectometry data

To approve the subdivision of the plasma polymer film into several layers in the fitting models, reflectivity curves resulting from models with a fewer number of layers are shown in comparison to the best fits in Figure 4.7 and Figure 4.8 for the HMDSO and SiO_x film, respectively.
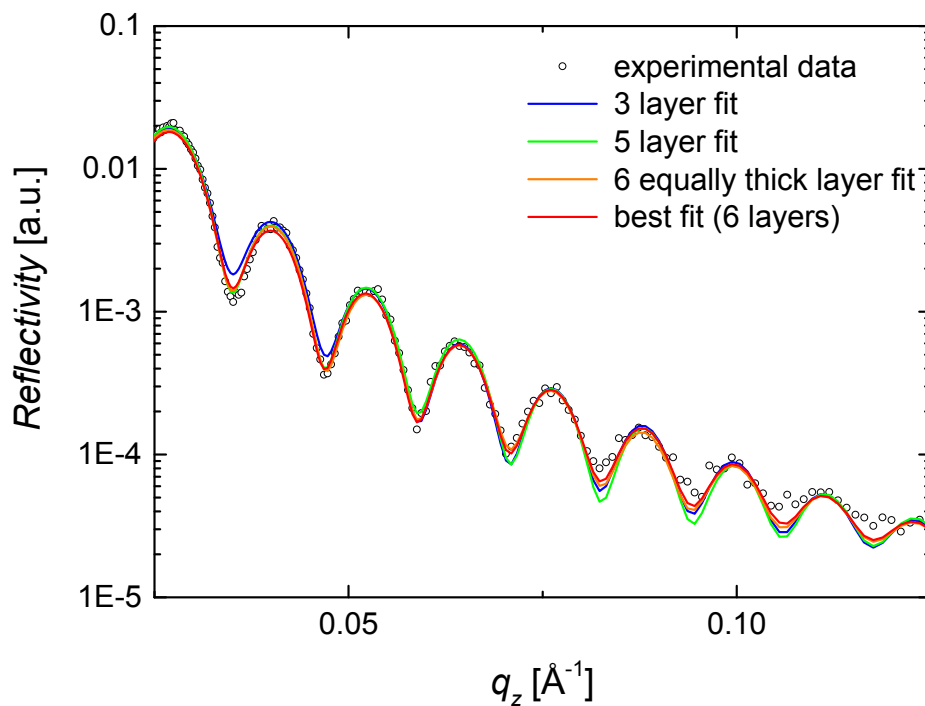
Figure 4.7: Neutron reflectivity curves and corresponding fits for the HMDSO film measured at 20°C in D_2O: best fit (red line), fit resulting from a model with a subdivision of the polymer layer into 3 (blue line), 5 (green line) and 6 equally thick (orange line) layers, respectively.

For the HMDSO film, also a fit resembling the best fit for the SiO_x film film (using a model based on six equally thick layers) was tested, but was shown to be worse than the proposed model. Adding more layers to the model did not significantly improve the agreement between the fit and the experimental data (curves not shown).
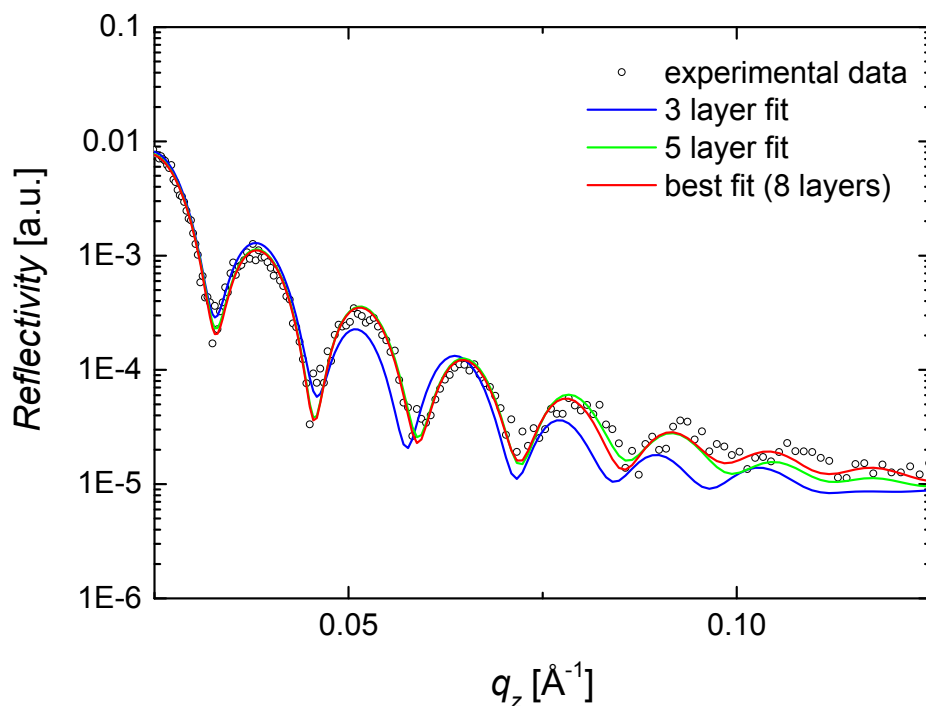
Figure 4.8: Neutron reflectivity curves and corresponding fits for the SiO$_x$ film measured at 20°C in D$_2$O: best fit (red line), fit resulting from a model with a subdivision of the polymer layer into 3 (blue line) or 5 (green line) layers, respectively.

4.5.2 IR spectra

Figure 4.9 shows the IR spectra of the HMDSO and SiO$_x$ films including the region below 1200 cm^{-1}, where the broad Si-O-Si band originating from an overlap of signals from the substrate and the film dominates the spectrum.
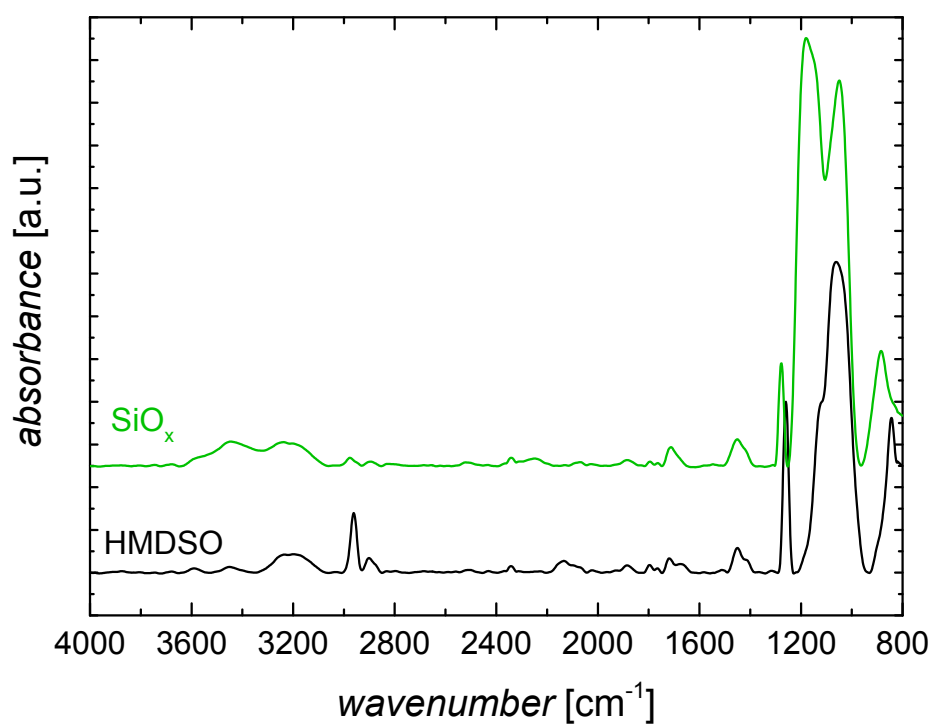
Figure 4.9: Baseline corrected IR spectra of the dry HMDSO and SiO$_x$ films, respectively. The very intense and broad band around 1050 cm^{-1} distorts the spectrum in this region and makes baseline correction and thus also quantitative comparison of spectra in the region below 1800 cm^{-1} difficult.

VERTICAL CHEMICAL GRADIENTS AND THEIR INFLUENCE
ON PROTEIN ADSORPTION

This chapter deals with the production of vertical chemical gradient films using plasma polymerization and their characterization. In addition, the adsorption of bovine serum albumin on these vertical chemical gradients is investigated. It is shown that the vertical chemical gradients significantly influence the adsorption of BSA and it is speculated that this is due to the interaction of sub-surface water within the gradient and the protein.

5.1 Introduction

Gradient surfaces are surfaces with gradually varying physical or chemical properties along a certain direction. Many excellent review articles discussing the fabrication and applications of surface gradients have been published (see e.g. [195–198]). Surface chemical gradients are nowadays mainly produced by coating a surface (with either a self-assembled monolayer (SAM) or a thin polymer

film) in a gradual manner. These methods usually depend on substrate chemistry. Another method of generating chemical gradient surfaces independent of substrate chemistry was introduced by Whittle et al. using plasma polymerization [199, 200]. Thereby, the feed composition containing two different monomers and plasma parameters were varied while a shutter was moved gradually over the substrate to obtain the desired (lateral) chemical gradient. Surface chemical gradients represent a widely used and efficient tool to study (biologically relevant) interfacial phenomena. On one hand, rather fundamental phenomena such as crystallization and morphology in isotactic polystyrene films, reaction kinetics of surface-initiated polymerization or the alignment of liquid crystals on chemical gradients were studied [201–203]. A well-known example is the movement of water droplets along a chemical gradient from the hydrophobic to the hydrophilic end first reported by Chaudhury and Whitesides [204] and further investigated by Daniel et al. [205, 206]. On the other hand, a large variety of studies related to biomedical or biosensing applications, such as the adsorption of (biological) molecules or cell adhesion on chemical gradient surfaces, were carried out [207–213]. The above mentioned studies were all conducted using lateral surface chemical gradients. However, more recently, vertical chemical gradients have attracted considerable interest in the community. These include vertical cross-link gradients in hydrogels [27], hydrophilic top layers on hydrophobic PDMS by controlled diffusion of amphiphilic block-co-polymers [28], gradient polymers, where the chemical composition gradually changes along the chain [29, 214], or vertical chemical gradients obtained by copolymerization of two monomers while gradually changing the composition of the reaction mixture [215, 216]. Vertical gradients are expected to affect the adsorption of amphiphilic molecules such as surfactants, lipids or biological macromolecules like proteins [30] if the length scale of the gradient is similar to the dimension of the adsorbing species.

Proteins are amphoteric polyelectrolytes composed of amino acid subunits, which exhibit different characteristics such as charge and hydrophobicity. Apolar parts tend to be buried inside the protein, while charged groups are likely to be found at the outside of the protein [217]. Proteins fold into unique three dimensional structures, which depend on the amino acid sequence and the interactions amongst the amino acids and their interaction with the surrounding solution. The protein surface is generally not homogenous, but rather composed of domains of different characteristics (charge, wettability, ...), which influence the interactions with the surface. Protein adsorption to various kinds of surfaces has been extensively studied due to the relevance of this phenomenon for many applications in biology, (bio-)medicine, biotechnology or food processing [12]. The adsorption of proteins is often the first event in biological processes and plays a key role in e.g. blood coagulation, cell adhesion and growth [15]. However, so far, no general consensus on the driving forces for protein adsorption exists (see e.g. review [11] and references therein). Several different interactions between the protein and the surface are discussed to be relevant. On one hand a complex interplay of pair-wise electrostatic or ionic interactions, van der Waals interactions and also hydrophobic interactions are proposed to drive protein adsorption [15, 18–20]. Others claim that the main driving force of protein adsorption are hydrophobic interactions causing the structuring of water around the molecules and at the interface, which will either favor or suppress protein adsorption depending on the strength of the water-surface interaction [11, 21–23]. In both views, the adsorption process is influenced by many factors such as buffer solution pH and ionic strength, temperature and surface free energy, either by directly including these factors into the models describing protein adsorption or by considering them indirectly via their influence on the water structure at the interface.

The adsorption of proteins is often described in terms of an adsorption isotherm relating the adsorbed amount to the concentration of protein in solution. The shape of the adsorption isotherm can give

insight into the affinity between the protein and the surface. However, to evaluate this affinity a model describing the protein-surface interactions is required, from which the adsorption isotherm can be derived and compared to experimental results [217]. The Langmuir isotherm [78] is an example of such a model (see also Chapter 2, section 2.3.2 for other adsorption isotherms). The kinetics of adsorption provide further understanding about the mechanisms driving the adsorption process. This adsorption/desorption process can be divided into several sub-processes: the transport of the protein toward the interface, attachment of the protein at the interface, conformational changes in the adsorbed protein, detachment of the protein from the interface and the transport of the protein away from the interface. In principle, each of these sub-processes can govern the overall kinetics of the adsorption process. At low protein concentrations, the transport of protein toward the interface is usually the limiting step, such that the measured kinetics provide information about the transport process to the surface, but not about the actual adsorption kinetics [217]. It has additionally been observed for mixtures of different proteins (as e.g. in body fluids) that the adsorption proceeds in several steps according to the so-called Vroman effect [218]. First, the smaller, more mobile proteins adsorb at the surface. In subsequent steps, these small proteins are then replaced by larger proteins having a higher affinity for the surface.

Considering all possible factors influencing protein adsorption, it is not surprising that, despite the advances made in the field in the last few years, a complete understanding of protein adsorption on surfaces is still missing. Surface free energy, long range van der Waals interactions as well as hydrophobic interactions are discussed as important (direct or indirect) driving forces for protein adsorption [21, 219–222].

Traditionally, adsorption is discussed in terms of the very surface properties, which indeed only

involves the top layer of atoms or molecules. Here, we would like to test the hypothesis that a gradient vertically lying below the surface will be able to affect the way molecules having amphiphilic functional groups adsorb. This vertical gradient has to be physically and chemically stable during such adsorption experiment. Plasma polymerization is a versatile technique to produce vertical gradients exhibiting the desired properties: the chemical composition of the deposited layer can easily be controlled by controlling the gas composition and energy input [34, 35] and the inherently high cross-linking degree of such films provides enhanced stability. Additionally, the chemistry of the substrate is not a limiting factor for this technique. For films deposited from hexamethyldisiloxane (HMDSO)/oxygen plasmas, it was shown that a broad range of wetting properties can be achieved by accurately controlling the O_2/HMDSO ratio and the power input into the plasma [97, 223]. Films exhibiting PDMS-like character are deposited from undiluted HMDSO discharges, while the admixture of oxygen to the plasma process leads to the abstraction of hydrocarbon groups in the gas phase yielding more inorganic, SiO_2-like films [223, 224]. For the production of vertical chemical gradients a deep understanding of the respective plasma and film forming processes is thus required. Hydrophilic-to-hydrophobic gradients can then be obtained in a controlled way by gradually removing the oxygen from the plasma and adjusting the process parameters to meet the desired gradient properties such as thickness and specific energy of the gradient.

In this chapter, we show that it is readily possible to produce vertical chemical gradients via plasma polymerization by precisely controlling the deposition conditions and the gas composition in the plasma. The obtained gradients were characterized by X-ray photoelectron spectroscopy (XPS) and contact angle measurements. In addition, the adsorption of bovine serum albumin (BSA) on these gradient surfaces was measured using the Transmission Interferometric Adsorption Sensor

(TInAS) [36] in order to test the hypothesis that protein adsorption is affected by the presence of the vertical chemical gradient structure.

5.2 Experimental section

5.2.1 Plasma polymerization

The plasma reactor and experimental setup are described in detail in Chapter 3 and reference [97]. Hydrophilic-to-hydrophobic gradients were produced in the following way: first, a more hydrophilic, nano-porous SiO_x film was deposited using a fixed oxygen-to-HMDSO-ratio of 10:1 or 15:1 and a nominal power input of 100 W (yielding a bias voltage of 123 and 109 V and deposition rates of $R = 25$ nm/min and $R = 22$ nm/min, respectively) according to well established protocols [97, 165]. Then, by removing the oxygen from the process and adjusting the nominal power input to 30 W ($R = 20$ nm/min) for the 15:1 SiO_x bottom layer or 50 W ($R = 28$ nm/min) for the 10:1 SiO_x bottom layer, respectively (yielding bias voltages of 38 V and 66 V, respectively), a gradient with a hydrophobic surface layer was obtained. For all deposition conditions, a pressure of 7 Pa was maintained within the plasma chamber. A computer-based control of the RF generator thereby ensured reproducible and well-controlled deposition times and conditions. For film characterization using XPS and contact angle measurements, the gradients were deposited onto silicon wafers, while for the adsorption measurements TInAS sensors (described below) were coated. To determine the deposition rate and the film density, reference glass slides and silicon wafers were coated. The deposited mass was determined by weighing the glass slides directly before and after the deposition process. The film thickness was measured over a masked film edge with a profilometer (Veeco,

Dektak 150) at minimum five positions along the film edge. The film density was then calculated from the volume and the mass of the coatings.

5.2.2 Surface characterization

Contact angle measurements

Water contact angles were determined using a software controlled drop shape analyzer (DSA 25, Krüss, Germany). For each sample, several drops at different positions on the sample were measured. The surface free energy was determined applying the OWRK method [73–75] using deionized water, hexadecane, ethylene glycol, glycerol and diiodomethane as measuring liquids. Contact angles and surface free energies were determined for the freshly prepared films as well as after storage in water for one day. The latter samples were taken out of the water, gently blown dry and contact angles were measured within 1-2 minutes. Measurements after one day in water were performed to estimate the surface free energy experienced by the adsorbing proteins in later adsorption studies, where the surfaces were stored in water overnight before starting the adsorption experiment.

Atomic force microscopy

Film morphology was assessed using atomic force microscopy at ambient conditions using a Nanosurf easyscan2 AFM (Nanosurf AG, Switzerland) in tapping mode with NCLR-20 cantilevers (resonance frequency = 190 kHz, force constant = 48 N/m from Nanoworld, Switzerland). An area of 1 μm by 1 μm was scanned in 256 lines with a speed of 1 s per line. For each sample, at least 3 different positions were imaged and gave reproducible results.

X-ray photoelectron spectroscopy

The chemical composition of the films was analyzed by X-ray photoelectron spectroscopy (XPS) measurements. For the gradients produced at 30 W nominal power input the utilized instrument and measurement conditions were described in Chapter 3 and reference [97]. The vertical gradient surfaces prepared at 50 W nominal power input were measured using a PHI VersaProbe II equipped with a hemispherical electron analyzer and a monochromatic Al Kα (25 W, 1486.6 eV) X-ray source. The base pressure was approximately $5 \cdot 10^{-8}$ Pa. For these samples, survey and high resolution spectra were recorded using pass energies of 187.85 and 29.35 eV and step widths of 0.800 and 0.125 eV, respectively. Charge neutralization was carried out with low energetic electrons as well as low energy Ar ions.

XPS is a surface sensitive technique because only photolectrons emitted near the surface can escape without energy loss and be detected. The distance the emitted photoelectrons travel within the sample without loss of energy or change of direction is the so-called attenuation length λ_X, which is related to the inelastic mean free path. Normal to the surface, 63% of the signal originates form an escape depth smaller than λ_X, 86% from an escape depth smaller than $2\lambda_X$ and 95% from an escape depth smaller than $3\lambda_X$. By increasing the take-off angle θ_X, the mean escape depth of the photoelectrons decreases by a factor of $\cos\theta_X$ as illustrated schematically in Figure 5.1.

In this way, the mean escape depth of the photoelectrons is varied and in-depth information of the atomic composition of the sample can be obtained in a non-destructive way. Thus, instead of depth profiling using sputtering with high energy argon ions, which is known to destroy and/or alter chemical bonds in polymeric materials [225], angle resolved measurements were performed at
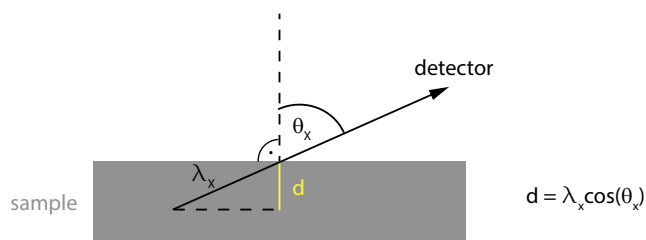
Figure 5.1: Illustration of measurement geometry for XPS measurements. The X-ray radiation hits the sample at an angle θ_X from the surface normal and has an attenuation length λ_X in the sample. The mean escape depth can then be calculated accordingly.

minimum three different take-off angles, θ_X: 20°, 45°, (55°) and 70° in order to assess the in-depth film composition. The inelastic mean free paths in the HMDSO and SiO_x films determined with the NIST electron Inelastic-Mean-Free-Path database, version 1.2, [226] using film compositions determined by neutron reflectometry [227] differed only by about 10% and were thus considered to be identical in the course of further analysis. The atomic concentrations were calculated using CasaXPS Version 2.3.12 software with instrument specific sensitivity factors. Charging effects were compensated by referencing the C 1s peak to 285.0 eV.

5.2.3 Protein adsorption measurements

The adsorption of bovine serum albumin (BSA, purchased from Sigma-Aldrich as lyophilized powder, purity $\geq 96\%$) was studied using the Transmission Interferometric Adsorption Sensor (TInAS), an optical technique based on thin-film interference [36]. Special sensors consisting of clean glass substrates coated by a thin layer of aluminum covered by 2.5 μm of sputtered SiO_2 are used. At each optical interface, partial reflections of the light passing through this sensor stack will interfere and generate an interference spectrum with characteristic maxima and minima. The transmitted light is

transferred to spectrometers (USB2000 and USB2000+, Ocean Optics, USA) via an optical fiber. A software is then used to detect the wavelengths corresponding to the interference maxima that are correlated to the optical film thickness. Typically, the sensor surface is exposed to a solution containing the desired adsorbate and the interference spectrum is monitored in real time. Upon adsorption of molecules to the sensor surface, the peak maxima are shifted in wavelength and from this shift, the optical thickness of the adsorbed layer can be determined. The adsorbed optical thickness D may then be transformed into adsorbed optical mass per unit area M using

$$M = \frac{n_A - n_s}{dn/dc} \cdot D \qquad (5.1)$$

with the solvent refractive index n_s, the dry refractive index of the adsorbate n_A and the refractive index increment dn/dc, respectively [228]. The TInAS allows measurements at high sampling rates (> 10 Hz) with a sensitivity of 1 ng/cm^2. For the here relevant substances (BSA and water) the following parameters were used: $n_A = 1.599$ [229], $dn/dc = 0.182$ cm^3/g [230] and $n_s = 1.337$. In a typical experiment, the sensor was coated with a plasma polymerized vertical gradient layer and mounted in the TInAS flow cell. A baseline in deionized water was measured overnight at 20°C. At time $t = 0$ min 1 ml of 5 mg/ml BSA solution was injected and the adsorption process was followed for 2.5 hours. A rinsing step with deionized water was then performed in order to remove proteins that were reversibly adsorbed on the surface. Over a time span of 1 hour no significant desorption could be detected indicating irreversible adsorption. The pH of this solution was determined to be 5-5.5, which is slightly higher than the isoelectric point of BSA at pH = 4.9 [231], i.e. the BSA molecules were slightly negatively charged. The protein adsorption on each vertical gradient was measured at least 3 times in order to ensure reproducibility.

5.3 Results and Discussion

5.3.1 Characterization of plasma polymerized vertical chemical gradients

Vertical chemical gradients of different nominal thicknesses and varying energy density were produced according to the protocol described in section 5.2.1 and characterized using X-ray photoelectron spectroscopy and contact angle measurements.

Water contact angle measurements

Water contact angles on the vertical chemical gradients of different thicknesses were determined and are reported in Figure 5.2.

With increasing gradient thickness, the water contact angle increases until eventually approaching the value of the hydrophobic HMDSO top layer at a gradient thickness of 4 nm. This is true, both, for freshly prepared samples as well as for samples that were stored in water for one day. As the contact angle probes the top 1-2 nm of a surface, it will react to changes in surface chemistry in the order of this length scale. We therefore define the surface of the gradient as the top nanometer, while the region below this depth will be referred to as sub-surface. The increasing contact angle thus indicates an increasing hydrophobicity at the film surface. An increase of the contact angle due to increased surface roughness can be excluded, as the mean square roughness R_{ms} is found to be constant for all gradients produced (see table 5.1). It has been suggested that plasma polymerization might proceed via an island-like film growth [174, 232], which would also affect the water contact angle. The tendency to form islands in the early stages of film growth is strongly dependent on the adhesion tension between the film-forming species and the substrate as well as on the cohesion
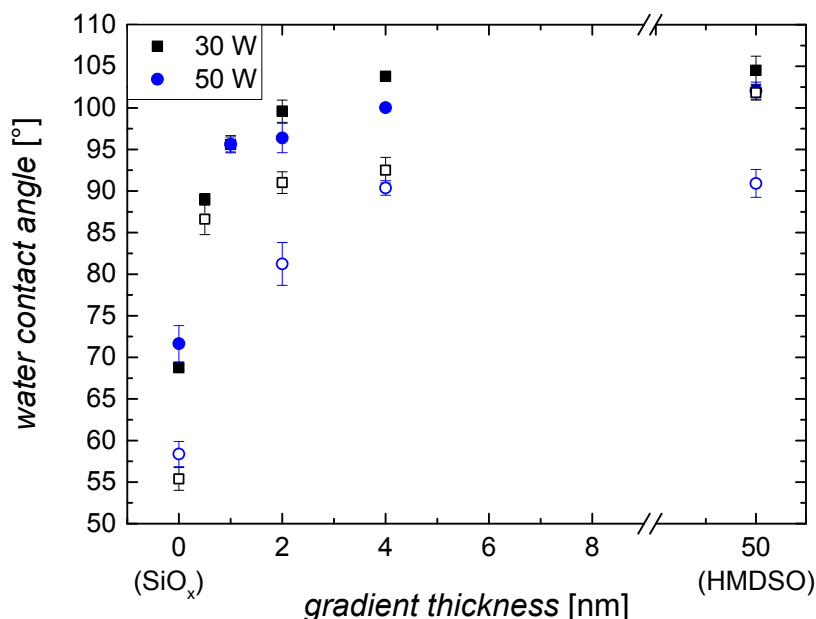
Figure 5.2: Water contact angle as a function of gradient thickness for gradients produced at nominal power inputs of 30 W (black squares) and 50 W (blue circles), respectively. Thereby a thickness of 0 nm corresponds to the plain hydrophilic SiO_x bottom layer and a thickness of 50 nm corresponds to the plain hydrophobic HMDSO top layer. Open symbols depict measurements after storage for one day in deionized water. Error bars represent standard deviations from several drops measured at different positions on the same sample.

energy and the mobility of the film-forming species. For film-forming species exhibiting a high mobility on the surface, but unfavorable adhesion energy, dewetting occurs and islands are formed. On the other hand, for species with a favorable adhesion energy, i.e. species that can readily form bonds with the substrate, a layer-by-layer growth is expected [232]. Due to the chemical similarity within the SiO_x/HMDSO interphase and the high surface mobility of the film-forming species in a plasma deposition environment, the vertical gradient is thus expected to grow layer by layer. Indeed, it has been shown that organosilicon plasma polymers form closed layers already at the early stage of film growth [233]. In the present case, island-like film growth is thus unlikely.

The interaction strength of the vertical chemical gradients can be characterized by a specific

energy (or energy density) given by the difference in surface free energy between the bottom and top layers $\Delta\gamma$ compared to the dimension of the gradient d, i.e. $\Delta\gamma/d$. Therefore, in addition to the water contact angle also the surface free energy was determined for the SiO_x and the HMDSO films for the freshly prepared films as well as for films that were stored in water for one day. Results of these measurements as well as the resulting specific gradient energies are reported in table 5.1.

Table 5.1: Surface roughness, surface free energy and specific energy of the vertical chemical gradients produced at 50 W nominal power input in comparison to the plain SiO_x and HMDSO films.

	SiO_x	1 nm	2 nm	4 nm	HMDSO
R_{ms} [nm]	0.33	0.30	0.30	0.29	0.33
surface free energy γ [mJ/m^2] (fresh)	33	-	-	-	24
specific gradient energy [MJ/m^3] (fresh)	-	9	4.5	2.25	-
surface free energy γ [mJ/m^2] (1 day in water)	43	-	-	-	29
specific gradient energy [MJ/m^3] (1 day in water)	-	14	7	3.5	-

The SiO_x film exhibits a slightly higher surface free energy, which is indicative of a more inorganic film that still contains some hydrocarbon groups (see Figure 5.3). This difference is enhanced after storage in water for one day and may be attributed to faster and more extensive water penetration into this film compared to the HMDSO film [97].

X-ray photoelectron spectroscopy

XPS measurements of the vertical chemical gradient films were carried out in two different ways: 1) measurements at a take-off angle of $45°$ of the differently thick gradients produced at 30 and 50 W and 2) angle resolved measurements at different take-off angles for individual gradients produced at 30 W. In method 1), all measurements were taken at the same take-off angle and thus the detected

photoelectrons originate from the same mean escape depth, assuming that the mean free path is the same in HMDSO and SiO$_x$ films. Thus for different gradient thicknesses, the X-ray radiation probes different parts of the vertical structure (see also Figure 5.4 for illustration). The sample compositions obtained by this method are reported in Figure 5.3 a).
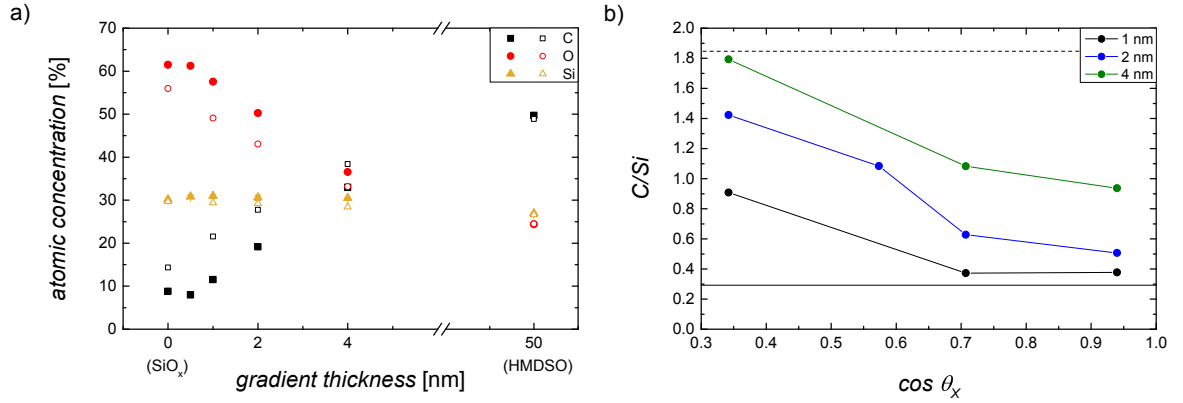
Figure 5.3: a) Atomic concentrations obtained for vertical gradients as a function of gradient thickness. Thereby a thickness of 0 nm corresponds to the plain hydrophilic SiO$_x$ bottom layer and a thickness of 50 nm corresponds to the plain hydrophobic HMDSO top layer. Filled and open symbols represent the gradients produced at 30 W and 50 W nominal power, respectively. b) C/Si atomic ratio for gradients produced at 30 W nominal power input as a function of $\cos\theta_X$, i.e. mean escape depth. The solid and dashed black lines indicate the C/Si value obtained for plain SiO$_x$ and HMDSO films, respectively.

The oxygen concentration gradually decreases from the plain hydrophilic bottom layer without gradient (thickness = 0 nm) to the plain hydrophobic top layer with a thickness of 50 nm. The opposite is true for the carbon content: as the gradient thickness is increased, more carbon is detected, eventually reaching maximum values of 49.7% C for the HMDSO film deposited at a nominal power input of 30 W and 48.9% C for the HMDSO film deposited at 50 W. Hence, these results confirm the trend observed for the water contact angle measurements. The silicon content within the films stays nearly constant for all gradient thicknesses for both deposition conditions. Figure 5.3 b) depicts the in depth variation of the C/Si atomic ratio of the vertical gradients produced at 30 W obtained by measurement method 2). For all gradients, the C/Si ratio gradually decreases with increasing escape

depth. The thinnest (1 nm) gradient thereby approaches the value for the hydrophilic SiO_x bottom layer (indicated by the black line) at the highest sampling depth, while closer to the surface, the value of the hydrophobic top layer (black dashed line) is not fully reached. On the other hand, for the 4 nm gradient, the measurement closest to the surface yields a value of C/Si approaching the value corresponding to the hydrophobic top layer, while at higher sampling depths C/Si is significantly higher than the value for the hydrophilic reference. As schematically illustrated in Figure 5.4 this difference arises from the photoelectrons collected at different take-off angles θ_x that probe different parts of the vertical structure.
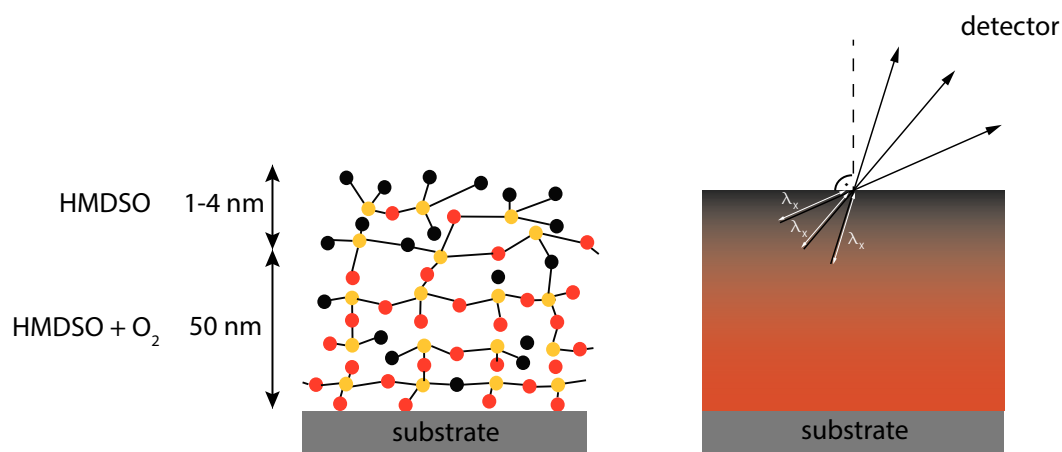
Figure 5.4: Schematic illustration of the produced vertical chemical gradient. On the right hand side the different sampling situations for angle resolved XPS are illustrated.

When the gradient is thick enough, i.e. reaching a minimal thickness of 4 nm, the hydrophobic layer "shields" the hydrophilic bottom layer, while for the very thin gradient the signal is dominated by the hydrophilic layer.

The results obtained from the characterization of the chemical gradients using XPS, AFM and contact angle measurements thus confirm the intended vertical chemical structure and the possibility

to tune the thickness as well as the specific energy of the gradient by accurately controlling the plasma process parameters.

5.3.2 Adsorption of bovine serum albumin on vertical chemical gradients

Protein adsorption is known to be controlled by physical and chemical properties of the surface like hydration, surface free energy, charges, polarity, roughness, etc, but also solution properties like composition and chemical potentials of the studied protein solution [15]. A simple comparison of the energy density contained in vertical gradients with the adsorption enthalpy of BSA [234] per protein free volume reveals the same order of magnitude (≈ 1 MJ/m^3) . Therefore, the vertical chemical gradients are indeed able to significantly alter the energetics of BSA adsorption provided the protein or surrounding water interacts with the gradient. To this end, the protein adsorption on vertical chemical gradients is explored in more detail.

The adsorption of bovine serum albumin (BSA), a globular protein, was measured using the Transmission Interferometric Adsorption Sensor (TInAS) [36], which allows following the adsorption process time-resolved and thus to determine adsorption kinetics together with the amount of adsorbed protein. As a reference, the adsorption on both types of plain plasma polymer films was investigated to establish reference values. In a second step, it was investigated how a vertical chemical gradient between the two types of plasma polymer films influences the adsorption of BSA. The measured adsorption curves were fitted to known models. Different kinetic models for the adsorption of proteins at the liquid/solid interface have been proposed [83, 88, 90, 92, 93] (c.f. Chapter 2, section 2.3.3). The mixed order equation [90] represents an intermediate behavior between first and second order kinetics and is therefore often applied successfully to describe experimental data [86, 235].

112

Its mathematical form is equivalent to the solution of to the Langmuir equation [78]. However, it can also be used to describe adsorption that does not fulfill the assumptions of Langmuir adsorption. Figure 5.5 shows the measured curves for the adsorption of BSA on the reference films of plain SiO$_x$ and plain HMDSO including the fits according to the mixed order model (Chapter 2, equation (2.37)). After rinsing with water no significant desorption was observed (not shown), i.e. the protein adsorbed irreversibly on both surfaces.
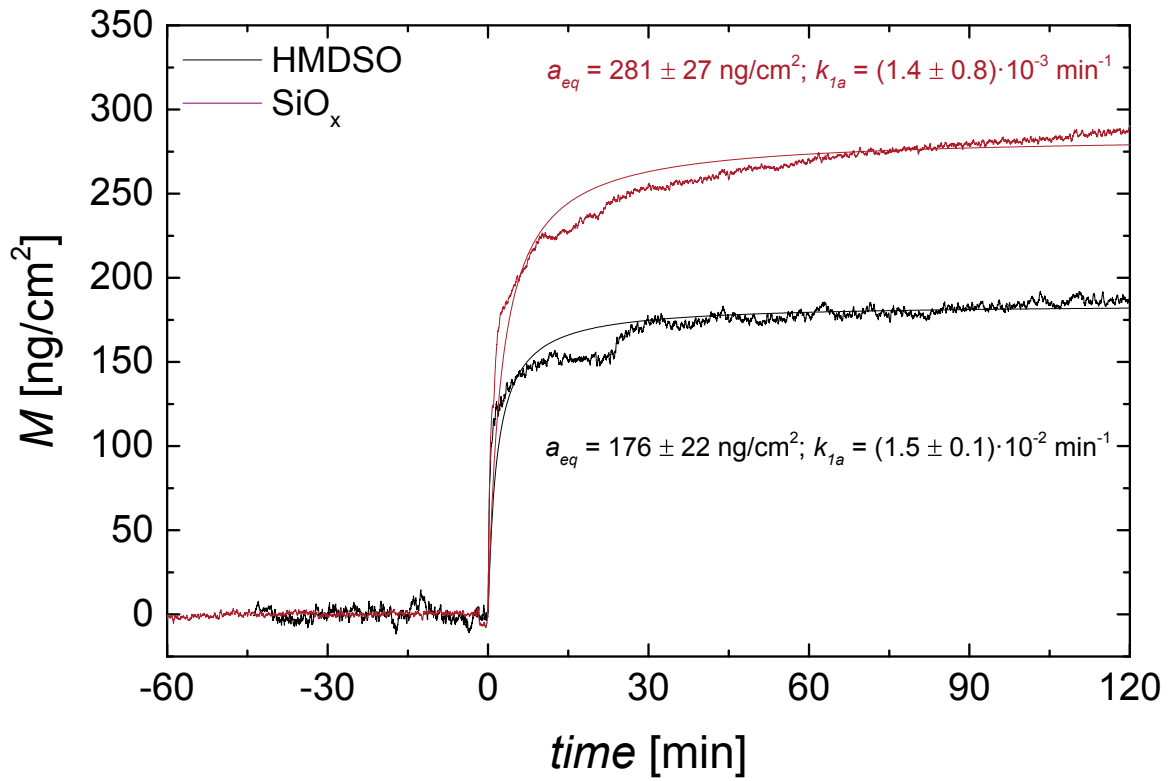
Figure 5.5: Adsorption curves of BSA on hydrophobic HMDSO films and more hydrophilic SiO$_x$ films. The smooth curves show the fit using a mixed order equation (Chapter 2, equation (2.37)). The mean values of the fitting parameters a_{eq} (adsorbed amount at equilibrium) and k_{1a} (adsorption rate constant) for all measurements on a specific surface are indicated in the graph.

A smaller amount of protein adsorbed on the plain hydrophobic HMDSO film (thickness of 50 nm). The adsorption kinetics is also faster on this plain HDMSO reference than on the plain SiO$_x$

film. A similar difference in adsorption kinetics has been observed for the adsorption of proteins onto polymer surfaces of varying hydrophobicity: a faster initial adsorption rate was observed on more hydrophobic surfaces and was attributed to the strong hydrophobic interaction between proteins and hydrophobic polymer surfaces [236]. The strong interaction between the hydrophobic groups located at the inside of the protein and the hydrophobic surface can lead to a conformational change of the soft proteins like BSA. The displacement of water molecules by the protein is thermodynamically favorable. Indeed, the measured mean optical thickness of the adsorbed BSA layer ($d \approx 1.2 \pm 0.1$ nm) is smaller than the diameter of BSA (dimensions of hydrated BSA, elongated ellipsoidal shape): 4 nm $\times$ 4 nm $\times$ 14 nm [237]) indicating a considerable flattening of the protein upon adsorption. Adsorption of BSA on the hydrophobic HMDSO films thus leads to a substantial change in the conformational structure of the protein.

For the more silica-like SiO_x electrostatic or polar interactions are responsible for a stronger surface hydration. Proteins compete for the surface with water. On hydrophilic surfaces proteins adsorb in a more native hydrated state and flatten less. As a result of the smaller surface area occupied per protein molecule the surface density of adsorbed proteins is larger and we measure higher adsorbed mass.

The energy density of a vertical chemical gradient is comparable to the adsorption enthalpy for BSA (per interaction volume) and we expect significant changes in adsorption energetics. Figure 5.6 depicts representative adsorption curves measured on vertical chemical gradients of different energy density (see table 5.1).

Indeed, the amount of protein adsorbed on the vertical chemical gradients is reduced compared to both the amount adsorbed on the plain HMDSO and SiO_x reference surfaces. Furthermore, the ad-
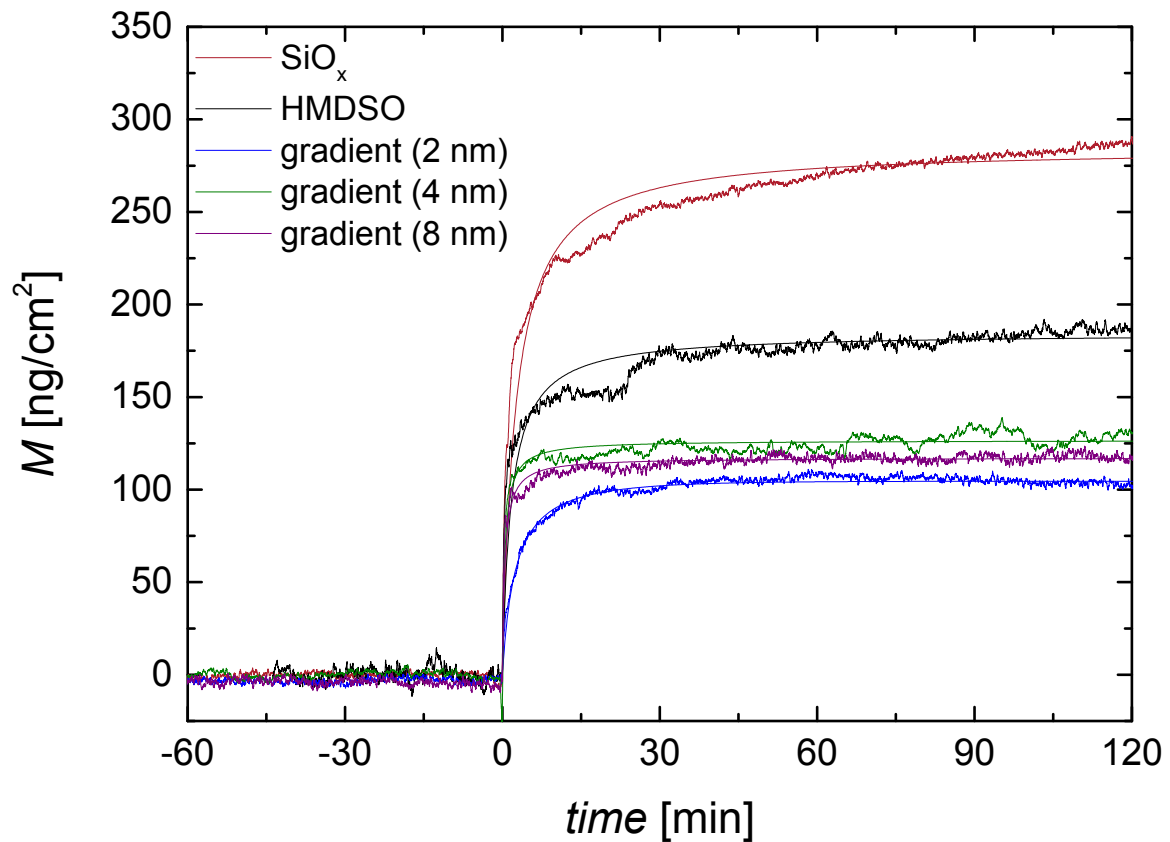
Figure 5.6: Adsorption curves of BSA on vertical chemical gradients produced at 50 W nominal power input with different specific energies in comparison to HMDSO and SiO$_x$ films. The smooth curves show the fits using a mixed order equation (Chapter 2, equation (2.37)).

sorption kinetics are slower on the vertical gradient coatings compared to the hydrophobic HMDSO film. This trend resembles protein adsorption on the more hydrophilic SiO$_x$ surface. It is interesting to note that the gradient thickness (i.e. gradient energy density) seems to play a minor role, since the observed differences were found to be small following no clear trend. To better illustrate the effects of the vertical chemical gradients on adsorption of BSA, the fitting parameters resulting from a fit using the mixed-order equation (Chapter 2, equation (2.37)), namely the adsorbed amount at equilibrium, a_{eq}, and the adsorption rate constant, k_{1a}, obtained for the different gradients investigated are reported in Figure 5.7.
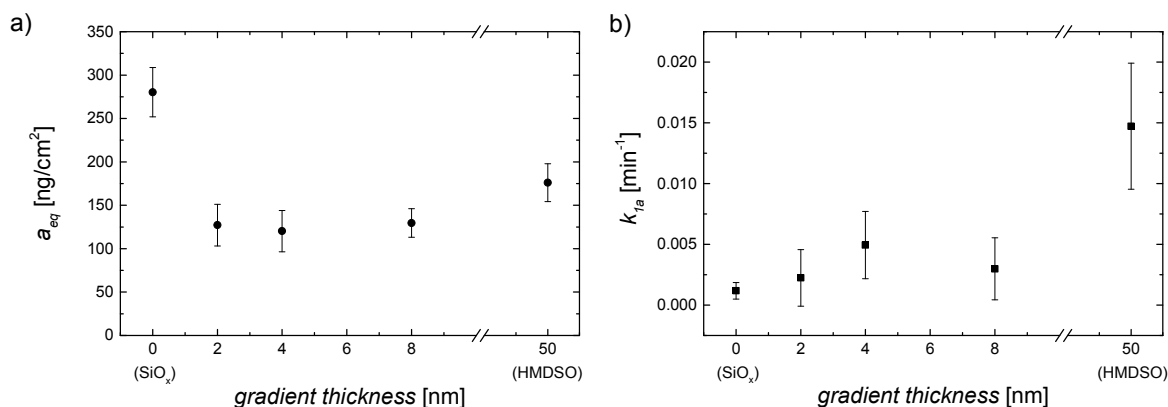
Figure 5.7: Parameters obtained from data fitting using a mixed order model (Chapter 2, equation (2.37)) as a function of gradient thickness (energy density): a) adsorbed amount of protein at equilibrium and b) adsorption rate constant. A thickness of 0 nm corresponds to the plain hydrophilic SiO_x bottom layer and a thickness of 50 nm corresponds to the plain hydrophobic HMDSO top layer.

Two trends can be recognized: 1) the amount of BSA adsorbed on the vertical chemical gradient surfaces is 20%-50% lower than on the plain reference coatings (Figure 5.7 a) and Figure 5.6) and 2) the adsorption kinetics on the vertical chemical gradient layers are similar to those on the more hydrophilic SiO_x plain reference film (Figure 5.7 b) and Figure 5.6). Both observations are independent of the gradient energy density within the examined range, as illustrated by the similarity of the average values a_{eq} and k_{1a} for gradients with energy densities (thicknesses) of 7 MJ/m^3 (2 nm), 3.5 MJ/m^3 (4 nm) and 1.75 MJ/m^3 (8 nm). As the vertical chemical gradients consists of a vertical transition between the plain SiO_x and the HMDSO films and therefore exhibit intermediate surface properties, an amount of adsorbed proteins between these two limiting reference cases could intuitively be expected. The amount of BSA that adsorbs on a surface is thus not solely determined by its surface free energy, but also by the sub-surface gradient structure.

The adsorption of proteins is driven by protein-surface interactions in competition with water-surface interactions. In the following, we invoke two hypotheses in an attempt to explain the observed

effects of sub-surface vertical chemical gradients to protein adsorption.

Hypothesis 1: Influence of sub-surface van der Waals interactions

Recently, it has been observed that slight changes in the sub-surface composition influence the orientation of proteins on surfaces, their adsorption kinetics and their enzymatic activity [220, 238–240]. Hähl et al. attribute these effects to van der Waals interactions that range over tens of nanometers [71]. In their study, they investigated protein adsorption on silicon wafers with different oxide layer thickness (i.e. different sub-surface composition) and surface chemistry. They could show that the sub-surface composition can influence the density of the adsorbed protein layer via long range polar or van der Waals forces, while the surface chemistry determines the degree of conformational changes upon adsorption. Van der Waals interactions depend on the polarizability of the interacting media. The polarizability of SiO_2 is about 1.5 times higher than the polarizability of PDMS [241, 242]. It is thus expected that the more SiO_2-like plasma polymerized SiO_x film exhibits a slightly higher polarizability and thus slightly stronger van der Waals attractions than the PDMS-like HMDSO film. A vertical chemical gradient with a more polarizable bottom layer (SiO_x) and less polarizable top layer (HMDSO) would thus exhibit intermediate attractive properties. However, the difference in polarizability and resulting van der Waals attractions is rather small and might not be strong enough to significantly affect protein adsorption. Furthermore, if protein adsorption on the vertical chemical gradients was predominantly driven by van der Waals interaction due to the higher polarizability of the sub-surface, an amount of adsorbed protein intermediate to both the plain SiO_x and HMDSO films would be expected, which is not what we observe (c.f. Figure 5.6 and Figure 5.7). The influence of water has so far been ignored in this hypothesis. However, water is an important system component known to influence protein adsorption and should therefore be considered. The

vertical chemical gradients may contain a larger amount of sub-surface water, which would lower the overall interaction energy and thus apparently reduce protein adsorption.

However, due to the extensive hydrogen bonding of water and its ability to structure around surfaces in order to minimize free energy, water will influence the energetics even more strongly via hydrophobic interactions. This will be further discussed in hypothesis 2.

Hypothesis 2: Influence of sub-surface water (structure)

The importance of water interactions with the surface for protein adsorption was pointed out by Kasemo [243] and has obtained ample attention in studies related to biological function [5, 244] and protein resistance [21–23, 221, 222]. Thereby, the interaction between the water present at the interface and the hydrated protein is crucial. The binding strength and resulting structural arrangement of water molecules at the interface depend on surface properties [11, 13, 22, 243]. Highly hydrophilic surfaces bind water molecules more strongly than they bind to themselves via hydrogen bonding and can resist protein adsorption because the displacement of the water molecules by the protein is energetically unfavorable. This is, for example, observed for self-assembled monolayers of poly(ethylene glycol) (PEG) [195, 245, 246]. At non-wetting surfaces, on the other hand, hydrogen bonding amongst water molecules is stronger than the water-surface bonds. In order to minimize free energy, water will adopt a structure, in which bonding with the surface is minimized. Along these lines, Vogler suggested that at a hydrophobic surface water is present in a less dense open structure while at hydrophilic surfaces a more dense water region forms. He proposed that the solvent properties at the interface control the adsorption of proteins and that the hydrophobic interactions are minimized in a region where the water structure at the interface resembles the bulk water structure (Berg limit) [21].

A similar argument could be applied to the vertical chemical gradient films. It was shown by neutron reflectometry that water diffuses into both, the SiO_x as well as the HMDSO film, in a sub-surface region of interest (c.f. Chapter 4). The vertical chemical gradient structure thus contains ample amounts of water and is wetted also from below. The surface free energy within the vertical chemical gradients gradually changes from a hydrophobic surface to a more hydrophilic sub-surface. This gradual change will affect the interaction of water with the gradient and also the structural arrangement of the water molecules present within the gradient. A protein approaching the vertical gradient does not only interact with the surface water but also with the sub-surface water contained in the gradient. The observed reduction in adsorbed amount of protein on the vertical chemical gradients compared to the plain films would thus suggest that this interaction of the protein with the sub-surface water in the gradient is less favorable than the water-gradient interaction. This situation is schematically illustrated in Figure 5.8 in comparison to the adsorption on the plain SiO_x and HMDSO films.

The interaction regions highlighted in yellow correspond to the sub-surface regions in the vertical chemical gradient, where the water structure would be altered in an energetically unfavorable way upon adsorption of a protein. These regions thus resist protein adsorption. Hence, the amount and structure of the sub-surface water largely influences protein adsorption on vertical chemical gradients.

Further studies will however be necessary to clarify the exact role of sub-surface water contained within the vertical gradient structure on protein adsorption. Suggestions for further investigations will be discussed in Chapter 6.
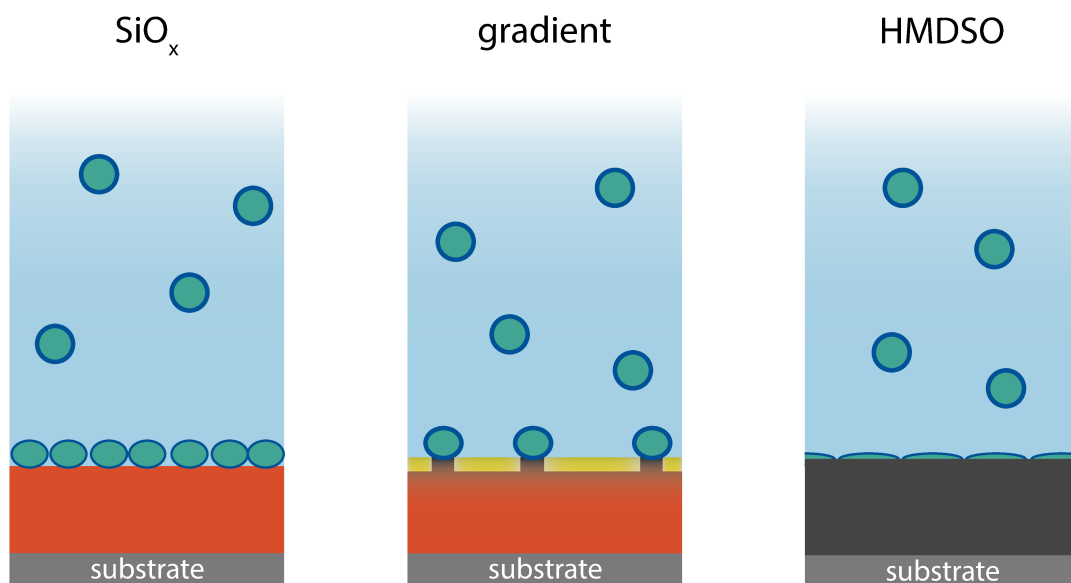
Figure 5.8: Schematic illustration of BSA (depicted as spherical objects here) adsorption on SiO$_x$, HMDSO and vertical chemical gradient surfaces, respectively, inspired by the scheme by Hähl et al. [219]. The gradient regions highlighted in yellow indicate the sub-surface regions of unfavorable interaction with the protein.

Conclusion

Novel vertical chemical gradient surfaces were produced using plasma polymerization and character-ized by X-ray photoelectron spectroscopy, atomic force microscopy and contact angle measurements. The thickness and chemical composition and therefore the specific energy of the gradient films can readily be tuned by precisely controlling the applied plasma parameters as well as the gas feed com-position. With increasing gradient thickness, an increasing surface hydrophobicity was detected by contact angle measurements along with an increase in carbon content and corresponding decrease in oxygen content assessed by XPS. The surface roughness of the films was found to be very low (≈ 0.3 nm) for all gradients investigated. The adsorption of bovine serum albumin on these vertical chemical gradient surfaces has been investigated using the TInAS and compared to the adsorption

on the plain SiO_x and HMDSO films. The highest amount of adsorbed protein was detected on the hydrophilic SiO_x film. This finding was attributed to the largely retained protein conformation on this surface leading to an enhanced diffusivity allowing for efficient packing of the proteins on the surface. Compared to this, the HMDSO film showed a reduced amount of protein indicating substantial conformational changes upon adsorption. A strong hydrophobic interaction between the inner parts of the protein and the surface is suspected, causing the substantial conformational changes of the protein upon adsorption. On the vertical chemical gradient films the adsorbed amount is reduced compared to the plain HMDSO and SiO_x films and the kinetics of adsorption resemble the slower kinetics observed on the more hydrophilic SiO_x film. The mechanisms governing this reduction are not evident and two hypotheses regarding the driving forces for this reduction are presented: the reduction of the adsorbed amount due to long range van der Waals interaction between the sub-surface and the protein as well as the interaction between the sub-surface water contained within the vertical gradient and the protein. However, further studies are necessary to clarify, which interactions govern the adsorption of proteins on these vertical chemical structures.

Remaining open questions concern the state of the adsorbed protein (hydrated or denatured), the amount of sub-surface water contained within the vertical chemical gradient and the structure of these water molecules.

CONCLUSIONS AND OUTLOOK

In this final chapter of the thesis the results obtained in the different experimental studies are summarized and strategies to test the hypotheses proposed in chapter 5 along with possible topics for further research as well as potential applications of the vertical chemical gradients are presented.

6.1 Conclusions

The plasma polymerization of hexamethyldisiloxane was investigated using a macroscopic approach and it was confirmed that it can be described using a quasi-Arrhenius approach with an apparent activation energy $\langle E_a \rangle$. We propose that, due to the complexity of the precursor, the observed activation energy results from the superposition of different chemical reaction pathways. Two main film-forming fragments have been identified: $(CH_3)_n SiO$ with $n = 2$ or 3. We found that for film densification not only surface processes such as energetic particle bombardment and momentum transfer are important, but also the extent of fragmentation of the precursor. Depending on the energy input

one or the other process prevails. We could further show that the film density along with the structure of the siloxane network within the films influences the surface wettability. Additional long term studies revealed aging effects in the films attributed to the slow oxidation of trapped radicals and the hydration of the films along the Si-O-Si network involving the formation of silanol groups.

The response of the plasma polymer films to aqueous environments was investigated in more detail using neutron reflectometry for two films exhibiting different surface wettabilities. We found that water penetrates into both films, but at different rates and to a different extent. The water penetration into the more hydrophilic SiO_x film is faster and the water penetrates deeper into this film. The top 5-10 nm of the film closest to the film-water interface contain a volume fraction of water of more than 10%. For the hydrophobic HMDSO film a volume fraction of water of less than 2% was determined for the same sub-surface region. The kinetics of water penetration into these two films are thus different and depend on the Si-O-Si content within the films. This can be explained by a combined diffusion-reaction mechanism taking into account the reaction of water with siloxane bonds to form silanols.

Further, thin vertical chemical gradients were produced using plasma polymerization of HMDSO and characterized using XPS, contact angle measurements and AFM. With a precise control over the energy input into and the gas composition of the plasma the thickness and energy density of these gradient films can be tuned. In addition, the adsorption of BSA on these gradient films was investigated in more detail. It was found that the amount of protein adsorbed on the vertical chemical gradients is reduced in comparison to the more hydrophilic SiO_x film and the hydrophobic HMDSO film. Also, the adsorption kinetics were found to be similar to those on the underlying SiO_x layer. Two hypotheses regarding the driving force for protein adsorption on the vertical chemical gradients

have been discussed: a change of the interaction of water with the protein due to the vertical gradient and the influence of the sub-surface via long range van der Waals interactions. It could not be clarified completely, which interactions govern protein adsorption on vertical chemical gradients. However, the interaction of sub-surface water contained within the gradient with the protein seems to be an important driving force. Further studies will be necessary to clarify this matter.

In conlcusion, we managed to create tunable vertical chemical gradient structures that significantly affect protein adsorption and are interesting for further studies related to the role of water in adsorption processes.

6.2 Outlook

In this section several suggestions to test the role of sub-surface water in protein adsorption are discussed. Furthermore, possible future research projects are proposed and potential applications of the vertical chemical gradient films are briefly outlined.

Further investigations on the influence of sub-surface water on protein adsorption

Several points regarding the role of sub-surface water contained within the gradient in adsorption processes remain open to question. These include the state of the adsorbed protein, the amount of water contained within the gradient and also the structure of this sub-surface water.

Assuming that the adsorbing protein is largely affected by the presence of the sub-surface water in the vertical chemical gradient, it is expected that the protein adsorbs in a more native state than on the plain hydrophobic reference surface. Circular dichroism spectroscopy can yield information about the fraction of α-helix and β-sheet structure of proteins in solution as well as of proteins adsorbed at an interface. By comparison of the α-helix and β-sheet fractions of native and adsorbed proteins, conclusions regarding the conformational state of the adsorbed proteins may be drawn [247]. Other methods that are able to simultaneously measure the thickness and the refractive index of an adsorbed layer, such as e.g. ellipsometry or a new implementation of the TInAS currently under development that also simultaneously measures the refractive index of the adsorbed layer, could yield additional insights into the density of the adsorbed protein layer and thus its conformational state.

To further investigate the role of sub-surface water on the adsorption of proteins several strategies could be followed:

- A combination of wet chemistry techniques and plasma polymerization could be envisaged to increase the amount of water present within the gradient. Thereby the hydrophilic bottom layer could consist of a hydrogel or a hydrophilic self-assembled monolayer (e.g. from poly(ethylene glycol)) that would then be coated by a thin hydrophobic plasma polymer film providing additional cross-linking and thus increased film stability, while ensuring that the water binding ability of the bottom layer remains high. The resulting effect of the increased water content within the sub-surface on protein adsorption could then be investigated.

- The structure of water molecules at interfaces is dependent on temperature [248, 249]. It would therefore be of interest to repeat the adsorption measurements of BSA on vertical chemical gradients at elevated temperatures, where the structuring of water is less stable. These measurements could add to a better understanding of the role of water structure in the adsorption of proteins on vertical chemical gradients.

- Additional insights into the role of sub-surface water in protein adsorption could also be gained by modeling the interaction of water molecules in the varying energy landscape of the vertical gradient and the proteins.

Also neutron reflectometry could contribute to a further understanding of the distribution and amount of water present within the gradient as sub-surface water. Furthermore, this technique could also give insights into the conformation of the adsorbed proteins.

Applications of vertical chemical gradients

The vertical chemical gradient films produced in this PhD thesis may be of interest for various applications in different fields. Examples of such applications are briefly outlined below.

- In addition to protein adsorption, it would be of interest to study the adsorption of other amphiphilic molecules, such as e.g. surfactants, on vertical chemical gradients. By systematically varying the dimensions of the hydrophobic and hydrophilic parts of the molecule additional insights into the effect of hydrophobic interactions and water structuring on the adsorption on vertical chemical gradients could be gained. Furthermore, for such systems a kinetic trapping of the molecules at the interface rather than an irreversible adsorption is expected. This trapping of molecules can be of interest for different applications such as re-loadable release systems for functional molecules.

- The gradually changing film properties and resulting water distribution within the vertical chemical gradients makes them potentially interesting also for tribological applications.

- These very thin plasma polymerized vertical gradient layers could also be interesting for coating other biosensors, which require coatings exhibiting long term stability, such as, for example, quartz crystal microbalance sensors or surface plasmon resonance sensors.

With this method, highly sophisticated model systems that allow for more systematic studies of the influence of water on protein adsorption were produced. These systems may have major impact on future technologies and developments.

Using the TInAS to detect biological substances

A further potentially interesting project involves the TInAS used in this thesis to measure the adsorption of BSA. As outlined below, this measurement technique might be of interest in biology and medicine, as many analytical and detection methods in these fields are based on specific interactions of substances with surfaces. A widely used method to detect substances such as antigens from solution is the enzyme-linked immunosorbent assay (ELISA). This test relies on the specific recognition between an antigen and its antibody and generally uses an enzymatic reaction resulting in a color change to quantify the amount of substance present in solution. As the TInAS can directly determine the amount of a substance adsorbed on a surface, a transfer of the ELISA test to the TInAS could be beneficial in terms of measurement time and added information about the kinetics of adsorption. A preliminary study using plasma polymers as substrates has shown that the TInAS is indeed a promising method to detect antigens from solution [250]. However, several issues should still be addressed:

- The coating used to immobilize the antibody on the surface should be optimized in the sense that as many antibodies as possible can be bound to the surface in the correct orientation.

- The influence of the concentration of the antibody and antigen in solution should be studied systematically in order to establish the detection limits of this method.

Solving these issues would make the TInAS a powerful technique to study biological phenomena and as a diagnostic tool. For example, the adsorption of different substances from cell culture supernatants could be analyzed in real-time. It would thus also be possible to study the impact of different substances such as nanoparticles on cell behavior. Such studies could contribute to a better under-

standing of the interaction of nanoparticles with cells and thus their dangers and chances for human health.

Over the curse of this PhD Studies, several methods were optimized and applied. A better understanding of HMDSO plasma polymerization and of the hydration and water uptake ability of the resulting films was achieved. With this knowledge, vertical chemical gradients could be produced and characterized. Furthermore, a reduction of protein adsorption on these vertical chemical gradients was observed, which was hypothesized to originate from unfavorable interactions between the sub-surface water within the gradient and the adsorbing protein. Vertical chemical gradients are thus interesting systems to study adsorption phenomena in more detail.

[1] F. H. Stillinger. *Water revisited*. Science, 209(4455), pp. 451–457 (1980).

[2] T. M. Raschke and M. Levitt. *Nonpolar solutes enhance water structure within hydration shells while reducing interactions between them*. Proceedings of the National Academy of Sciences of the United States of America, 102(19), pp. 6777–6782 (2005).

[3] Y. L. A. Rezus and H. J. Bakker. *Observation of immobilized water molecules around hydrophobic groups*. Phys. Rev. Lett., 99, p. 148301 (2007).

[4] B. Widom, P. Bhimalapuram and K. Koga. *The hydrophobic effect*. Phys. Chem. Chem. Phys., 5, pp. 3085–3093 (2003).

[5] P. Ball. *Water as an active constituent in cell biology*. Chemical Reviews, 108(1), pp. 74–108 (2008).

[6] N. T. Southall, K. A. Dill and A. D. J. Haymet. *A view of the hydrophobic effect*. The Journal of Physical Chemistry B, 106(3), pp. 521–533 (2002).

[7] M. Morra. *On the molecular basis of fouling resistance*. Journal of Biomaterials Science, Polymer Edition, 11(6), pp. 547–569 (2000).

[8] M. J. Stevens and G. S. Grest. *Simulations of water at the interface with hydrophilic self-assembled monolayers (review)*. Biointerphases, 3(3), pp. FC13–FC22 (2008).

[9] M. Tanaka and A. Mochizuki. *Clarification of the blood compatibility mechanism by controlling the water structure at the blood-poly(meth)acrylate interface*. Journal of Biomaterials Science – Polymer Edition, 21(14), pp. 1849 – 1863 (2010).

[10] B. O. Leung, Z. Yang, S. S. H. Wu and K. C. Chou. *Role of interfacial water on protein adsorption at cross-linked polyethylene oxide interfaces*. Langmuir, 28(13), pp. 5724–5728 (2012).

[11] E. A. Vogler. *Protein adsorption in three dimensions*. Biomaterials, 33(5), pp. 1201 – 1237 (2012).

[12] K. Nakanishi, T. Sakiyama and K. Imamura. *On the adsorption of proteins on solid surfaces, a common but very complicated phenomenon*. Journal of Bioscience and Bioengineering, 91(3), pp. 233 – 244 (2001).

[13] A. Ponche, L. Ploux and K. Anselme. *Protein/material interfaces: Investigation on model surfaces*. Journal of Adhesion Science and Technology, 24(13-14), pp. 2141–2164 (2010).

[14] Q. Wei, T. Becherer, S. Angioletti-Uberti, J. Dzubiella, C. Wischke, A. T. Neffe, A. Lendlein, M. Ballauff and R. Haag. *Protein interactions with polymer coatings and biomaterials*. Angewandte Chemie International Edition, 53(31), pp. 8004–8031 (2014).

[15] M. Rabe, D. Verdes and S. Seeger. *Understanding protein adsorption phenomena at solid surfaces*. Advances in Colloid and Interface Science, 162(1-2), pp. 87 – 106 (2011).

[16] B. Milthorpe. *Protein adsorption to surfaces and interfaces*. In P. Vadgama (ed.), *Surfaces and Interfaces for Biomaterials*, Woodhead Publishing Series in Biomaterials, pp. 763 – 781. Woodhead Publishing (2005).

[17] W. Norde, T. A. Horbett and J. L. Brash. *Proteins at Interfaces III: Introductory Overview*, pp. 1–34. American Chemical Society (2012).

[18] J. M. Mollerup. *A review of the thermodynamics of protein association to ligands, protein adsorption, and adsorption isotherms.* Chemical Engineering & Technology, 31(6), pp. 864–874 (2008).

[19] C. A. Haynes and W. Norde. *Globular proteins at solid/liquid interfaces.* Colloids and Surfaces B: Biointerfaces, 2(6), pp. 517 – 566 (1994).

[20] J. J. Ramsden. *Concentration scaling of protein deposition kinetics.* Phys. Rev. Lett., 71, pp. 295–298 (1993).

[21] E. A. Vogler. *Structure and reactivity of water at biomaterial surfaces.* Advances in Colloid and Interface Science, 74(1 - 3), pp. 69 – 117 (1998).

[22] M. Tanaka, T. Hayashi and S. Morita. *The roles of water molecules at the biointerface of medical polymers.* Polymer Journal, 45, p. 701–710 (2013).

[23] M. J. Penna, M. Mijajlovic and M. J. Biggs. *Molecular-level understanding of protein adsorption at the interface between water and a strongly interacting uncharged solid surface.* Journal of the American Chemical Society, 136(14), pp. 5323–5331 (2014).

[24] E. A. Vogler. *Wettability, Surfactant Science Series*, vol. 49, chap. Interfacial chemistry in biomaterials science, pp. 184–250. Marcel Dekker, New York (1993).

[25] I. Banerjee, R. C. Pangule and R. S. Kane. *Antifouling coatings: Recent developments in the design of surfaces that prevent fouling by proteins, bacteria, and marine organisms.* Advanced Materials, 23(6), pp. 690–718 (2011).

[26] C. Blaszykowski, S. Sheikh and M. Thompson. *Surface chemistry to minimize fouling from blood-based fluids.* Chem. Soc. Rev., 41, pp. 5599–5612 (2012).

[27] M. Guvendiren, J. A. Burdick and S. Yang. *Kinetic study of swelling-induced surface pattern formation and ordering in hydrogel films with depth-wise crosslinking gradient.* Soft Matter, 6(9), pp. 2044–2049 (2010).

[28] Z. Wu and K. Hjort. *Surface modification of PDMS by gradient-induced migration of embedded pluronic.* Lab on a chip, 9(11), pp. 1500–1503 (2009).

[29] K. Karaky, C. Derail, G. Reiter and L. Billon. *Tuning the surface/bulk properties by the control of the amphiphilic profile in gradient copolymer.* Macromolecular Symposia, 267(1), pp. 31–40 (2008).

[30] M. Wang, G. Wildburg, J. Van Esch, P. Bennema, R. Nolte and H. Rinsdorf. *Surface-tension-gradient-induced pattern formation in monolayers.* Physical Review Letters, 71(24), pp. 4003–4006 (1993).

[31] A. J. Choudhury, S. A. Barve, J. Chutia, A. R. Pal, R. Kishore, Jagannath, M. Pande and D. S. Patil. *RF-PACVD of water repellent and protective HMDSO coatings on bell metal surfaces: Correlation between discharge parameters and film properties.* Applied Surface Science, 257(20), pp. 8469–8477 (2011).

[32] T. F. Wang and H. K. Yasuda. *Modification of wettability of a stainless-steel plate by cathodic plasma polymerization of trimethylsilane-oxygen mixtures.* Journal of Applied Polymer Science, 55(6), pp. 903–909 (1995).

[33] R. Kleber, M. Weiler, A. Krüger, S. Sattel, G. Kunz, K. Jung and H. Ehrhardt. *Influence of ion energy and flux composition on the properties of plasma-deposited amorphous carbon and amorphous hydrogenated carbon films.* Diamond and Related Materials, 2(2-4), pp. 246–250 (1993).

[34] D. Hegemann, C. Oehr and A. Fischer. *Design of functional coatings.* Journal of Vacuum Science & Technology A, 23(1), pp. 5–11 (2005).

[35] D. Hegemann, U. Schuetz and E. Koerner. *Macroscopic approach to plasma polymerization using the concept of energy density.* Plasma Processes and Polymers, 8(8), pp. 689–694 (2011).

[36] M. Heuberger and T. E. Balmer. *The transmission interferometric adsorption sensor.* Journal of Physics D: Applied Physics, 40(23), pp. 7245–7254 (2007).

[37] W. Crookes. *"Radiant matter": a resumé of the principal lectures and papers of Prof. William Crookes, on the "fourth state of matter"*. James W. Queen & Co, Philadelphia, Pa (1881).

[38] I. Langmuir. *Oscillations in ionized gases*. Proceedings of the National Academy of Sciences, 14(8), pp. 627–637 (1928).

[39] M. A. Lieberman and A. J. Lichtenberg. *Principles of plasma discharges and materials processing*. Wiley, New York, N.Y (1994).

[40] J. R. Roth. *Industrial plasma engineering*, vol. 1. Institute of Physics Publishing, Bristol (1995).

[41] H. Yasuda. *Plasma polymerization*. Academic Press (1985).

[42] A. Grill. *Cold plasma in materials fabrication : From fundamentals to applications*. IEEE Press, Piscataway, N.J (1994).

[43] M. J. Druyvesteyn and F. M. Penning. *The mechanism of electrical discharges in gases of low pressure*. Rev. Mod. Phys., 12, pp. 87–174 (1940).

[44] International Telecommunication Union. *Radio regulations* (2012).

[45] H. Conrads and M. Schmidt. *Plasma generation and plasma sources*. Plasma Sources Science and Technology, 9(4), p. 441 (2000).

[46] S. G. Walton. *An Overview of Plasma Processes* (2007).

[47] F. Fracassi. *Plasma Processing of Polymers*, chap. Architecture of Plasma Reactors, pp. 47–64. Springer (1997).

[48] D. Hegemann, U. Schuetz and C. Oehr. *RF-Plasma Deposition of SiOx and a-C:H as Barrier Coatings on Polymers*, pp. 23–37. Wiley-VCH Verlag GmbH & Co. KGaA (2005).

[49] J. Goodman. *The formation of thin polymer films in the gas discharge*. Journal of Polymer Science, 44(144), pp. 551–552 (1960).

[50] A. Bradley and J. P. Hammes. *Electrical properties of thin organic films*. Journal of The Electrochemical Society, 110(1), pp. 15–22 (1963).

[51] M. Stuart. *Dielectric properties of cross-linked polystyrene film formed in the glow discharge*. Nature, 199, pp. 59–60 (1963).

[52] H. Biederman and Y. Osada. *Plasma polymerization processes*. Elsevier (1992).

[53] N. Morosoff. *An introduction to plasma polymerization*. In R. d'Agostino (ed.), *Plasma Deposition, Treatment, and Etching of Polymers*, Plasma - Materials Interactions, pp. 1 – 93. Academic Press, San Diego (1990).

[54] A. Bell. *The mechanism and kinetics of plasma polymerization*. In S. Veprek and M. Venugopalan (eds.), *Plasma Chemistry III*, *Topics in Current Chemistry*, vol. 94, pp. 43–68. Springer Berlin Heidelberg (1980).

[55] J. van Dijk, G. M. W. Kroesen and A. Bogaerts. *Plasma modelling and numerical simulation*. Journal of Physics D: Applied Physics, 42(19), p. 190301 (2009).

[56] Z. Donkó, P. Hartmann and K. Kutasi. *On the reliability of low-pressure DC glow discharge modelling*. Plasma Sources Science and Technology, 15(2), p. 178 (2006).

[57] E. Warburg. *Jahrbuch der Radioaktivität und der Elektronik*, vol. 6, chap. Über chemische Reaktionen, welche durch die stille Entladung in gasförmigen Körpern herbeigeführt werden, pp. 181–229. S. Hirzel, Leipzig (1909).

[58] H. Becker. *Wissenschaftliche Verffentlichungen aus dem Siemens-Konzern*, chap. Über die extrapolation und Berechnung der Konzentration und Ausbeute von Ozonapparaten, pp. 76–106. Springer (1920).

[59] A. Rutscher and H. E. Wagner. *The model of macroscopic kinetics in non-equilibrium plasma chemical reactions I. general considerations and basic relations.* Beitraege aus der Plasmaphysik, 25(4), pp. 337–350 (1985).

[60] H.-E. Wagner. *Low temperature plasma physics: fundamental aspects and applications*, chap. Reactive non-thermal plasmas - chemical quasi-equilibria, similarity principles and macroscopic kinetics, pp. 305–330. Wiley-VCH (2001).

[61] H. Schlemm and M. Matthes. *Magnetic field enhanced plasma etching and glow polymerization at a low-frequency dischrge.* Wissenschaftliche Zeitschrift - Technische Hochschule Karl-Marx-Stadt, 28(2), pp. 219–224 (1986).

[62] D. Hegemann. *Plasma polymer deposition and coatings on polymers*, vol. 4, pp. 201–228. Elsevier Ltd., Oxford, UK (2014).

[63] H. Yasuda and T. Hirotsu. *Critical evaluation of conditions of plasma polymerization.* Journal of Polymer Science: Polymer Chemistry Edition, 16(4), pp. 743–759 (1978).

[64] D. Hegemann, M. M. Hossain, E. Koerner and D. J. Balazs. *Macroscopic description of plasma polymerization.* Plasma Processes and Polymers, 4(3), pp. 229–238 (2007).

[65] Y. Matsuda and H. Yasuda. *Evaluation of plasma polymers of silanes as adhesion promoters for organic paint.* Thin Solid Films, 118(2), pp. 211 – 224 (1984).

[66] D. Hegemann and M.-M. Hossain. *Influence of non-polymerizable gases added during plasma polymerization.* Plasma Processes and Polymers, 2(7), pp. 554–562 (2005).

[67] A. Manenschijn and W. J. Goedheer. *Angular ion and neutral energy distribution in a collisional rf sheath.* Journal of Applied Physics, 69(5), pp. 2923–2930 (1991).

[68] H. Windischmann. *An intrinsic stress scaling law for polycrystalline thin films prepared by ion beam sputtering.* Journal of Applied Physics, 62(5), pp. 1800–1807 (1987).

[69] C. Davis. *A simple model for the formation of compressive stress in thin films by ion bombardment.* Thin Solid Films, 226(1), pp. 30 – 34 (1993).

[70] D. Hegemann, E. Korner, N. Blanchard, M. Drabik and S. Guimond. *Densification of functional plasma polymers by momentum transfer during film growth.* Applied Physics Letters, 101(21), pp. 211603–4 (2012).

[71] J. N. Israelachvili. *Intermolecular and Surface Forces.* Academic Press, San Diego, third edition edn. (1992).

[72] H. Hamaker. *The London-van der Waals attraction between spherical particles.* Physica, 4(10), pp. 1058 – 1072 (1937).

[73] D. K. Owens and R. C. Wendt. *Estimation of the surface free energy of polymers.* Journal of Applied Polymer Science, 13(8), pp. 1741–1747 (1969).

[74] W. Rabel. *Einige Aspekte der Benetzungstheorie und ihre Anwendung auf die Untersuchung und Veränderung der Oberflächeneigenschaften von Polymeren.* Farbe und Lacke, 77(10), pp. 997–1005 (1971).

[75] D. H. Kaelble. *Dispersion-polar surface tension properties of organic solids.* The Journal of Adhesion, 2(2), pp. 66–81 (1970).

[76] P. Atkins and J. de Paula. *Atkins' Physical Chemistry.* OUP Oxford (2010).

[77] H. Freiser and G. H. Nancollas. *Compendium of analytical nomenclature : definitive rules 1987.* Blackwell Science, Oxford, 2nd edn. (1987).

[78] I. Langmuir. *The adsorption of gases on plane surfaces of glass, mica and platinum.* Journal of the American Chemical Society, 40(9), pp. 1361–1403 (1918).

[79] T. E. Balmer, H. K. Christenson, N. D. Spencer and M. Heuberger. *The effect of surface ions on water adsorption to mica*. Langmuir, 24(4), pp. 1566–1569 (2008).

[80] S. Brunauer, P. H. Emmett and E. Teller. *Adsorption of gases in multimolecular layers*. Journal of the American Chemical Society, 60(2), pp. 309–319 (1938).

[81] M. Temkin and V. Pyzhev. Acta Physicochimica URSS, 12, p. 217 (1940).

[82] H. Freundlich. *Kapillarchemie*. Academishe Bibliothek, Leipzig (1909).

[83] S. Lagergren. *Zur Theorie der sogenannten Adsorption gelöster Stoffe*. Kungliga Svenska Vetenskapsakademiens Handlingar, 24(4), pp. 1–39 (1898).

[84] Y. Ho and G. McKay. *Sorption of dye from aqueous solution by peat*. Chemical Engineering Journal, 70(2), pp. 115 – 124 (1998).

[85] R. M. A. Azzam, P. G. Rigby and J. A. Krueger. *Kinetics of protein adsorption and immunological reactions at a liquid/solid interface by ellipsometry*. Physics in Medicine and Biology, 22(3), p. 422 (1977).

[86] Y. Liu and L. Shen. *From Langmuir kinetics to first- and second-order rate equations for adsorption*. Langmuir, 24(20), pp. 11625–11630 (2008).

[87] M. Islam, M. Khan and M. Mozumder. *Adsorption equilibrium and adsorption kinetics: A unified approach*. Chemical Engineering & Technology, 27(10), pp. 1095–1098 (2004).

[88] Y. Ho and G. McKay. *Pseudo-second order model for sorption processes*. Process Biochemistry, 34(5), pp. 451 – 465 (1999).

[89] S. Azizian. *Kinetic models of sorption: a theoretical analysis*. Journal of Colloid and Interface Science, 276(1), pp. 47 – 52 (2004).

[90] A. Marczewski. *Application of mixed order rate equations to adsorption of methylene blue on mesoporous carbons*. Applied Surface Science, 256(17), pp. 5145 – 5152 (2010). Seventh International Symposium Effects of Surface Heterogeneity in Adsorption and Catalysis on Solids - ISSHAC-7.

[91] A. W. Marczewski. *Analysis of kinetic Langmuir model. part I: Integrated kinetic Langmuir equation (ikl): A new complete analytical solution of the Langmuir rate equation*. Langmuir, 26(19), pp. 15229–15238 (2010).

[92] V. Krisdhasima, J. McGuire and R. Sproull. *Surface hydrophobic influences on β-lactoglobulin adsorption kinetics*. Journal of Colloid and Interface Science, 154(2), pp. 337 – 350 (1992).

[93] B. Widom. *Random sequential addition of hard spheres to a volume*. The Journal of Chemical Physics, 44(10), pp. 3888–3894 (1966).

[94] P. Schaaf and J. Talbot. *Kinetics of random sequential adsorption*. Phys. Rev. Lett., 62, pp. 175–178 (1989).

[95] A. Fick. *Ueber Diffusion*. Annalen der Physik, 170(1), pp. 59–86 (1855).

[96] R. H. Doremus. *Diffusion of water in silica glass*. Journal of Materials Research, 10, pp. 2379–2389 (1995).

[97] N. E. Blanchard, B. Hanselmann, J. Drosten, M. Heuberger and D. Hegemann. *Densification and hydration of HMDSO plasma polymers*. Plasma Processes and Polymers, 12(1), pp. 32–41 (2015).

[98] D. Music, U. Kreissig, Z. Czigany, U. Helmersson and J. M. Schneider. *Elastic modulus-density relationship for amorphous boron suboxide thin films*. Applied Physics A, 76(2), pp. 269–271 (2003).

[99] S. Peter, K. Graupner, D. Grambole and F. Richter. *Comparative experimental analysis of the a-C : H deposition processes using CH_4 and C_2H_2 as precursors*. Journal of Applied Physics, 102(5) (2007).

[100] A. M. Wrobel and M. R. Wertheimer. *Plasma-Polymerized Organosilicones and Organometallics*, pp. 163–268. Academic Press, San Diego (1990).

[101] R. Barni, S. Zanini and C. Riccardi. *Characterization of the chemical kinetics in an O2/HMDSO RF plasma for material processing*. Advances in Physical Chemistry, 2012, p. 6 (2012).

[102] G. F. Leu, A. Brockhaus and J. Engemann. *Diagnostics of a hexamethyldisiloxane/oxygen deposition plasma*. Surface and Coatings Technology, 174-175(0), pp. 928–932 (2003).

[103] D. Hegemann. *Macroscopic investigation of reaction rates yielding plasma polymer deposition*. Journal of Physics D: Applied Physics, 46(20) (2013).

[104] C. Rau and W. Kulisch. *Mechanisms of plasma polymerization of various silico-organic monomers*. Thin Solid Films, 249(1), pp. 28–37 (1994).

[105] K. Ruegner, R. Reuter, D. Ellerweg, T. de los Arcos, A. von Keudell and J. Benedikt. *Insight into the reaction scheme of SiO$_2$ film deposition at atmospheric pressure*. Plasma Processes and Polymers, 10(12), pp. 1061–1073 (2013).

[106] S. Y. Park, N. Kim, U. Y. Kim, S. I. Hong and H. Sasabe. *Plasma polymerization of hexamethyldisilazane*. Polymer Journal, 22, pp. 242–249 (1990).

[107] D. Hegemann, E. Koerner, S. Chen, J. Benedikt and A. von Keudell. *Functional plasma polymers deposited in capacitively and inductively coupled plasmas*. Applied Physics Letters, 100(5), pp. 051601–051601 (2012).

[108] S. Engelmann, R. L. Bruce, F. Weilnboeck, G. S. Oehrlein, D. Nest, D. B. Graves, C. Andes and E. A. Hudson. *Dependence of polymer surface roughening rate on deposited energy density during plasma processing*. Plasma Processes and Polymers, 6(8), pp. 484–489 (2009).

[109] J. Trieschmann and D. Hegemann. *Plasma polymerization at different positions in an asymmetric ethylene discharge*. Journal of Physics D: Applied Physics, 44(47) (2011).

[110] L. Martinu, J. E. Klembergsapieha and M. R. Wertheimer. *Dual-mode microwave radio-frequency plasma deposition of dielectric thin-films*. Applied Physics Letters, 54(26), pp. 2645–2647 (1989).

[111] C. Vautrin-Ul, F. Roux, C. Boisse-Laporte, J. L. Pastol and A. Chausse. *Hexamethyldisiloxane (HMDSO)-plasma-polymerised coatings as primer for iron corrosion protection: influence of RF bias*. Journal of Materials Chemistry, 12(8), pp. 2318–2324 (2002).

[112] D. Hegemann, B. Hanselmann, N. Blanchard and M. Amberg. *Plasma-substrate interaction during plasma deposition on polymers*. Contributions to Plasma Physics, 54(2), pp. 162–169 (2014).

[113] R. P. Gandhiraman, M. K. Muniyappa, M. Dudek, C. Coyle, C. Volcke, A. J. Killard, P. Burham, S. Daniels, N. Barron, M. Clynes and D. C. Cameron. *Interaction of plasma deposited HMDSO-based coatings with fibrinogen and human blood plasma: The correlation between bulk plasma, surface characteristics and biomolecule interaction*. Plasma Processes and Polymers, 7(5), pp. 411–421 (2010).

[114] N. Guermat, A. Bellel, S. Sahli, Y. Segui and P. Raynaud. *Thin plasma-polymerized layers of hexamethyldisiloxane for humidity sensor development*. Thin Solid Films, 517(15), pp. 4455–4460 (2009).

[115] W. Jianhua, T. Igarashi, N. Okumori, T. Maetani, L. Baolin and M. Yoshinari. *Influence of surface wettability on competitive protein adsorption and initial attachment of osteoblasts*. Biomedical Materials, 4(4), pp. 045002 –045002 (2009).

[116] C. Saulou, B. Despax, P. Raynaud, S. Zanna, A. Seyeux, P. Marcus, J.-N. Audinot and M. Mercier-Bonin. *Plasma-mediated nanosilver-organosilicon composite films deposited on stainless steel: Synthesis, surface characterization, and evaluation of anti-adhesive and anti-microbial properties on the model yeast saccharomyces cerevisiae*. Plasma Processes and Polymers, 9(3), pp. 324–338 (2012).

[117] F. Xiangli, Y. Chen, W. Jin and N. Xu. *Polydimethylsiloxane (PDMS)/ceramic composite membrane with high flux for pervaporation of ethanol-water mixtures*. Industrial & Engineering Chemistry Research, 46(7), pp. 2224–2230 (2007).

[118] S. Zanini, E. Grimoldi and C. Riccardi. *Development of controlled releasing surfaces by plasma deposited multi-layers*. Materials Chemistry and Physics, 138(2-3), pp. 850–855 (2013).

[119] N. Alissawi, T. Peter, T. Strunskus, C. Ebbert, G. Grundmeier and F. Faupel. *Plasma-polymerized HMDSO coatings to adjust the silver ion release properties of Ag/polymer nanocomposites*. Journal of Nanoparticle Research, 15(11), pp. 1–12 (2013).

[120] B. Janocha, D. Hegemann, C. Oehr, H. Brunner, F. Rupp and J. Geis-Gerstorfer. *Adsorption of protein on plasma-polysiloxane layers of different surface energies*. Surface and Coatings Technology, 142-144(0), pp. 1051–1055 (2001).

[121] S. Guimond, U. Schuetz, B. Hanselmann, E. Koerner and D. Hegemann. *Influence of gas phase and surface reactions on plasma polymerization*. Surface and Coatings Technology, 205, Supplement 2(0), pp. S447–S450 (2011).

[122] M. R. Alexander, R. D. Short, F. R. Jones, W. Michaeli and C. J. Blomfield. *A study of HMDSO/O2 plasma deposits using a high-sensitivity and -energy resolution XPS instrument: curve fitting of the Si 2p core level*. Applied Surface Science, 137(1-4), pp. 179–183 (1999).

[123] A. Sonnenfeld, T. M. Tun, L. Zajickova, K. V. Kozlov, H. E. Wagner, J. F. Behnke and R. Hippler. *Deposition process based on organosilicon precursors in dielectric barrier discharges at atmospheric pressure - a comparison*. Plasmas and Polymers, 6(4), pp. 237–266 (2001).

[124] Y. Wang, J. Zhang and X. Shen. *Surface structures tailoring of hexamethyldisiloxane films by pulse RF plasma polymerization*. Materials Chemistry and Physics, 96(2â€"3), pp. 498–505 (2006).

[125] R. Basner, R. Foest, M. Schmidt, K. Becker and H. Deutsch. *Absolute total and partial electron impact ionization cross sections of hexamethyldisiloxane*. International Journal of Mass Spectrometry, 176(3), pp. 245–252 (1998).

[126] Y.-R. Luo. *Comprehensive Handbook of Chemical Bond Energies*. CRC Press, Boca Raton (2007).

[127] I. Vinogradov and A. Lunk. *Film deposition in the dielectric barrier discharge at atmospheric pressure in He/O2/HMDSO and He/N2O/HMDSO mixtures*. Plasma Processes and Polymers, 6(S1), pp. S514–S518 (2009).

[128] Y. Kudriavtsev, A. Villegas, A. Godines and R. Asomoza. *Calculation of the surface binding energy for ion sputtered particles*. Applied Surface Science, 239(3-4), pp. 273–278 (2005).

[129] M. R. Alexander, F. R. Jones and R. D. Short. *Radio-frequency hexamethyldisiloxane plasma deposition: A comparison of plasma- and deposit-chemistry*. Plasmas and Polymers, 2(4), pp. 277–300 (1997).

[130] D. Hegemann, H. Brunner and C. Oehr. *Evaluation of deposition conditions to design plasma coatings like SiOx and a-C:H on polymers*. Surface and Coatings Technology, 174-175(0), pp. 253–260 (2003).

[131] M. R. Alexander, R. D. Short, F. R. Jones, M. Stollenwerk, J. Zabold and W. Michaeli. *An X-ray photoelectron spectroscopic investigation into the chemical structure of deposits formed from hexamethyldisiloxane/ oxygen plasmas*. Journal of Materials Science, 31(7), pp. 1879–1885 (1996).

[132] A. Morinaka and Y. Asano. *Residual stress and thermal expansion coefficient of plasma polymerized films*. Journal of Applied Polymer Science, 27(6), pp. 2139–2150 (1982).

[133] B. Eliasson, M. Hirth and U. Kogelschatz. *Ozone synthesis from oxygen in dielectric barrier discharges*. Journal of Physics D: Applied Physics, 20(11), pp. 1421–1437 (1987).

[134] V. D. Rusanov, A. A. Fridman and G. V. Sholin. *The physics of a chemically active plasma with nonequilibrium vibrational excitation of molecules*. Soviet Physics - Uspekhi, 24(6), pp. 447–474 (1981).

[135] J. Roepcke, G. Revalde, M. Osiac, K. Li and J. Meichsner. *Tunable diode laser absorption studies of hydrocarbons in RF plasmas containing hexamethyldisiloxane*. Plasma Chemistry and Plasma Processing, 22(1), pp. 137–157 (2002).

[136] Y. Sawada, S. Ogawa and M. Kogoma. *Synthesis of plasma-polymerized tetraethoxysilane and hexamethyldisiloxane films prepared by atmospheric-pressure glow-discharge*. Journal of Physics D-Applied Physics, 28(8), pp. 1661–1669 (1995).

[137] D. Theirich, C. Soll, F. Leu and J. Engemann. *Intermediate gas phase precursors during plasma CVD of HMDSO*. Vacuum, 71(3), pp. 349–359 (2003).

[138] X. Zhu, F. Arefi-Khonsari, C. Petit-Etienne and M. Tatoulian. *Open air deposition of SiO2 films by an atmospheric pressure line-shaped plasma*. Plasma Processes and Polymers, 2(5), pp. 407–413 (2005).

[139] T. R. Gengenbach and H. J. Griesser. *Post-deposition ageing reactions differ markedly between plasma polymers deposited from siloxane and silazane monomers*. Polymer, 40(18), pp. 5079–5094 (1999).

[140] H. Yasuda and T. S. Hsu. *Some aspects of plasma polymerization of fluorine-containing organic compounds*. Journal of Polymer Science: Polymer Chemistry Edition, 15(10), pp. 2411–2425 (1977).

[141] M. Drabik, J. Kousal, C. Celma, P. Rupper, H. Biederman and D. Hegemann. *Influence of deposition conditions on structure and aging of C:H:O plasma polymer films prepared from acetone/CO2 mixtures*. Plasma Processes and Polymers, 11(5), pp. 496–508 (2014).

[142] R. N. Lamb and D. N. Furlong. *Controlled wettability of quartz surfaces*. Journal of the Chemical Society, Faraday Transactions 1: Physical Chemistry in Condensed Phases, 78(1), pp. 61–73 (1982).

[143] G. A. Parks. *Surface and interfacial free energies of quartz*. Journal of Geophysical Research: Solid Earth, 89(B6), pp. 3997–4008 (1984).

[144] V. Purohit, E. Mielczarski, J. A. Mielczarski and L. Akesso. *Evidence of coexistence of micro and nanoporosity of organo-silica polymeric films deposited on silicon by plasma deposition*. Materials Chemistry and Physics, 141(2–3), pp. 602–612 (2013).

[145] C. L. Wang, Y. Kobayashi, H. Togashi, K. Kato, T. Hirotsu, K. Hirata, R. Suzuki, T. Ohdaira and T. Mikado. *Plasma-polymerized hexamethyldisiloxane films characterized by variable-energy positron lifetime spectroscopy*. Journal of Applied Polymer Science, 74(10), pp. 2522–2528 (1999).

[146] A. Henglein. *Physicochemical properties of small metal particles in solution: "microelectrode" reactions, chemisorption, composite metal particles, and the atom-to-metal transition*. The Journal of Physical Chemistry, 97(21), pp. 5457–5471 (1993).

[147] A. Henglein. *Colloidal silver nanoparticles: Photochemical preparation and interaction with O2, CCl4, and some metal ions*. Chemistry of Materials, 10(1), pp. 444–450 (1998).

[148] C.-N. Lok, C.-M. Ho, R. Chen, Q.-Y. He, W.-Y. Yu, H. Sun, P.-H. Tam, J.-F. Chiu and C.-M. Che. *Silver nanoparticles: partial oxidation and antibacterial activities*. JBIC Journal of Biological Inorganic Chemistry, 12(4), pp. 527–534 (2007).

[149] T. R. Gengenbach, R. C. Chatelier and H. J. Griesser. *Correlation of the nitrogen 1s and oxygen 1s XPS binding energies with compositional changes during oxidation of ethylene diamine plasma polymers*. Surface and Interface Analysis, 24(9), pp. 611–619 (1996).

[150] D. J. Menzies, A. Nelson, H.-H. Shen, K. M. McLean, J. S. Forsythe, T. Gengenbach, C. Fong and B. W. Muir. *An X-ray and neutron reflectometry study of PEG-like plasma polymer films*. Journal of The Royal Society Interface, 9(70), pp. 1008–1019 (2012).

[151] I. Nouicer, S. Sahli, M. Kihel, Z. Ziari, A. Bellel and R. P. *Superhydrophobic surface produced on polyimide and silicon by plasma enhanced chemical vapour deposition from hexamethyldisiloxane precursor*. International Journal of Nanotechnology, 12(8/9), pp. 597 – 607 (2015).

[152] S. Zanini, R. Bami, R. D. Pergola and C. Riccardi. *Development of super-hydrophobic PTFE and PET surfaces by means of plasma processes*. Journal of Physics: Conference Series, 550(1), p. 012029 (2014).

[153] A. Bieder, A. Gruniger and R. von Rohr. *Deposition of SiOx diffusion barriers on flexible packaging materials by PECVD*. Surface and Coatings Technology, 200(1-4), pp. 928 – 931 (2005).

[154] F. L. Mobarakeh, J. R. and F. M. *Superhydrophobic surface elaboration using plasma polymerization of hexamethyldisiloxane (HMDSO)*. Advanced Materials Research, 409, pp. 783–787 (2011).

[155] A. Nelson, B. W. Muir, J. Oldham, C. Fong, K. M. McLean, P. G. Hartley, S. K. Oiseth and M. James. *X-ray and neutron reflectometry study of glow-discharge plasma polymer films*. Langmuir, 22(1), pp. 453–458 (2006).

[156] B. Duncan, J. Urquhart and S. Roberts. *Review of measurement and modelling of permeation and diffusion in polymers*. Tech. rep., National Physical Laboratory (2005).

[157] S. Russell and D. Weinkauf. *Vapor sorption in plasma polymerized vinyl acetate and methyl methacrylate thin films*. Polymer, 42(7), pp. 2827 – 2836 (2001).

[158] E. Favre, P. Schaetzel, Q. Nguygen, R. Clément and J. Néel. *Sorption, diffusion and vapor permeation of various penetrants through dense poly(dimethylsiloxane) membranes: a transport analysis*. Journal of Membrane Science, 92(2), pp. 169 – 184 (1994).

[159] J. Watson and M. Baron. *The behaviour of water in poly(dimethylsiloxane)*. Journal of Membrane Science, 110(1), pp. 47–57 (1996).

[160] M. Tsige and G. Grest. *Interdiffusion of solvent into glassy polymer films: A molecular dynamics study*. Journal of Chemical Physics, 121(15), pp. 7513–7519 (2004).

[161] R. H. Doremus. *Diffusion of water in crystalline and glassy oxides: Diffusion-reaction model*. Journal of Materials Research, 14, pp. 3754–3758 (1999).

[162] A. G. Erlat, R. J. Spontak, R. P. Clarke, T. C. Robinson, P. D. Haaland, Y. Tropsha, N. G. Harvey and E. A. Vogler. *Siox gas barrier coatings on polymer substrates: Morphology and gas transport considerations*. The Journal of Physical Chemistry B, 103(29), pp. 6047–6055 (1999).

[163] B. W. Muir, A. Nelson, A. Fairbrother, C. Fong, P. G. Hartley, M. James and K. M. McLean. *A comparative X-Ray and neutron reflectometry study of plasma polymer films containing reactive amines*. Plasma Processes and Polymers, 4(4), pp. 433–444 (2007).

[164] H. Jeon, J. Wyatt, D. Harper-Nixon and D. Weinkauf. *Characterization of thin polymer-like films formed by plasma polymerization of methylmethacrylate: A neutron reflectivity study*. Journal of Polymer Science Part B: Polymer Physics, 42(13), pp. 2522–2530 (2004).

[165] D. Hegemann, E. Koerner and S. Guimond. *Macroscopic approach to investigate plasma polymer growth*. In *53rd Annual Technical Conference Proceedings*, vol. 17-22, pp. 409–413. Society of Vacuum Coaters (2010).

[166] D. Clemens, P. Gross, P. Keller, N. Schlumpf and M. Könnecke. *AMOR - the versatile reflectometer at SINQ*. Physica B: Condensed Matter, 276-278(0), pp. 140 – 141 (2000).

[167] L. G. Parratt. *Surface studies of solids by total reflection of X-Rays*. Phys. Rev., 95, pp. 359–369 (1954).

[168] C. Braun. *Parratt32, v 1.6.0, build 242* (2002).

[169] H.-B. Liu, N. V. Venkataraman, T. E. Bauert, M. Textor and S.-J. Xiao. *Multiple transmission-reflection infrared spectroscopy for high-sensitivity measurement of molecular monolayers on silicon surfaces.* The Journal of Physical Chemistry A, 112(48), pp. 12372–12377 (2008).

[170] W. Sellmeier. *Zur Erklärung der abnormen Farbenfolge im Spectrum einiger Substanzen.* Annalen der Physik und Chemie, 219, pp. 272–282 (1871).

[171] H. Kiessig. *Interferenz von Roentgenstrahlen an duennen Schichten.* Annalen der Physik, 402(7), pp. 769–788 (1931).

[172] T. Russell. *X-ray and neutron reflectivity for the investigation of polymers.* Materials Science Reports, 5(4), pp. 171 – 271 (1990).

[173] H. Hillborg, J. Ankner, U. Gedde, G. Smith, H. Yasuda and K. Wikström. *Crosslinked polydimethylsiloxane exposed to oxygen plasma studied by neutron reflectometry and other surface specific techniques.* Polymer, 41(18), pp. 6851 – 6863 (2000).

[174] E. Grimoldi, S. Zanini, R. A. Siliprandi and C. Riccardi. *AFM and contact angle investigation of growth and structure of pp-HMDSO thin films.* European Physical Journal D, 54(2), pp. 165–172 (2009).

[175] R. Siliprandi, S. Zanini, E. Grimoldi, F. Fumagalli, R. Barni and C. Riccardi. *Atmospheric pressure plasma discharge for polysiloxane thin films deposition and comparison with low pressure process.* Plasma Chemistry and Plasma Processing, 31(2), pp. 353–372 (2011).

[176] H. Zabel. *X-ray and neutron reflectivity analysis of thin films and superlattices.* Applied Physics A, 58(3), pp. 159–168 (1994).

[177] H. Yasuda and T. Hsu. *Some aspects of plasma polymerization investigated by pulsed R.F. discharge.* Journal of Polymer Science: Polymer Chemistry Edition, 15(1), pp. 81–97 (1977).

[178] A. M. Wrobel. *Aging process in plasma-polymerized organosilicon thin films.* Journal of Macromolecular Science: Part A - Chemistry, 22(8), pp. 1089–1100 (1985).

[179] B. Despax and P. Raynaud. *Deposition of "polysiloxane" thin films containing silver particles by an RF asymmetrical discharge.* Plasma Processes and Polymers, 4(2), pp. 127–134 (2007).

[180] P. J. Launer. *Infrared Analysis of Organosilicon Compounds: Spectra-Structure Correlations*, p. 100. Petrarch Systems, Bristol, PA (Bartram Rd., Bristol 19007) (1987).

[181] D. D. Burkey and K. K. Gleason. *Structure and mechanical properties of thin films deposited from 1,3,5-trimethyl-1,3,5-trivinylcyclotrisiloxane and water.* Journal of Applied Physics, 93(9), pp. 5143–5150 (2003).

[182] R. Anderson, B. Arkles and G. Larson. *Silicon compounds review and register.* Tech. rep., Petrarch Systems, Bristol, PA (1987).

[183] G. Lucovsky. *Chemical effects on the frequencies of Si-H vibrations in amorphous solids.* Solid State Communications, 29(8), pp. 571 – 576 (1979).

[184] K. Aumaille, C. Vallée, A. Granier, A. Goullet, F. Gaboriau and G. Turban. *A comparative study of oxygen/organosilicon plasmas and thin SiOxCyHz films deposited in a helicon reactor.* Thin Solid Films, 359(2), pp. 188–196 (2000).

[185] F. Fanelli, S. Lovascio, R. d'Agostino, F. Arefi-Khonsari and F. Fracassi. *Ar/HMDSO/O2 fed atmospheric pressure DBDs: Thin film deposition and GC-MS investigation of by-products.* Plasma Processes and Polymers, 7(7), pp. 535–543 (2010).

[186] W. A. Pliskin. *Comparison of properties of dielectric films deposited by various methods.* Journal of Vacuum Science & Technology, 14(5), pp. 1064–1081 (1977).

[187] J. Fang, H. Chen and X. Yu. *Studies on plasma polymerization of hexamethyldisiloxane in the presence of different carrier gases*. Journal of Applied Polymer Science, 80(9), pp. 1434–1438 (2001).

[188] D. S. Wavhal, J. Zhang, M. L. Steen and E. R. Fisher. *Investigation of gas phase species and deposition of SiO2 films from HMDSO/O2 plasmas*. Plasma Processes and Polymers, 3(3), pp. 276–287 (2006).

[189] S. Zanini, C. Riccardi, M. Orlandi, P. Esena, M. Tontini, M. Milani and V. Cassio. *Surface properties of HMDSO plasma treated polyethylene terephthalate*. Surface and Coatings Technology, 200(1-4), pp. 953 – 957 (2005).

[190] K. Li, O. Gabriel and J. Meichsner. *Fourier transform infrared spectroscopy study of molecular structure formation in thin films during hexamethyldisiloxane decomposition in low pressure rf discharge*. Journal of Physics D-Applied Physics, 37(4), pp. 588–594 (2004).

[191] http://www.ncnr.nist.gov/resources/activation/ (2014).

[192] N. Guermat, A. Bellel, S. Sahli, Y. Segui and P. Raynaud. *Water molecule sensitive layers deposited from hexamethyldisiloxane/oxygen mixture at low temperature*. Materials Science Forum, 609, pp. 69–73 (2009).

[193] K. Siderakis and D. Pylarinos. *Room Temperature Vulcanized Silicone Rubber Coatings: Application in High Voltage Substations*, pp. 1–17. John Wiley & Sons, Inc. (2014).

[194] H. Yang, Q. T. Nguyen, Y. Ding, Y. Long and Z. Ping. *Investigation of poly(dimethyl siloxane) (PDMS)-solvent interactions by {DSC}*. Journal of Membrane Science, 164(1-2), pp. 37 – 43 (2000).

[195] S. Morgenthaler, C. Zink and N. D. Spencer. *Surface-chemical and -morphological gradients*. Soft Matter, 4, pp. 419–434 (2008).

[196] J. Genzer and R. R. Bhat. *Surface-bound soft matter gradients*. Langmuir, 24(6), pp. 2294–2317 (2008).

[197] H. Elwing and C.-G. Goelander. *Protein and detergent interaction phenomena on solid surfaces with gradients in chemical composition*. Advances in Colloid and Interface Science, 32(4), pp. 317 – 339 (1990).

[198] T. Ruardy, J. Schakenraad, H. van der Mei and H. Busscher. *Preparation and characterization of chemical gradient surfaces and their application for the study of cellular interaction phenomena*. Surface Science Reports, 29(1), pp. 3 – 30 (1997).

[199] J. D. Whittle, D. Barton, M. R. Alexander and R. D. Short. *A method for the deposition of controllable chemical gradients*. Chemical Communications, 0(14), pp. 1766–1767 (2003).

[200] M. R. Alexander, J. D. Whittle, D. Barton and R. D. Short. *Plasma polymer chemical gradients for evaluation of surface reactivity: epoxide reaction with carboxylic acid surface groups*. J. Mater. Chem., 14, pp. 408–412 (2004).

[201] K. L. Beers, J. F. Douglas, E. J. Amis and A. Karim. *Combinatorial measurements of crystallization growth rate and morphology in thin films of isotactic polystyrene*. Langmuir, 19(9), pp. 3935–3940 (2003).

[202] M. R. Tomlinson and J. Genzer. *Formation of grafted macromolecular assemblies with a gradual variation of molecular weight on solid substrates*. Macromolecules, 36(10), pp. 3449–3451 (2003).

[203] A. D. Price and D. K. Schwartz. *Anchoring of a nematic liquid crystal on a wettability gradient*. Langmuir, 22(23), pp. 9753–9759 (2006).

[204] M. K. Chaudhury and G. M. Whitesides. *How to make water run uphill*. Science, 256(5063), pp. 1539–1541 (1992).

[205] S. Daniel, M. K. Chaudhury and J. C. Chen. *Fast drop movements resulting from the phase change on a gradient surface*. Science, 291(5504), pp. 633–636 (2001).

[206] S. Daniel, S. Sircar, J. Gliem and M. K. Chaudhury. *Ratcheting motion of liquid drops on gradient surfaces*. Langmuir, 20(10), pp. 4085–4092 (2004).

[207] L. M. van de Steeg and C.-G. Goelander. *Adsorption of ethylene oxide/propylene oxide copolymers on hydrophobicity gradient surfaces.* Colloids and Surfaces, 55(0), pp. 105 – 119 (1991).

[208] V. Hlady. *Spatially resolved adsorption kinetics of immunoglobulin G onto the wettability gradient surface.* Appl. Spectrosc., 45(2), pp. 246–252 (1991).

[209] V. Hlady and C.-H. Ho. *Human low density lipoprotein (LDL) and human serum albumin (HSA) co-adsorption onto the C18-silica gradient surface.* Materialwissenschaft und Werkstofftechnik, 32(2), pp. 185–192 (2001).

[210] H. Elwing. *Wettability gradient surfaces for protein adsorption.* Biological Chemistry Hoppe-Seyler, 368, p. 740 (1987).

[211] R. C. Gunawan, J. Silvestre, H. R. Gaskins, P. J. A. Kenis and D. E. Leckband. *Cell migration and polarity on microfabricated gradients of extracellular matrix proteins.* Langmuir, 22(9), pp. 4250–4258 (2006).

[212] F. Fang, J. Satulovsky and I. Szleifer. *Kinetics of protein adsorption and desorption on surfaces with grafted polymers.* Biophysical journal, 89(3), pp. 1516–1533 (2005).

[213] Y. Ding and V. Hlady. *Competitive adsorption of three human plasma proteins onto sulfhydryl-to-sulfonate gradient surfaces.* Croat Chem Acta, 84(2), pp. 193–202 (2011).

[214] K. Karaky, L. Billon, C. Pouchan and J. Desbrie. *Amphiphilic gradient copolymers shape composition influence on the surface/bulk properties.* Macromolecules, 40(3), pp. 458–464 (2007).

[215] C. Xu, T. Wu, Y. Mei, C. M. Drain, J. D. Batteas and K. L. Beers. *Synthesis and characterization of tapered copolymer brushes via surface-initiated atom transfer radical copolymerization.* Langmuir, 21(24), pp. 11136–11140 (2005).

[216] C. Xu, S. E. Barnes, T. Wu, D. A. Fischer, D. M. DeLongchamp, J. D. Batteas and K. L. Beers. *Solution and surface composition gradients via microfluidic confinement: Fabrication of a statistical-copolymer-brush composition gradient.* Advanced Materials, 18(11), pp. 1427–1430 (2006).

[217] V. Hlady, J. Buijs and H. Jennissen. *Methods for studying protein adsorption.* Methods in enzymology, 309, pp. 402–429 (1999).

[218] L. Vroman, A. Adams, G. Fischer and P. Munoz. *Interaction of high molecular weight kininogen, factor XII, and fibrinogen in plasma at interfaces.* Blood, 55(1), pp. 156–159 (1980).

[219] H. Haehl, F. Evers, S. Grandthyll, M. Paulus, C. Sternemann, P. Loskill, M. Lessel, A. K. Haesecken, T. Brenner, M. Tolan and K. Jacobs. *Subsurface influence on the structure of protein adsorbates as revealed by in situ X-ray reflectivity.* Langmuir, 28(20), pp. 7747–7756 (2012).

[220] M. Bellion, L. Santen, H. Mantz, H. Hähl, A. Quinn, A. Nagel, C. Gilow, C. Weitenberg, Y. Schmitt and K. Jacobs. *Protein adsorption on tailored substrates: long-range forces and conformational changes.* Journal of Physics: Condensed Matter, 20(40), p. 404226 (2008).

[221] P. Harder, M. Grunze, R. Dahint, G. M. Whitesides and P. E. Laibinis. *Molecular conformation in oligo(ethylene glycol)-terminated self-assembled monolayers on gold and silver surfaces determines their ability to resist protein adsorption.* The Journal of Physical Chemistry B, 102(2), pp. 426–436 (1998).

[222] M. Heuberger, T. Drobek and N. D. Spencer. *Interaction forces and morphology of a protein-resistant poly(ethylene glycol) layer.* Biophysical journal, 88(1), pp. 495–504 (2005).

[223] W. Michaeli, K. Telgenbuescher, J. Striffler, J. Leiber and M. Stollenwerk. *Broad range variation in surface tension by plasma-polymerized coatings on polymethyl methacrylate.* Surface and Coatings Technology, 59(1-3), pp. 338–341 (1993).

[224] D. Hegemann, H. Brunner and C. Oehr. *Improving the adhesion of siloxane-based plasma coatings on polymers with defined wetting properties.* In *45th Annual Technical Conference Proceedings*, pp. 174–178 (2002).

141

[225] N. Sanada, A. Yamamoto, R. Oiwa and Y. Ohashi. *Extremely low sputtering degradation of polytetrafluoroethylene by C60 ion beam applied in XPS analysis*. Surface and Interface Analysis, 36(3), pp. 280–282 (2004).

[226] C. J. Powell and A. Jablonski. *NIST electron Inelastic-Mean-Free-Path Database*. National Institute of Standards and Technology, Gaithersburg, USA, version 1.2 edn. (2010).

[227] N. E. Blanchard, V. Naik, T. Geue, O. Kahle, D. Hegemann and M. Heuberger. *The response of HMDSO plasma polymer films to aqueous environments*. Langmuir, submitted (2015).

[228] J. A. De Feijter, J. Benjamins and F. A. Veer. *Ellipsometry as a tool to study the adsorption behavior of synthetic and biopolymers at the air-water interface*. Biopolymers, 17(7), pp. 1759–1772 (1978).

[229] T. L. McMeekin, M. L. Groves and N. J. Hipp. *Refractive Indices of Amino Acids, Proteins, and Related Substances*, chap. 4, pp. 54–66. American Chemical Society (1964).

[230] R. Barer and S. Tkaczyk. *Refractive index of concentrated protein solutions*. Nature, 173, pp. 821 – 822 (1954).

[231] A. Conway-Jacobs and L. M. Lewin. *Isoelectric focusing in acrylamide gels: Use of amphoteric dyes as internal markers for determination of isoelectric points*. Analytical Biochemistry, 43(2), pp. 394 – 400 (1971).

[232] A. Michelmore, P. Martinek, V. Sah, R. D. Short and K. Vasilev. *Surface morphology in the early stages of plasma polymer film growth from amine-containing monomers*. Plasma Processes and Polymers, 8(5), pp. 367–372 (2011).

[233] G. Grundmeier and M. Stratmann. *Interfacial processes during plasma polymer deposition on oxide covered iron*. Thin Solid Films, 352(1-2), pp. 119 – 127 (1999).

[234] D. R. Jackson, S. Omanovic and S. G. Roscoe. *Electrochemical studies of the adsorption behavior of serum proteins on titanium*. Langmuir, 16(12), pp. 5449–5457 (2000).

[235] A. Derylo-Marczewska, M. Blachnio, A. Marczewski, A. Swiatkowski and B. Tarasiuk. *Adsorption of selected herbicides from aqueous solutions on activated carbon*. Journal of Thermal Analysis and Calorimetry, 101(2), pp. 785–794 (2010).

[236] M. Hasegawa and H. Kitano. *Adsorption kinetics of proteins onto polymer surfaces as studied by the multiple internal reflection fluorescence method*. Langmuir, 8(6), pp. 1582–1586 (1992).

[237] P. G. Squire, P. Moser and C. T. O'Konski. *Hydrodynamic properties of bovine serum albumin monomer and dimer*. Biochemistry, 7(12), pp. 4261–4272 (1968).

[238] K. E. Michael, V. N. Vernekar, B. G. Keselowsky, J. C. Meredith, R. A. Latour and A. J. Garia. *Adsorption-induced conformational changes in fibronectin due to interactions with well-defined surface chemistries*. Langmuir, 19(19), pp. 8033–8040 (2003).

[239] G. Anand, S. Sharma, A. K. Dutta, S. K. Kumar and G. Belfort. *Conformational transitions of adsorbed proteins on surfaces of varying polarity*. Langmuir, 26(13), pp. 10803–10811 (2010).

[240] C. F. Wertz and M. M. Santore. *Adsorption and reorientation kinetics of lysozyme on hydrophobic surfaces*. Langmuir, 18(4), pp. 1190–1199 (2002).

[241] W. Noll. *The Polymeric Organosiloxanes*. Academic Press (1968).

[242] P. R. Gray, P. J. Hurst, S. H. Lewis and R. G. Meyer. *Analysis and Design of Analog Integrated Circuits*. Wiley, New York, 5th edition edn. (2009).

[243] B. Kasemo. *Biological surface science*. Current Opinion in Solid State and Materials Science, 3(5), pp. 451 – 459 (1998).

[244] V. Conti Nibali and M. Havenith. *New insights into the role of water in biological function: Studying solvated biomolecules using terahertz absorption spectroscopy in conjunction with molecular dynamics simulations*. Journal of the American Chemical Society, 136(37), pp. 12800–12807 (2014).

[245] J. Harris, S. Zalipsky, A. C. S. D. of Polymer Chemistry and A. C. S. Meeting. *Poly(ethylene Glycol): Chemistry and Biological Applications*. No. v. 680 in ACS symposium series. American Chemical Society (1997).

[246] M. Heuberger, T. Drobek and J. Voeroes. *About the role of water in surface-grafted poly(ethylene glycol) layers*. Langmuir, 20(22), pp. 9445–9448 (2004).

[247] B. Sivaraman, K. P. Fears and R. A. Latour. *Investigation of the effects of surface chemistry and solution concentration on the conformation of adsorbed proteins using an improved circular dichroism method*. Langmuir, 25(5), pp. 3050–3056 (2009).

[248] R. Shevchuk, D. Prada-Gracia and F. Rao. *Water structure-forming capabilities are temperature shifted for different models*. The Journal of Physical Chemistry B, 116(25), pp. 7538–7543 (2012).

[249] Y. A. Mantz, B. Chen and G. J. Martyna. *Temperature-dependent water structure: Ab initio and empirical model predictions*. Chemical Physics Letters, 405(4â€"6), pp. 294 – 299 (2005).

[250] M. Lemesle. *Transfer of the ELISA on the TInAS*. Master's thesis, Ecole européenne de Chimie, Polymères et Matériaux and Empa, Swiss Federal Laboratories for Science and Technology, Strasbourg, France and St. Gallen, Switzerland (2015).

Tobi, you have always supported me with your love during my PhD studies. You helped me leaving work behind and gain new energy. You always believed in me and my work. Thank you for everything.

<div align="right">THANK YOU</div>

CURRICULUM VITAE

Personal Information

Noémi Blanchard
Allmendstrasse 6
CH-1712 Tafers
Email: noemi.blanchard@gmx.ch
Date of Birth: April 27, 1987
Hometown: Tafers, Switzerland

Current Occupation

04/2012–07/2015	PhD Student at EMPA, Swiss Federal Laboratories for Materials Science and Technology, St. Gallen, Switzerland and the Laboratory for Surface Science and Technology at ETH Zurich, Zürich, Switzerland. *The role of sub-surface water in plasma-deposited vertical chemical gradients* Supervised by Dr. Dirk Hegemann and Prof. Dr. Manfred Heuberger.

Education

09/2009–10/2011	MSc in Physics, University of Fribourg, Switzerland.
Master Thesis (9 months)	*Elasticity of dense microgel suspensions*; Grade 6.0 Supervised by Dr. Véronique Trappe at the University of Fribourg, Switzerland.
10/2006–07/2009	BSc in Physics, University of Fribourg, Switzerland.
08/2002–07/2006	Highschool (Matura), Kollegium St. Michael, Freiburg, Switzerland.

Language Skills

German	Mother Tongue
English	Very good oral and writing skills.
French	Good oral and writing skills.
Spanish	Basic oral and writing skills.

Publications

submitted, 2015. *The response of HMDSO plasma polymers to aqueous environments.* **N.E. Blanchard**, V. Naik, T. Geue, O. Kahle, D. Hegemann, M. Heuberger.

Plasma Processes and polymers, 12(1), pp. 32-41, 2015 *Densification and hydration of HMDSO plasma polymers.* **N.E. Blanchard**, B. Hanselmann, J. Drosten, M. Heuberger, D. Hegemann.

submitted, 2015. *Deposition of functional plasma polymers influenced by reactor geometry in capacitively coupled discharges.* D. Hegemann, M. Michlicek, **N.E. Blanchard**, U. Schütz, D. Lohmann, M. Vandenbossche, L. Zajickova, M. Drabik.

Contributions to Plasma Physics 54 (2), pp. 162-169, 2014 *Plasma-Substrate Interaction during Plasma Deposition on Polymers.* D. Hegemann, B. Hanselmann, **N.E. Blanchard**, M. Amberg.

Applied Physics Letters 101 (21), 211603, 2012. *Densification of functional plasma polymers by momentum transfer during film growth.* D. Hegemann, E. Koerner, **N.E. Blanchard**, M. Drabik.

Conference contributions

Oral presentations:

04/2015 Interdisciplinary Surface Science Conference, Birmingham, United Kingdom; *Plasma polymerized vertical chemical gradients and their influence on protein adsorption.*

10/2014 Empa PhD Symposium, St. Gallen, Switzerland; *Hydration of HMDSO plasma polymer films.* Winner of the best-presentation award.

09/2013 International Conference on Plasma Processes, Paris, France; *Effect of aqueous environment on properties of Ag/a-C:H:O nanocomposite films.*

Poster presentations:

09/2014 International Conference on Plasma Surface Engineering, Garmisch-Partenkirchen, Germany; *Hydration of Hydrophobic HMDSO Plasma Polymers.*

06/2014 International Symposium on Surfactants in Solution, Coimbra, Portugal; *Trapping of amphiphilic molecules on vertical chemical gradients.*

10/2013 Empa PhD Symposium, Dübendorf, Switzerland; *Stability of hexamethyldisiloxane plasma polymers in aqueous environments.*

09/2013 International Conference on Plasma Processes, Paris, France; *Plasma polymer coatings with nanometer sized vertical chemical gradients.*

02/2013 Fachtagung für Plasmatechnologie, Greifswald, Germany; *Thin Plasma Polymer Coatings Exhibiting a Stable Vertical Chemical Gradient.*

11/2012   Empa PhD Symposium, Dübendorf, Switzerland; *Kinetic adsorption trapping via vertical chemical gradients.*